Studies Towards The Development Of Novel Multidentate Ligands

A THESIS

Submitted in fulfilment of the requirements for the degree of

Master of Science

of

Rhodes University

by

Nceba Magqi
B.Sc. Hons. (Rhodes University)

January 2007

ABSTRACT

In this study, attention has been given to the design and synthesis of novel multidentate ligands for use in the construction of ruthenium-based metathesis catalysts, and their chelating potential has been explored by computer modelling at the Density Functional Theory (DFT) level. Both Kemp's triacid (1,3,5-trimethyl-1,3,5-cyclohexanetricarboxylic acid) and D-(+)-camphor have been investigated as molecular scaffolds for the development of such ligands. However selective elaboration of the functional groups in Kemp's triacid proved difficult to achieve, and the research has focused on the development of camphor derivatives.

The synthesis of the camphor-based ligands has involved C-8 functionalisation and ring-opening of the bicyclic system to afford tridentate products. The formation of 9-iodocamphorquinone bis(ethylene ketal) together with the desired product, the 8-iodo isomer, has been confirmed by single crystal X-ray analysis of both compounds. Formation of the 9-iodo analogue has provided new insights into the intramolecular rearrangement of camphor skeleton, and the mechanistic implications have been assessed by coset analysis. Attempts to effect nucleophilic displacement of the 8-halogeno groups by nucleophilic donor moieties proved unexpectedly difficult and, coupled with the susceptibility of the carbonyl groups to nucleophilic attack, has led to the formation of novel tricyclic products, *viz.*, 1,6-dimethyl-3-(2-pyridylamino)-4-oxatricyclo[4.3.0.0^{3,7}]-2-nonanone and 6,7-dimethyl-3-(2-pyridylamino)-4-oxatricyclo -[4.3.0.0^{3,7}]-2-nonanone. However the diphenylphosphine group was successfully introduced at C-8 and oxidative ring-opening of the camphor skeleton has afforded the tridentate ligands, 2-(diphenylphosphinoylmethyl)-1,2-dimethyl-1,3-cyclopentane-dicarboxylic acid and 2-(diphenylphosphinoylmethyl)-1,3-bis(hydroxymethyl)1,2-dimethylcyclopentane.

One- and two-dimensional NMR and, where appropriate, high-resolution MS methods have been used to characterise the products. Three ^{13}C NMR chemical shift prediction programmes, *viz.,* ChemWindow and the MODGRAPH neural network and HOSE (Hierachially Ordered Spherical description of Environment), have been applied to representative compounds to assess their efficacy. While the predicted shifts

correlated reasonably well with the experimental data, they proved to be insufficiently accurate to differentiate the isomeric systems examined.

ACKNOWLEDGEMENTS

I would like to thank my supervisor, Professor P.T. Kaye for allowing me to conduct this research under his supervision and all his time, support and guidance given during my post-graduate studies.

Thank you to Mr A. Sonemann for running low resolution mass spectrometry, Mr Tommy van der Merwe from the University of Witwatersrand for running high-resolution mass spectrometry and Mr Andy Soper for technical support with the NMR spectrometer. Many thanks to Mr Kevin Lobb for assistance in coset analysis, Professor Mino Caira from the University of Cape Town for X-ray crystallography, and Mr Dokes Ntebe for ordering and dispensing chemicals. Thanks to Dr W. Meyer, my Sasol mentor, from Sasol R&D for fruitful discussions.

I would also like to thank my fellow students and friends for their support during this research. A special thank you to Mlu Ganto for being willing to proof-read my introduction. Also to my family for their constant support and encouragement in all the years I have spent at university.

I would like to express my gratitude to Sasol and Rhodes University for generous financial support.

LIST OF ABBREVIATIONS

COSY	1H - ^{1}H shift-correlated spectroscopy
DEPT	Distortionless Enhancement by Polarization Transfer
DFT	Density Functional Theory
DMF	Dimethylformamide
DMSO	Dimethylsulfoxide
DNP	'double numerical plus polarization'
GGA	Generalised Gradient Approximation
HMBC	Heteronuclear Multiple Bond Coherence
HMQC or HSQC	Heteronuclear Multiple Quantum Coherence
HPLC	High Performance Liquid Chromatography
IR	Infrared
LAH	Lithium aluminium hydride
LDA	Lithium diisopropylamide
NBS	*N*-Bromosuccinimide
NMR	Nuclear Magnetic Resonance
PTSA	*p*-Toluenesulfonic acid
PW91	Perdew and Wang
THF	Tetrahydrofuran
TMSCl	Trimethylsilyl chloride

1. INTRODUCTION

1.1. CATALYSIS: BASIC PRINCIPLES

Catalytic processes date back as early as the 1800s when metal surfaces were first used as catalysts to speed up chemical reactions.[1] The attempts to study and define catalytic processes were first made towards the end of 19th century by Ostwald,[2] whose work on catalytic processes was recognised in the award of a Nobel Prize in Chemistry in 1909. In the first scientific analyses of catalytic processes, only thermodynamic factors were given attention. Subsequently, kinetic data were formulated by Langmuir[3] in his work on chemisorption. Although the early catalysts were mainly solid metals or metal complexes, nowadays catalysts can be anything from soluble acids or bases to organometallic systems.[4] Regardless of the complex nature of different catalysts, their main function is to speed up a chemical reaction by reducing the free energy of activation.[4,5]

There is clearly a very wide range of catalysts, varying in chemical and physical properties, but the discussion in this chapter will be limited to metal-based catalysts. Among such catalysts, transition metals tend to be favoured due to their particular properties, which are outlined in the following sections.

1.1.1. Transition Metals as Catalysts

Various characteristics of transition metals make these metals ideal catalysts. These characteristics include bonding ability, ligand effects, variability in oxidation state and coordination potential.[5]

1.1.1.1. *Bonding ability*

The *d*-block transition metal ions have nine valence shell orbitals, *viz.*, *s*, p_x, p_y, p_z, d_{z^2}, $d_{x^2-y^2}$, d_{xz}, d_{yz}, d_{xy}. These orbitals can form sigma and/or pi bonds with coordinated ligands, and determine the characteristic geometry of the resulting complexes.[5]

1.1.1.2. *Ligand effects*

The catalytic cycle of a metal complex usually involves the dissociation and/or association of ligands.[6] A ligand *trans* to the dissociating ligand in a complex can have electronic and/or steric effects on the dissociation of the leaving ligand. This phenomenon is known as the "*trans effect*".[7] The electron donor-acceptor properties of phosphorous ligands may also play an important role. The infrared stretching frequency of a carbon monoxide (CO) ligand in a metal complex varies according to the nature and the number of ligands present in a complex.[8,9] This variation can, for example, be used to understand the electron donor/acceptor properties of trivalent phosphorus ligands.[9,10]

1.1.1.3. *Variability in oxidation state and coordination potential*

Since transition metal ions can exist in a wide range of oxidation states, it is possible to form complexes with ligands that prefer either high oxidation state metal ions or low oxidation state metal ions. The variation in the oxidation states of transition metal ions is particularly useful in catalytic cycles in which certain ligands might be added or removed from the metallic complex. [6,5]

1.1.2. Types of Catalysts

The main feature that is used to classify catalysts is solubility or insolubility in the reaction medium.[4] Thus, the two general classes of catalysts are homogeneous and heterogeneous catalysts. Homogeneous catalysts are soluble in the reaction medium while heterogeneous catalysts are usually not soluble. However, the use of solubility as the sole criterion for classifying catalysts is not really adequate since soluble catalysts, for example, may form insoluble metal-particles *in situ.* These metal particles can then function as heterogeneous catalysts.[11] In the following sub-section, the general characteristics of homogeneous and heterogeneous catalysts are outlined.

1.1.2.1. *Homogeneous catalysts*

Homogeneous catalysts are soluble chemical substances that exist in the same phase as the other constituents of the chemical reaction. Usually, the catalyst is dissolved in a solvent to form a homogeneous mixture with the other reagents.[4] In solution, a catalyst often forms discrete species with catalytically active sites.[5] This, for example,

can be seen in organometallic catalytic cycle where an 18-electron and 16-electron complexes alternate.[6] 16-Electron complexes are usually the catalytically active species that initiate the reaction.

It has been observed that, in a number of chemical reactions, homogeneous catalysis has very attractive qualitative advantages in terms of the purity of the product. Homogeneous catalysts are, generally, more highly selective than their heterogeneous counterparts[4] and, thus, fewer by-products are formed with homogeneous catalysis. The soluble nature of homogeneous catalysts is also a major advantage since the catalytic mechanisms can be studied using modern techniques and that may lead to modification and optimization of the catalyst.[5] Modified and optimized rhodium catalysts, for an example, have been developed by complexation with rationally designed ligands.[12] However, there are often major disadvantages involved in the use of homogeneous catalysis; these include expensive separation procedures, the problem of disposing of toxic liquid waste after a catalytic reaction and expenses due to corrosion problems.[4]

1.1.2.2. *Heterogeneous catalysts*

Catalysts in this category exist in a different phase from the reactants and, sometimes, from the products. The catalyst is usually a solid, and the reactants and products are in the liquid or gas phase. The heterogeneous catalytic reaction takes place on the surface of the catalyst.[4]

A typical and major advantage of heterogeneous catalysis is the simple separation of the catalyst from the reaction mixture and product(s), especially if the product is in the liquid or gaseous phase. Moreover, heterogeneous catalysts are usually thermally stable, solid substances that can be easily regenerated *in situ*.[4,5] However, there are major drawbacks that include uncontrollable use of energy, low selectivity and the practical difficulty of studying the catalytic reaction on the surface of the catalyst. Understanding the reaction mechanism is essential in finding ways to control the undesirable products that are usually formed using heterogeneous catalysts.[4,5]

1.1.3. Catalysis in Chemical Industry

Catalysts are used in wide range of chemical reactions. They are used in both large-scale chemical reactions for commercial purposes and small-scale reactions in universities and, industrial research and development laboratories. It is estimated that 80% of industrial reactions are assisted by catalysts.[13] Some of the well known arch-catalytic processes currently in use in the chemical industry include the Wacker, Wilkinson, Ziegler-Natta and Fischer-Tropsch catalytic reactions.

The factors that motivated the development of early industrial catalysts were mainly quantitative. The development of aircraft during World War II, the wide use of automobiles after the war and the availability of cheap raw materials, such as coal, motivated many industries to mass-produce synthetics. In this day and age new catalysts need to be developed to meet the standards required of modern catalytic processes. The general characteristics required of an industrial catalyst include the following:-[4]

i) *Activity*, which refers to the amount of product produced relative the amount of catalyst or reactant used. Higher activity leads mainly to higher productivity even under milder conditions.
ii) *Selectivity*, which refers to the amount of desired product produced per reactant consumed in a catalytic reaction.
iii) *Lifetime, i.e.* the time a catalyst can be used without losing its activity.
iv) Ease of regeneration of used catalyst.
v) *Toxicity*, in terms of being user-friendly and leading to less toxic waste problems.
vi) *Price*, which refers to all the operations that lead to additional costs when the catalyst has been used in a reaction. These operations include the expensive procedures of separation, corrosion problems and the treatment of toxic waste.

There have been major advantages, such as durability and easy of separation, shown by heterogeneous catalysis in industrial applications.[4,13b] There are, however, some disadvantages; these include low selectivity and high energy consumption. Growing

concerns over the use of energy and greenhouse gas emissions during energy production, and growing demands for fine chemicals (for use in pharmaceuticals, agricultural chemicals and specialty polymers) suggest the need for more efficient catalytic methods. Efficient methods would, for example, be more selective and less energy-consuming and could, include the use of homogeneous catalysis.[13b,14,15]

Organometallic catalysts, especially those containing transition metals, have been developed as efficient and low-temperature catalysts.[14] These catalytic complexes gained popularity because of their high selectivity and activity under mild conditions. The solubility of organometalic catalysts in a medium is also a major advantage since catalytic pathways can be monitored and novel catalysts developed by the replacement of certain ligands.[12]

While homogeneous catalysts have been used in the chemical industry since 1910,[13b] some of the industrial homogeneous catalytic processes developed in the 1970s are shown in **Table 1**.[13b] Other commercially viable chemical reactions, in which homogeneous catalytic systems have been used, include isomerization, carbonylation, hydroformylation, oligomerization, polymerization, oxidation and olefin metathesis reactions.[5] Olefin metathesis is the focus of the present study, with particular emphasis on ruthenium-based catalysts.

Table 1: Homogeneous catalytic processes developed in the 1970s.[13b]

Process	Company	Start Up
Adiponitrile from HCN and butadiene	Du Pont	1971
Linear α-olefins from ethylene	Shell	1977
Rh-catalysed hydroformylation	Celanese, Carbide Union	1976
Acetic Acid from CO and MeOH	Monsanto	1970
L-DOPA by asymmetric hydrogenation	Monsanto	1974

1.2. OLEFIN METATHESIS

The general concept of metathesis is essentially the exchange of "radicals" between two compounds that decompose simultaneously to form new compounds.[16] The application of this concept in the synthesis of alkenes has led to useful catalytic processes that are generally known as olefin metathesis processes.[17,18] These processes can be generally be defined as the statistical redistribution of alkylidene entities such that, under steady state conditions, equilibrium concentrations of reactants and products are formed (**Scheme 1**).[5] When the equilibrium is reached, the more thermodynamically stable isomers predominate.

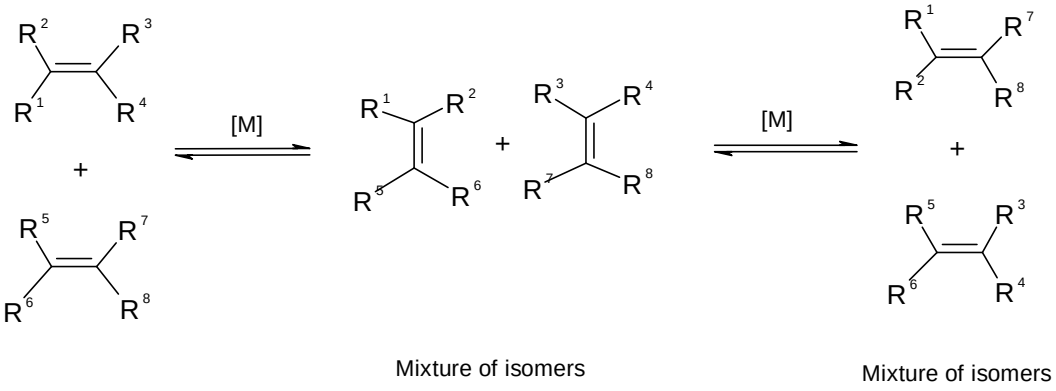

Scheme 1. Olefin Metathesis[5]

1.2.1. Types of Metathesis Reactions

The redistribution of unsaturated carbon-carbon bonds during olefin metathesis occurs in five closely related types of reaction, *viz.*, ring opening metathesis polymerization (ROMP), ring closing metathesis (RCM), acyclic diene metathesis polymerization (ADMET), ring opening metathesis (ROM), and cross metathesis (CM or XMET) (**Scheme 2**). Since these reactions are closely related, tandem or domino processes may occur involving two or more metathesis reactions.

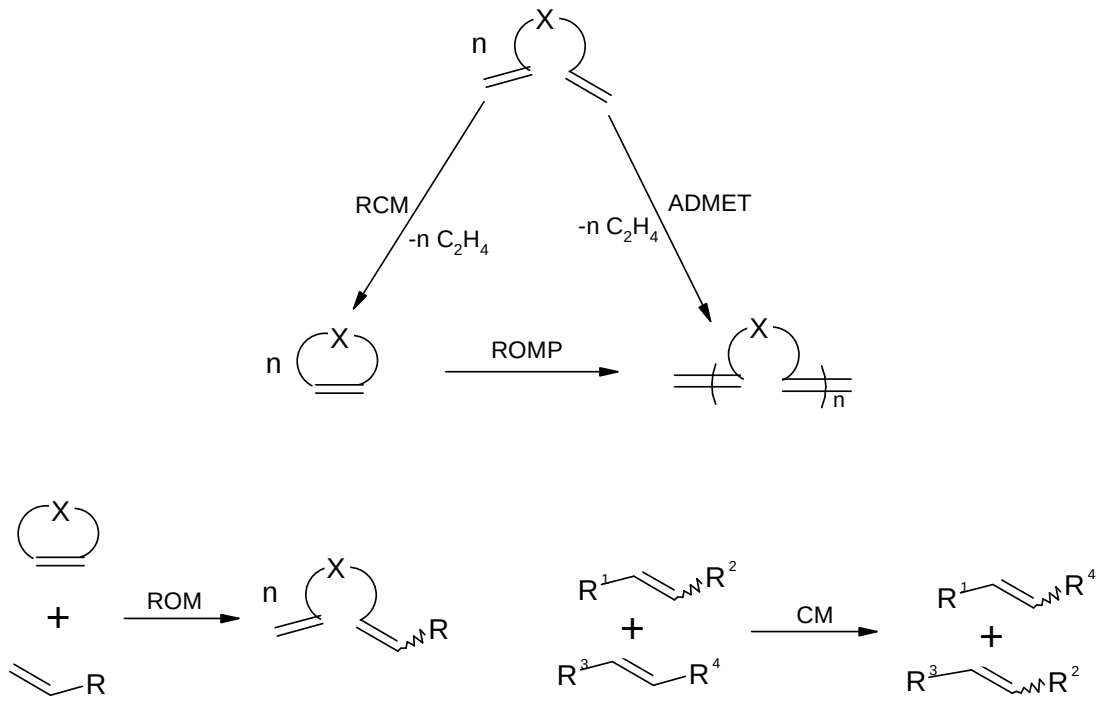

Scheme 2: Types of olefin metathesis reactions.[19]

1.2.1.1. *Ring opening metathesis polymerization (ROMP)*

In the early stages, ROMP was confused with Ziegler-Natta addition polymerization. However, ROMP was later elucidated independently by Eleuterio and Calderon[20] and by Natta[21] (**Scheme 3**). The first living polymerization of ROMP products,[22,20] was first reported by Grubbs and Gillion.[23] After the discovery of living polymerization, several controlled polymers were discovered.[20] The two ends of the ROMP polymer can be defined by the alkyl group on the carbene of the initiator species and the group coupled to the polymeric carbene during work-up to form an end-cap[24,25] as shown in **Scheme 3c**.

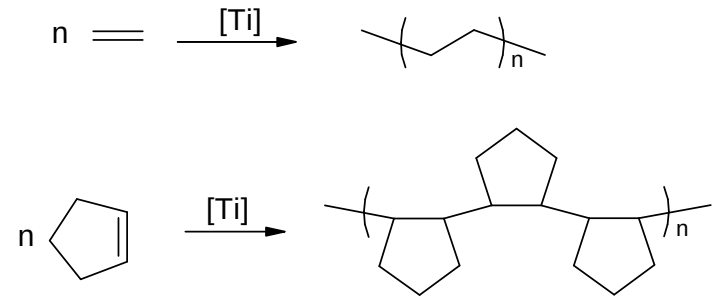

a) Ziegler-Natta addition polymerization

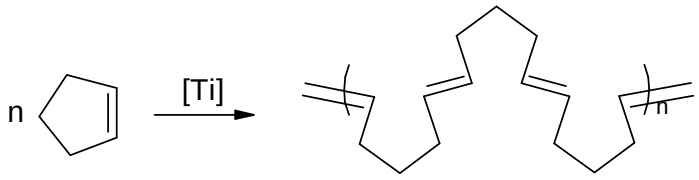

b) Ring Opening Metathesis Polymerization

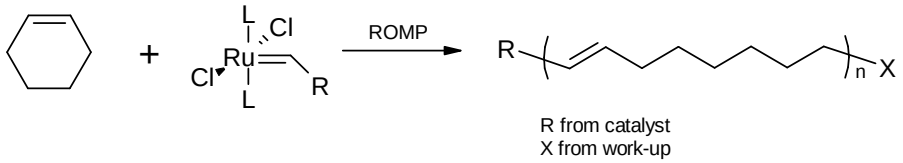

c) Ring Opening Metathesis Polymerization

Scheme 3: a) Ziegler-Natta addition polymerization, b) ROMP catalysed by different Ti complexes and c) ROMP catalysed by a Ru complex.

1.2.1.2. *Acyclic diene metathesis polymerization (ADMET)*

The search for versatile polymerization processes led to the discovery of acyclic diene metathesis (ADMET) polymerization.[26] ADMET complements ROMP in polymerizing acyclic α,ω-dienes. The ADMET reaction usually affords polymers with vinylic end groups (**Scheme 4**).[25,26,27] In order to drive the reaction towards the formation of products, ethylene (a by-product), needs to be constantly removed from the system.[26]

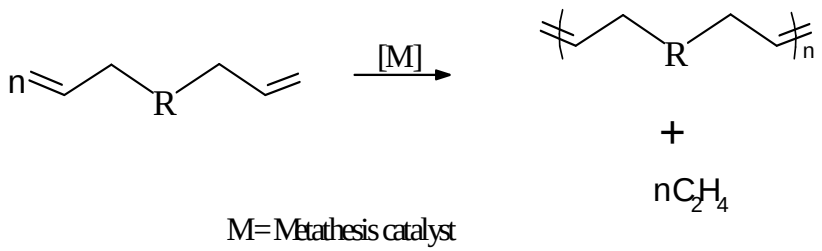

Scheme 4: Acyclic diene metathesis polymerization

1.2.1.3. *Ring-closing metathesis (RCM)*

Research has shown that both ROMP and ADMET competition products form during a RCM reaction (**Scheme 5**).[28] ROMP products may be favoured depending on the thermodynamic or kinetic characteristics of the competing reactions. In some cases, microwave irradiation has been used to increase the rate of RCM.[29] Despite the existence of competing reaction pathways, RCM has been used to synthesize a number of cyclic products[30,31] as shown in Section 1.2.2.2.

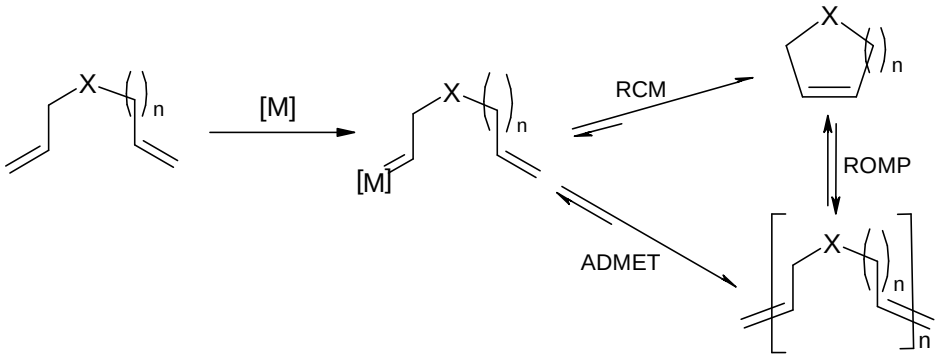

Scheme 5: RCM reaction and competing reactions.[28]

1.2.1.4. *Cross metathesis (CM)*

Cross metathesis reactions have not received as much attention as ROMP[20] and RCM[31e] reactions. This is due to the lack of selectivity and stereoselectivity in the formation of CM products since self-olefin metathesis may compete leading to similar products (**Scheme 6**).

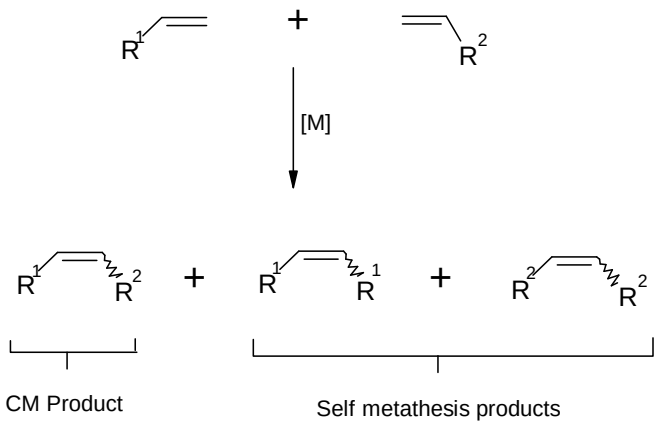

Scheme 6: Cross metathesis and self-metathesis.

The availability of efficient catalysts such as the Grubbs first- and second-generation catalysts has encouraged significant investigation into the selectivity of olefin cross metathesis reactions. Grubbs and co-workers discovered a "general model" that assists in the prediction of the selectivity and stereochemistry of CM products.[32] The "general model" suggests that different types of olefins could be matched based on their relative reactivity and ability to form consumable homodimmers. For instance, CM products can be obtained by reacting a highly active olefin with less reactive olefin. The homodimers formed by the highly reactive olefin react with the less reactive olefin to form CM products (**Scheme 7**).

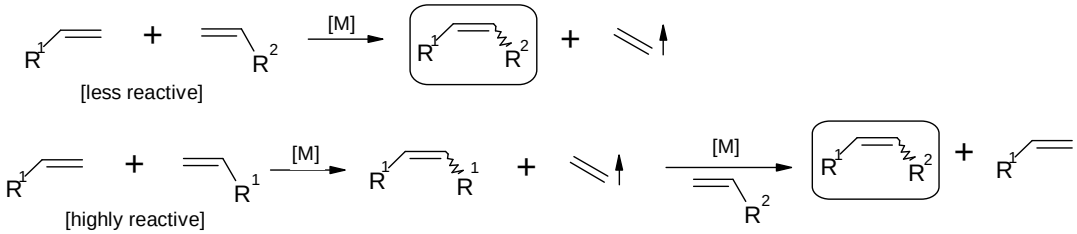

Scheme 7: CM "general moldel"[32]

1.2.1.5. *Ring opening metathesis (ROM)*

Ring opening metathesis (ROM) may be followed by cross metathesis (CM). Thus, strained ring systems are opened and subsequently coupled with acyclic olefins in the presence of a metal catalyst.[33] Application limitations such as product selectivity, stereoselectivity and regioselectivity,[34] that are common in CM reactions, also hamper

the application of ROM in organic synthesis. The additional problem in ROM reactions is the polymerization of cyclic olefins, *i.e.* the ROMP reaction. As a result, low concentrations of strained ring substrates are coupled with excess amounts of acyclic olefins to avoid ROMP.[31c,31e] Immobilization of the acyclic olefin has also been attempted to minimise polymerization and self-metathesis.[31g]

Besides the types of olefin metathesis reactions outlined above, Chen and Adlhart[35] further divide these reactions into the following four classes, depending on the substrate used.

i) *Acyclic degenerate*: in which the product is the same as the substrate; the model substrate for this reaction is ethylene.

ii) *Acyclic exothermic*: the model substrate is ethyl vinyl ether.

iii) *ROMP with an unstrained cyclic substrate*: the model substrate is cyclopentene

iv) *ROMP with a strained substrate*: the model substrate is norbonene.

1.2.2. Applications of Olefin Metathesis Reactions

Numerous reviews and reports on the applications of olefin metathesis reactions may be found in literature.[31,36] For the sake of brevity and clarity, only selected applications are discussed here.

1.2.2.1. *Industrial applications*

A number of industrial processes use or incorporate olefin metathesis in the production of useful chemical products, such as petrochemicals, polymers, specialty chemicals and so forth.[36]

1.2.2.1.1. *Petrochemicals*[37]

The two main olefin metathesis processes used in the production of petrochemicals are olefin conversion technology (OCT) processes and the Shell higher olefins process (SHOP).

The tungsten-catalysed OCT process, licensed by ABB Lummus Global, is basically a cross metathesis (CM) reaction used mainly in the industrial production of propene from ethene and 2-butene (**Scheme 8)**.[37] This reversible CM reaction was previously observed by Rooney and O'Neil in a small-scale Mo-catalysed reaction.[38]

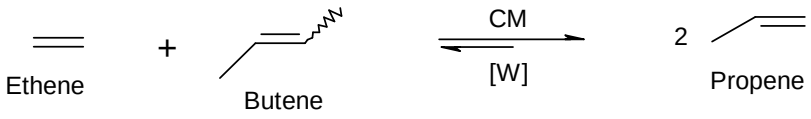

Scheme 8: The OCT Process

Propene is characterized by an allylic methyl group and a double bond and can be modified into wide range of petrochemicals. Propene is used as a building block for the synthesis of products such as polypropylene, oxo alcohols, acrolein, acrylic acid and other petrochemicals.[37] Due to the high demand for propene, OCT has been licensed to a number of chemical companies including BASF, Fina and Mitsui Chemicals.

SHOP is a three-stage industrial process that leads to the formation of C_{11}-C_{14} linear internal olefins.[39] The first stage of this process is the oligomerization of ethene into light and heavy olefins. These olefins are, in turn, isomerized in the second stage. Cross metathesis (CM) of olefin isomers in the presence of a Mo metathesis catalyst constitutes the last stage (**Scheme 9**). The linear olefins produced through this process can be converted into detergent alcohols or detergent alkylates.[37]

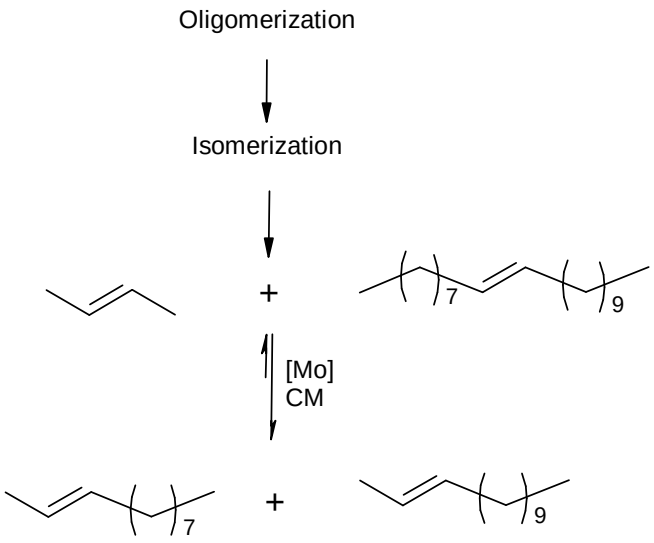

Scheme 9: The SHOP Process.

1.2.2.1.2. *Polymer synthesis*

Ring Opening Metathesis Polymerization (ROMP) is a well-used metathetic process in the industrial synthesis of light and heavy polymers. The first commercial use of ROMP involved the tungsten-catalysed reaction of highly strained 2-norbonene. Useful elastomers such as Norsorex are synthesized by ROMP of 2-norbonene (**Scheme 10**).[36]

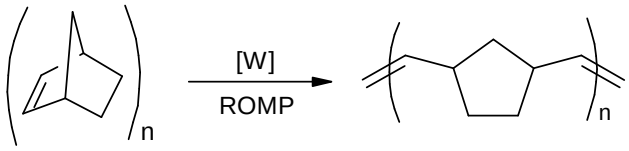

Scheme 10: The Norsorex Process

Other industrial processes that use ROMP in the synthesis of polymers are Reaction Injection Molding (RIM) technology, which is licensed by BFGoodrich, Hercules and Degussa-Huls AG. RIM is used in the production of Vestenamer products (**Scheme 11**).[36] The Nippon Zeon Corporation also uses ROMP in the production of cyclo-olefin polymers, which are marketed as Zeonex® and Zeonor® products.[40]

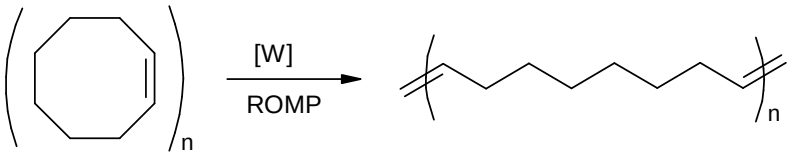

Scheme 11: The Vestenamer Process

1.2.2.1.3. *Fragrance industry*

Macrocyclic compounds with a musk odour are used in the fragrance industry to make perfumes. The traditional method to obtain natural musk was through extraction from living organisms.[41] A few of these macrocyclic musks are synthesised *via* RCM. Eh and Worner,[42] for example, have reported the metathetic preparation of 1,4-dioxacycloalkan-2-ones and 1,4-dioxacycloalkene-2-ones, used as ingredients in perfumes. The application of olefin metathesis in the synthesis of natural macrocyclic musks is discussed in the following subsection.

1.2.2.2. *Applications in natural products synthesis*

Several reports on the total synthesis of natural products using metathesis reactions (mostly RCM) appear in the literature.[31d,43] **Figure 1** illustrates some of the cyclic natural products that have been prepared *via* RCM.

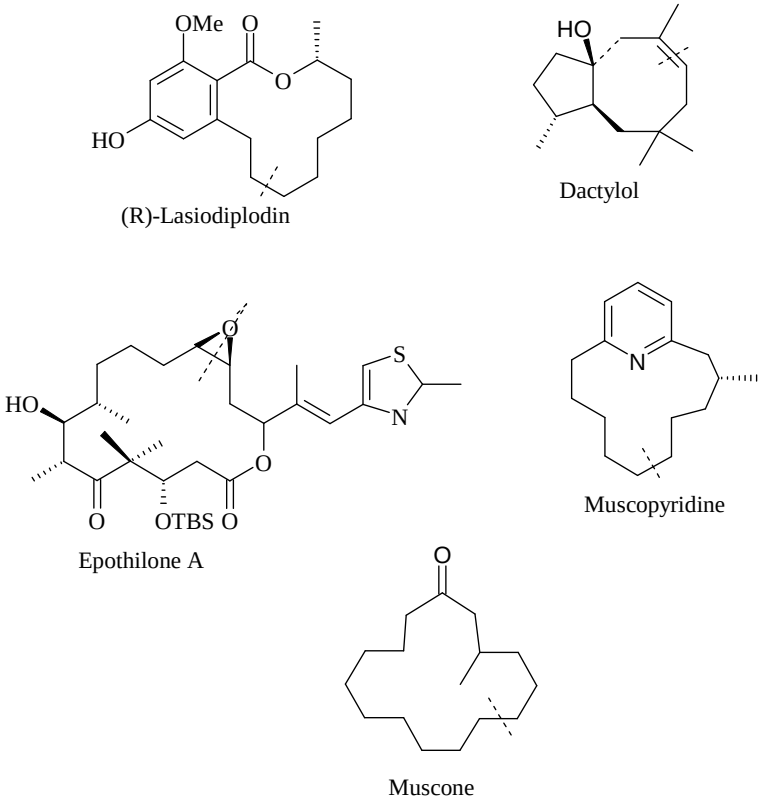

Figure 1. Cyclic natural products accessed *via* RCM. The broken lines show the site of ring closure.

Muscopyridine and muscone are macrocyclic musks isolated from *Moschus moschiferus*.[44,45] The total synthesis of these two musks can be achieved by Grubbs 1st- and 2nd-generation catalysts, respectively.[44,45] (Ruthenium-based catalysts are discussed in Section 1.2.3). (*R*)-(+)-Lasiodiplodin and epothilone A have also been prepared using Grubbs 1st- and 2nd-generation catalysts, respectively. Epothilone A is very useful in cancer therapy.[31d]

Recently, considerable attention has been given to the use of CM in natural products synthesis.[46,43] In one of the early reports on the use of CM in natural product synthesis, Blechert and co-workers reported the total synthesis of the plant pheromone, jasmonic acid (**Scheme 12).**[31e]

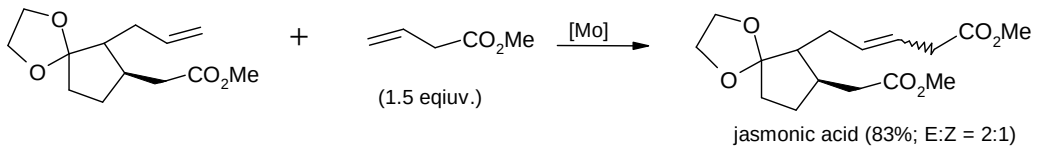

Scheme 12: Synthesis of jasmonic acid via CM[31e]

While ring opening metathesis (ROM) has not received significant attention in natural products synthesis, it is important to note its application in the synthesis of the brown algae pheromones, multifidene and viridiene (**Scheme 13**).[31c]

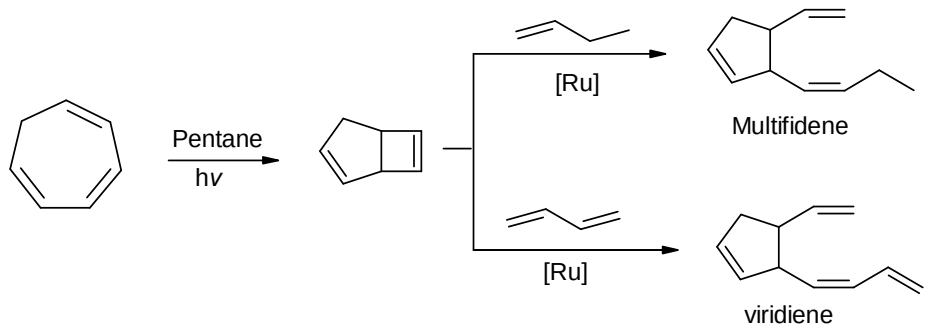

Scheme 13: Synthesis of multifidene and viridiene via ROM[31c]

1.2.3. Olefin Metathesis Catalysts

Olefin metathesis catalysts are divided into heterogeneous and homogeneous catalysts. The first catalysts to be used in olefin metathesis reactions were heterogeneous catalysts.[5,17]

1.2.3.1. *Heterogeneous olefin metathesis catalysts*

The three metals that have been mainly used for heterogeneous catalysts in olefin metathesis are molybdenum, rhenium and tungsten.[31f] The oxides or halides (mostly chlorides) of the metals are supported on alumina,[17] silica or other inert surfaces.[31f] The most common feature of heterogeneous metathesis catalysts is the lack of an alkylidene moiety in their original co-ordination sphere, which is a common feature of most homogeneous counterparts. The catalytically active metal carbene intermediate is formed from the catalyst and the olefin itself.[47] Sometimes, pre-treatment of the metal catalyst with certain additives or promoters before initiation of the metathesis reaction is necessary. The pre-treatment generates the catalytically active species that can initiate metathesis.[48,49,50] Tetraalkyl-tin, -lead, -silicon and -germanium compounds are commonly used as promoters in the pre-treatment of metal catalysts.

Besides their thermal stability and separation advantages, heterogeneous catalysts show little or no activity for the metathesis of functionalized olefins such as unsaturated acid esters.[49] Rhenium shows better functionality tolerance and can operate under milder conditions compared to Mo and W catalysts.[48,50]

1.2.3.2. *Homogeneous olefin metathesis catalysts*

Early work on single component, homogeneous catalysts was conducted on a number of metal complexes with different transition metal spheres. The main aim of this early research was to develop alkylidene and metallacyclobutane complexes[51] that would follow the Chauvin mechanism[20] in olefin metathesis. Transition metals examined in the early homogeneous catalysts included molybdenum, tungsten, ruthenium and titanium. Titanium complexes have been extensively used for the living ROMP of norbornenes.[20] However, the current literature on well-defined metathesis catalysts is dominated by molybdenum-based (Schrock's catalysts)[52] and ruthenium-based (Grubbs' catalysts)[31] metal complexes.

Grubbs' comparative study on ROMP[53] showed that the Ru-based Grubbs' 1st-generation catalyst **4** is more selective than the highly reactive Schrock catalysts (NAr)(OR')$_2$Mo=CHR **3** and (NAr)(OR')$_2$W=CHR **2** (**Table 2**). The other disadvantage of the Schrock catalysts is their sensitivity to oxygen and moisture due to the high oxophilicity of the W and Mo metal spheres. The selectivity shown by Ru-

based catalysts is due to the relative softeness of the Ru metal ion. Thus, in the presence of oxygen functional groups, Ru catalysts prefer to react with soft Lewis bases, *e.g.*, olefins.

Table 2. Grubbs' comparative study of different olefin metathesis catalysts.[53]

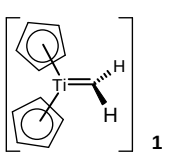 **1**	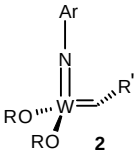 **2**	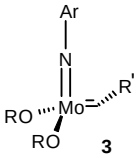 **3**	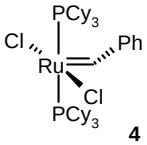 **4**
Acids	Acids	Acids	***Olefins***
ROH, H_2O	ROH, H_2O	ROH, H_2O	Acids
Aldehydes	Aldehydes	Aldehydes	ROH, H_2O
Ketones	Ketones	***Olefins***	Aldehydes
Esters	***Olefins***	Ketones	Ketones
Olefins	Esters	Esters	Esters

Increasing order of reactivity.

Functional group tolerance

1.3. RUTHENIUM-BASED OLEFIN METATHESIS CATALYSTS

The first homogeneous Ru-based olefin metathesis catalysts were reported in the 1960s; simple salts such as $RuCl_3$(hydrate)[54] and $Ru(H_2O)_6(TsO)_2$ (*TsO* = *p*-toluenesulfonate)[55] were used to catalyse ROMP reactions. However, these complexes had very low catalytic rates.

1.3.1. Grubbs' Catalysts: 1st and 2nd Generation

The first report of a catalytically active Ru alkylidene species was in 1992 when Grubbs reported the synthesis of the distorted square pyramidal L_2X_2Ru=CHR complex **6** (**Scheme 14**).[56]

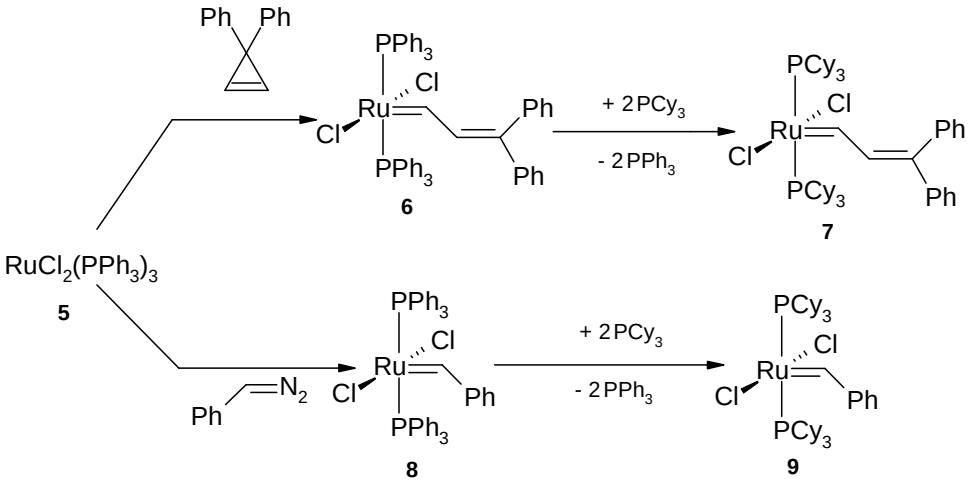

Scheme 14: Synthesis of Grubbs first generation catalysts.

The Grubbs catalyst **6** showed significant functional group tolerance but its catalytic activity was limited to ROMP of highly strained monomers. Subsequently, the matathetic activity of **6** was improved by replacement of the triphenylphosphine (PPh_3) ligands with the more basic and larger tricyclohexylphosphine (PCy_3) ligands to form analogue **7**.[57] The revised Grubbs catalyst **7** extended the scope of utility of Ru alkylidenes to include ROMP of low-strained monomers and CM of acyclic olefins. Furthermore, the catalyst **7** showed improved functional group tolerance and less sensitivity to air and water. Since the synthesis of diphenylcyclopropene (which

leads to the formation of catalysts **6** and **7**) was difficult, the reaction of $RuCl_2(PPh_3)_3$ with alkyl- and aryldiazoalkanes provided an alternative route which led to the formation of the highly active analogue **9** (**Scheme 14)**.[58]

Mechanistic studies by Grubbs' research group have shed some light on alternative ways of fine-tuning Ru olefin metathesis catalysts.[59] A number of modifications of the Grubbs' first-generation Ru catalyst have been investigated by varying the halide, phosphine or the alkylidene ligands. This led to the successful development of Grubbs' second-generation catalysts (**Figure 2**), in which one or two of the phosphine ligands are replaced by a stronger σ-donor ligand, the nitrogen heterocylic carbene (NHC).[60] The monosubstituted analogues **11** and **12** showed greater catalytic activity than the bis-substituted complex **10**.

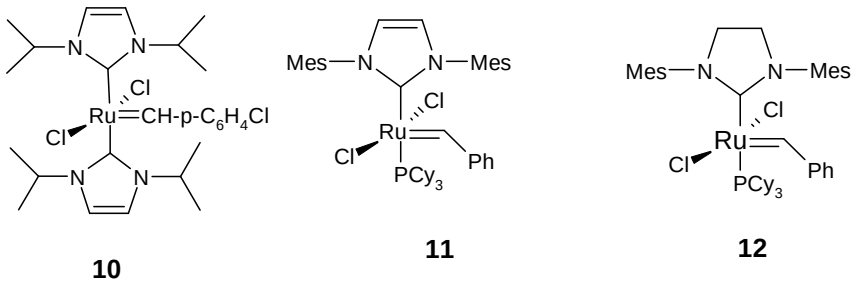

10 **11** **12**

Cy = Cyclohexyl
Mes = Mesityl

Figure 2. Grubbs second-generation catalysts.

1.3.2. Other Ruthenium Catalysts

A further class of ruthenium olefin metathesis catalysts was discovered by introducing chelating ligands to Grubbs' type systems. There are two main types within this class of catalysts.

a) *Hofmann-type catalysts*.[61] There are characterised by the rigid *cis*-stereochemistry of the phosphine donors of the η^2-bis(di-*tert*-butylphosphanyl)methane (η^2-dtbpm) ligand in the square-pyramidal structure **14 –** an arrangement which contrasts with the *trans*-stereochemistry of the phosphine ligands in the Grubbs-type system **13** (**Figure 3).**

b) *Grubbs-Hoveyda type catalysts.*[63,62] These Ru chelates contains a styrenyl ether ligand as shown in complex **15** (**Figure 3**). The Grubbs-Hoveyda type catalysts have shown promising results in catalytic recycling as well as immobilization potential. These aspects will be discussed later in this section.

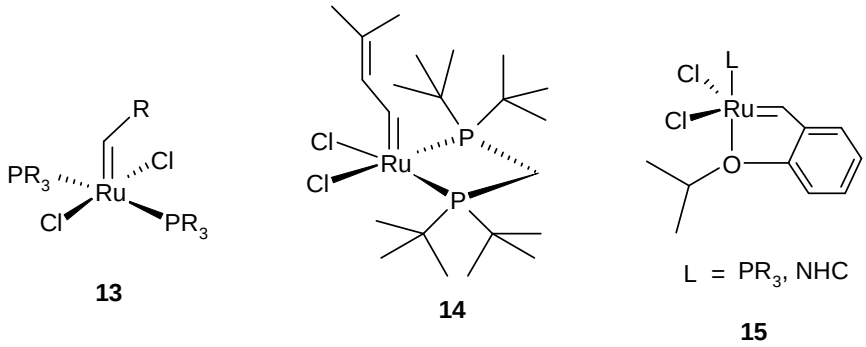

Figure 3: Grubbs first-generation catalyst **13** and Ru catalysts with chelating ligands.

1.3.3. Mechanistic Studies

The catalytic behaviour of $L_2X_2Ru{=}CHR$ complexes has been extensively explored in order to understand the mechanism by which these catalysts facilitate olefin metathesis. Experimental data were used initially to explore mechanistic pathways [59] but, lately a number of research groups have employed theoretical methods, using computer programmes to study the mechanism involved in $L_2X_2Ru{=}CHR$ catalysis.[35]

Grubbs and co-workers[59] pioneered mechanistic studies involving distorted square pyramidal $L_2X_2Ru{=}CHR$ complexes[58] by proposing two possible catalytic pathways, *i.e.* the associative and dissociative pathways,[6] based on a pathway first proposed by Chauvin in 1970 (**Scheme 15**). [20]

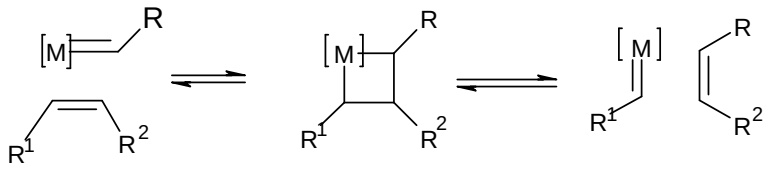

Scheme 15: The Chauvin mechanism.[20]

The associative pathway is characterised by an 18-electron olefin π-complex formed by olefin coordination (**Scheme 16**). Limited research has been reported on the associative pathway[59,35] since it appears to play an insignificant role in catalystic turnover.[59]

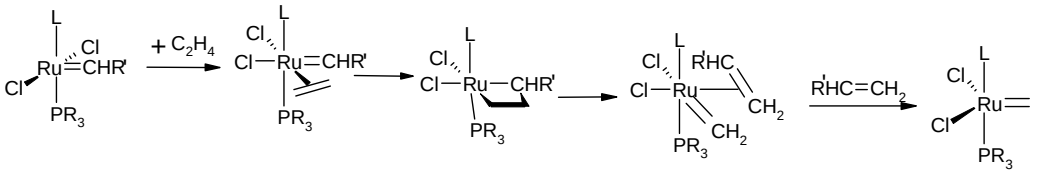

Scheme 16: The **a**ssociative pathway.[59]

The alternative, dissociative pathway is characterised by the dissociation of one phosphine ligand to form a highly active monophosphine intermediate **17**, which subsequently coordinates the olefinic substrate. The dissociative mechanism has been rationalised in a number of publications[31,35] and kinetic data suggest that this mechanism is responsible for 95% of the catalystic turnover.[59] The general dissociative pathway is shown in **Scheme 17.**

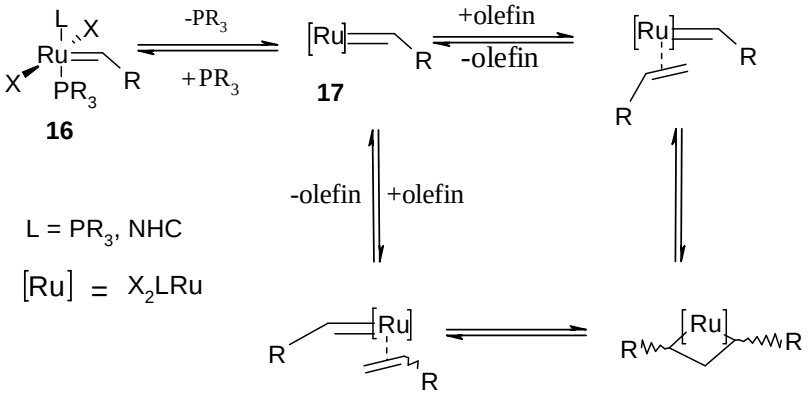

Scheme 17: Generalised dissociative catalytic cycle.[64]

It should be noted that the stereochemistry of the ligands around the metal centre of the monophosphine complexes is not shown. This is because there are a number of possible ways in which an olefin can coordinate to a metal centre. The orientation of an olefin bound to a metal to form a π-complex can affect the stereochemistry of the other ligands around the metal centre.[35,59] In the original Grubbs' proposal of the dissociative mechanism,[59] it was suggested that an olefin could bind *cis* or *trans* to the remaining phosphine ligand (**Scheme 18)**. It was further suggested that the *cis*-dissociative pathway is more favourable.

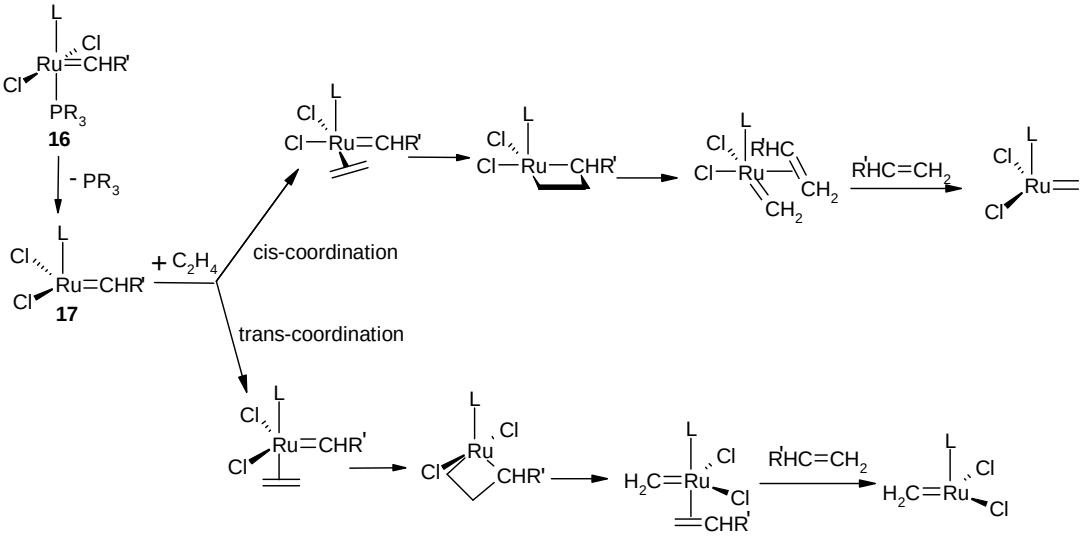

Scheme 18: *Cis*- and *trans*-dissociative catalytic pathways.[64]

Further experimental and computational work from different research groups has helped to elucidate the dissociative mechanism involving Grubbs catalysts. Most of the reported experimental work has been done in solution. Grubbs' second-generation catalysts exhibit greater activity and also follow the basic dissociative mechanism. Kinetic studies show that active species **17** (**Scheme 18**) has a very high affinity towards olefins, but the initiation step that leads to **17** is very slow.[64] The Grubbs[65] and Snapper[66] π-complexes **18** and **19**, respectively, have been isolated confirming their role as intermediates in the dissociative mechanism. The existence of a metallacyclic intermediate of the type illustrated in **Scheme 18** has also been detected spectroscopically by Piers and Romero.[67]

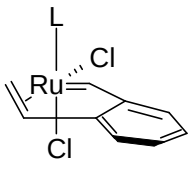

18

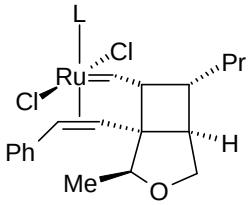

19

One of the few reported experiments conducted in the gas phase is Chen's electro-spray ionization tandem mass spectrometry (ESI-MS/MS) experiment.[68] The results suggested that the metallacycle complex in both the *cis* and *trans* dissociative mechanisms exists as a transition state rather than an intermediate. However, the computational work done by the same research group[68] and several other groups has indicated that the metallacyclic complex is, in fact, an intermediate species.[69,70,71,72]

As mentioned above, computational methodology is fast becoming a significant tool in the elucidation of some of the steps in the dissociative mechanism that cannot be studied experimentally. There is still an ongoing debate about the favourable binding mode of the olefin to active metal complex (*cis* or *trans*), the rate-limiting step and the factors influencing the increased activity of Grubbs second-generation catalysts. The coordination of an olefin *cis* to the ligand (L) has been supported by Meier and co-workers using Car-Parrinello molecular dynamics.[69] The results from this study show a 180^{o} rotation of the carbene in the Cl-Ru-Cl plane and a facile "*trans-cis* configurational exchange" of chloride ligands.

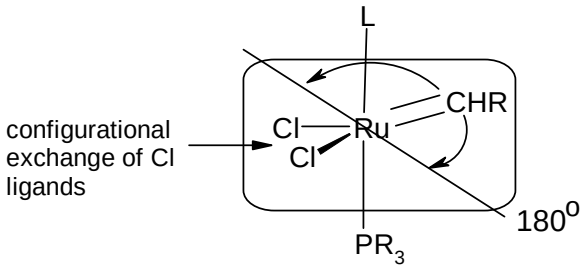

These rearrangements and other individual steps of the *cis* dissociative pathway could be observed in simulations conducted at ambient temperatures. However, phosphine dissociation required an elevated temperature. These findings were very consistent with the Grubbs *cis*-dissociative mechanism.[59] Thiel and co-workers' [70] DFT study has indicated the existence of both *cis*- and *trans*-binding of the olefin, but a

preference for *trans*-binding. Many other reported DFT calculations also favour *trans*-binding over *cis*-binding of the olefin.[35,70]

DFT calculations indicate that the rate-limiting step using Grubbs' first-generation systems is associated with the formation of the metallacycle.[70,73] Moreover, a DFT theoretical study conducted in our research group indicated that the π-complex and the metallacycle have similar energies and are both likely to influence the reaction rate.[74] In the case of Grubbs second-generation systems, however, the rate-limiting step appears to involve the slow dissociation of the phosphine to form an active species.[35] Cavallo's[72] theoretical study suggested that the slow dissociation of the phosphine in second-generation catalysts is due to the steric pressure exerted by the bulky mesityl groups on the chloride and alkylidene ligands. The resulting 14-electron Ru complex is destabilised by the interaction between the mesityl groups and the chlorides and the alkylidene ligands. It further suggested that the same steric pressure favours the subsequent steps of the catalytic cycle and thus increases the catalytic rate for second-generation systems. However, Thiel and co-workers[70] have suggested that the electronic influence exerted by the remaining ligand determines the rate of phosphine dissociation and the subsequent steps in the catalytic cycle for Grubbs' second-generation catalysts.

Several other possibilities regarding the dissociative catalytic cycle have been raised by computational studies. Bottoni and co-workers' [71] results, obtained at the DFT level suggest three possible catalytic pathways for the Grubbs' first-generation catalysts. The most likely pathways were: i) a pathway that involves the normal dissociation of a phosphine ligand followed by re-coordination after olefin binding; ii) a pathway that involves the migration of one chloride ligand from the metal centre to the coordinated olefin to afford a carbenoid species [$(PR_3)_2ClRu\text{-}CH_2Cl$], which undergoes further rearrangement to form the products. These results suggested that a monophosphine complex **17** is not the main active complex in the catalytic cycle of Grubbs' type catalysts.[71] However, separate theoretical results strongly contradicting the formation of the 18-electron π-complex implicated in the associative pathway (**Scheme 16**) were reported by Fomine and co-workers.[75]

1.3.4. Recent Advances in Ruthenium Catalysts: Design and Application

The detailed mechanistic studies on Grubbs' first-generation catalysts revealed fascinating facts that encouraged numerous research groups to fine-tune ruthenium catalysts to match the standard industrial catalysts. Several variations of Grubbs' first-generation catalyst have been developed to extend the application, to enhance catalytic activity, selectivity, stability and life-time and to improve the ease of regeneration of used catalyst. In this section, recent advances in the development of Ru-based catalysts are outlined.

1.3.4.1. *Activity*

The discovery of Grubbs second-generation catalysts increased the scope of application[33,60] and activity[60] of Ru-based catalysts. The catalytic activity of these catalysts matched Schrock's catalysts in RCM yet retained the functional group tolerance shown by Grubbs first-generation catalysts. Notwithstanding the impressive catalytic activity shown by Grubbs' second-generation catalysts, ways to increase the initiation rate were investigated.[76] Herrmann's[77] research group attempted to replace the phosphine ligand in complexes **11**[76] and **12**[77] by a labile ligand to form complexes such as **20** and **21** (**Fig. 5**). Both of these complexes showed better initiation rates but decomposed readily in metathesis reactions conducted at elevated temperatures (*ca*. 55°C).[78]

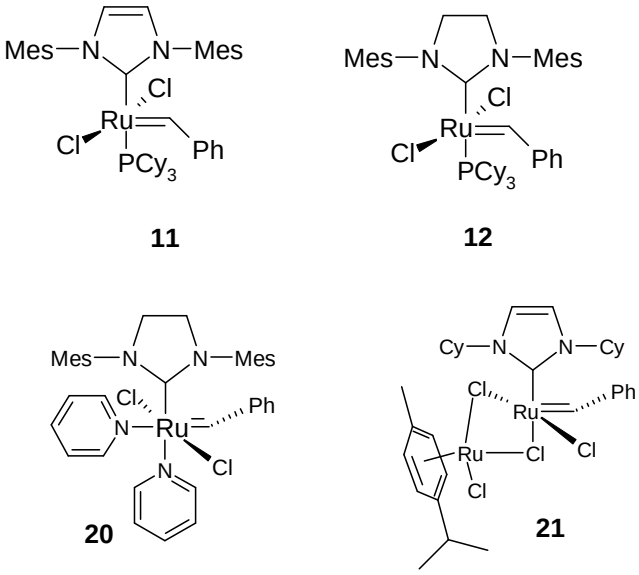

Figure 5: Grubbs' second-generation catalysts and analogues.

Complex **20** also facilitated the synthesis of active NHC catalysts **22** containing triarylphosphine ligands such as triphenylphosphine (**Scheme 19**). These triarylphosphine ruthenium complexes **22** exhibit activity of up to 2 orders of magnitude better than complex **12**.[76]

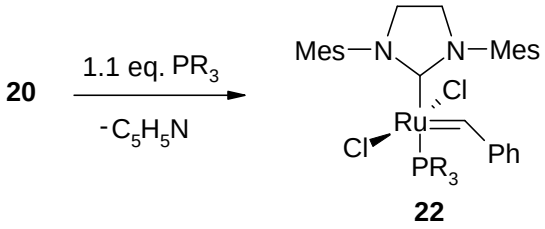

22

R = Ph, p-$CF_3C_6H_4$, p-ClC_6H_4, p-$MeOC_6H_4$

Scheme 19: Synthesis of triarylphosphine catalysts.[76]

1.3.4.2. *Thermal stability*

Robust olefin metathesis catalysts that can maintain high catalytic activity for a long time at high temperatures are clearly desirable.[78] Complexes **23**, **24** and **25,** which contain a chelating Schiff base ligand (**Figure 6**), show impressive stability to air, moisture and elevated temperatures.[79,80] Although the catalytic activity is not as pronounced as in Grubbs' first-generation and second-generation catalysts, catalyst **23** can catalyse metathesis reactions in polar protic solvents.[79] Catalyst **24,** with an NHC ligand, is catalytically active under mild conditions.[81] The proposed olefin metathesis mechanism of Schiff base type catalysts involves the de-coordination and re-coordination of "one-arm" of the Schiff base.[80,81]

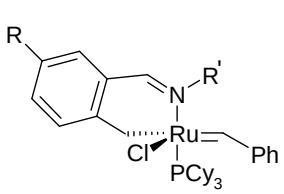

23

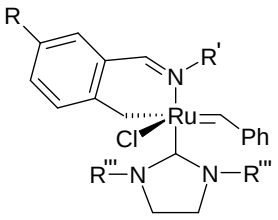

24

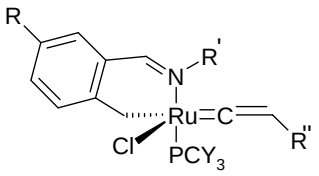

25

R' = H, NO_2
R'' = Substituted aliphatic/aromatic group
R''' = 2,4,6-trimethylphenyl

Figure 6: Robust metathesis catalysts with Schiff base bidentate ligand.

1.3.4.2. *Catalyst recovery and immobilization*

The discovery of the Grubbs-Hoveyda catalysts **15**[63,62] prompted research on the immobilization of Ru-based catalysts on solid supports. The advantage of the Grubbs-Hoveyda catalysts in this context is their ease of recycling. The tethered styrenyl ether ligand in **15** is released in the initiation step and returned at the end of catalytic cycle as in **Scheme 20.**[82] The complex that is formed after the "release and return" process is stable enough to be separated on silica.

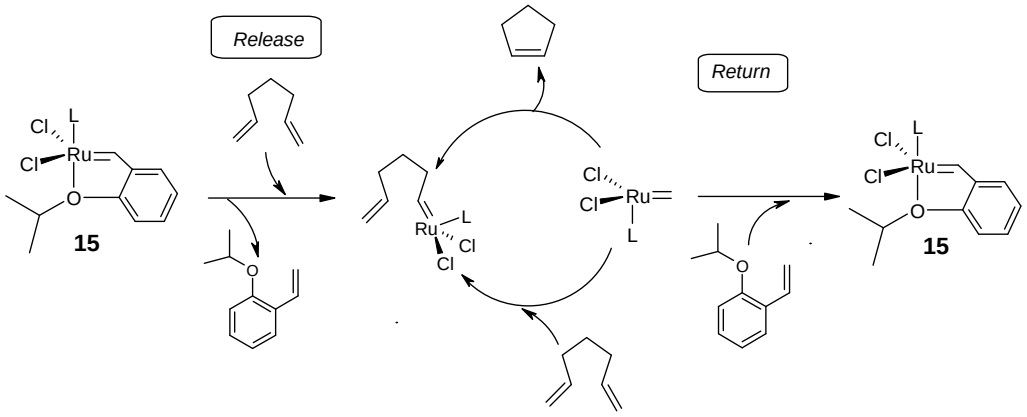

Scheme 20: Release and return mechanism for the Gubbs-Hoveyda catalyst.[82]

Attempts to enhance the recyclability of catalyst **15** by immobilisation of the styrenyl ether to a polymer have been reported. The immobilization of single component catalysts such as **15** is attractive in large-scale applications and successful developments in this direction include the development of active dendritic and recyclable ruthenium complexes.[82] Yao and Motta[83] have reported an active ruthenium complex supported on poly(ethylene glycol), while Buchmeiser and co-workers' approach to the immobilization of Grubbs-Hoveyda catalysts has involved the replacement of the two Cl ligands with electron withdrawing ligands that can be attached to a support.[84]

1.3.4.3. *Selectivity.*

Olefin metathesis reactions often lead to a mixture of *cis* and *trans* alkenes or a mixture of enantiomers. The selective formation of one enentiomer can be controlled by the use of chiral catalysts,[85] that can function at controlled temperatures or that are

tolerant to polar protic solvents.[79] However, relatively few reports on chiral Ru-based olefin metathesis catalysts are found in the literature.[85,86,87] The first report on the development of chiral Ru metathesis catalysts was based on the chiral monodentate ligand in complex **26**. Up to 90% enantiomeric excess was achieved using this catalyst[85] Chiral catalysts such as complex **27,** which contain a bidentate ligand and which are based on Grubbs-Hoveyda catalysts, have also been reported to catalyse asymmetric ring-opening/cross metathesis in unpurified solvents.[86] The modified version of complex **27**, catalyst **28**, was prepared *in situ* by the same research group, and exhibited the same catalytic activity as **27** but shorter reaction times.[87]

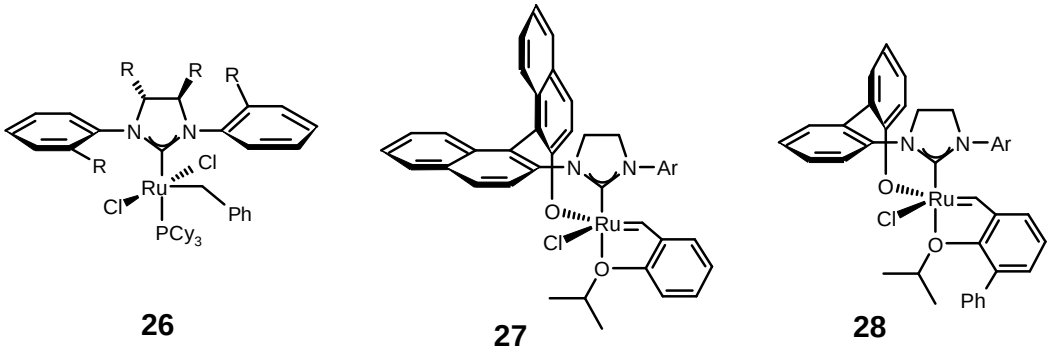

Figure 7. Chiral Ru-based catalysts.

1.3.4.4. *Catalyst decomposition*

Olefin metathesis catalyst decomposition is still a challenge in the catalysis of highly substituted or electron-deficient olefins at elevated temperatures. Unfortunately, highly active catalysts, such as Grubbs' second-generation catalysts, that can catalyse olefin metathesis of such olefins, decompose at high temperatures.[88] A thorough investigation of the decomposition of Grubbs' second-generation catalyst led to the isolation of the homodinuclear complex **30** (**Scheme 21a**).[88] The mechanism proposed for the formation of complex **30** involves a chloride bridged intermediate **31** (**Scheme 21b**).

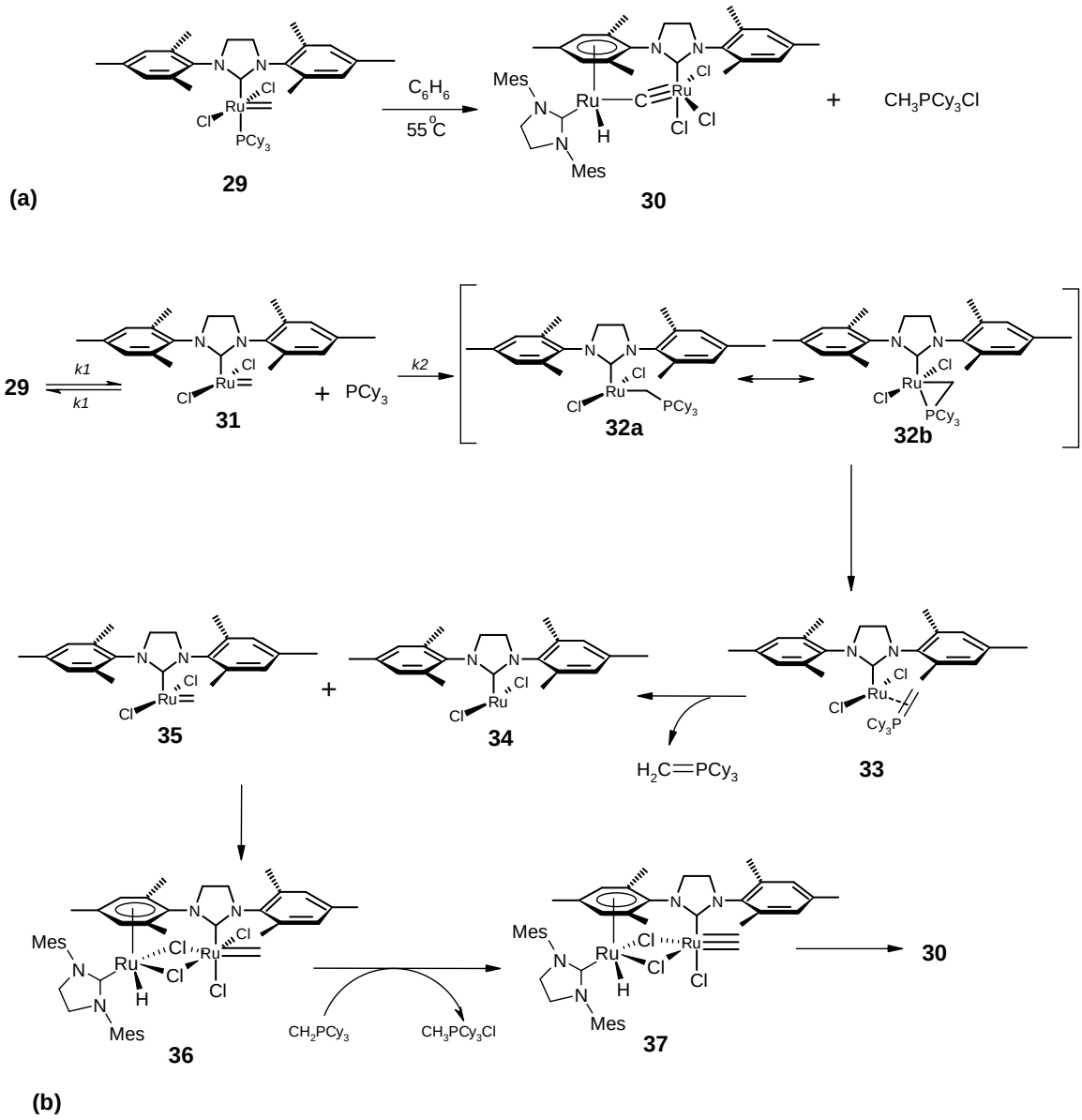

Scheme 22: Decomposition of Grubbs' second-generation catalysts.[88]

Chloride bridging has also been implicated in the decomposition of metathesis catalysts with *cis*-chelating phosphines,[89] while, a theoretical study on the decomposition of Grubbs' type catalysts to inactive hydride and unsaturated complexes has also been reported.[90]

1.3.4.5. *Other factors in catalyst design and application*

In living ROMP, chain transfer and termination are slow relative to the initiation rate.[22,20] However, it is desirable to have a highly active catalytic system with slow initiation rates to allow longer handling of the monomer before polymerization starts. It is for this reason that Grubbs and co-workers[91] synthesized isomers of latent second-generation analogues **38** containing a pyridine moiety; these complexes showed catalytic activity in both RCM and ROMP but with elongated initiation times.

Variations of the Ru-metal carbene moiety led to the introduction of linear alkyl carbene complexes.[58] Such complexes are useful in ROMP since they incorporate a linear alkyl group into a polymer[24,25] and thus improve the diversity of ROMP polymers. Recently, Wagener and Lehman[25] synthesized a second-generation analogue with a linear alkyl carbene moiety.

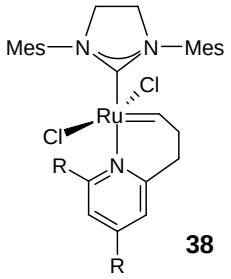

38 R = H, Me

Another area that has been explored in the development of Ru-based catalysts is solubility in aqueous media.[54,55,92] The introduction of ammonium chloride moities in Grubbs first-generation systems, such as complexes **39** and **40**[93] improved the solubility in water-based media. These polar catalysts have been effectively applied in RCM[94] and ROMP[95] in protic solvents. Recently, water solubility has been introduced into the Grubbs' second-generation (**41**)[96] and Grubbs-Hoveyda (**42**)[30] type catalysts with poly(ethylene glycol) as a solubilizing agent. Use of catalyst **42** permitted the extension of water-based olefin metathesis to include RCM of simple α,ω-dienes.

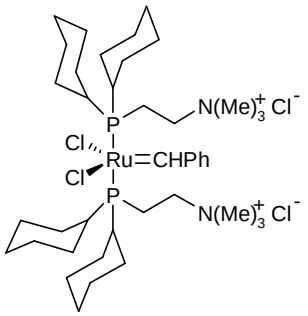
N(Me)3+ Cl-
P
Cl
Ru=CHPh
Cl
P
N(Me)3+ Cl-

39

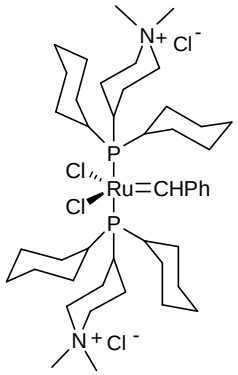
N+ Cl-
P
Cl
Ru=CHPh
Cl
P
N+ Cl-

40

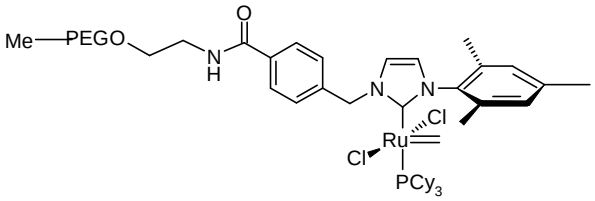
Me—PEGO
O
N
H
N
N
Cl
Ru
Cl
PCy3

41

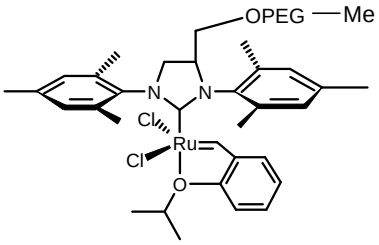
OPEG —Me
N
N
Cl
Ru
Cl
O

42

1.4. PREVIOUS WORK IN THE GROUP AND AIMS OF THE PRESENT STUDY

In previous years, our research group has shown interest in the development of multidentate ligands to be used in various studies. For example, attention has been given to the design and synthesis of novel diamido, diamino and diimino ligands, and their evaluation in the formation of copper(II), cobalt(II), nickel(II) and platinum(II) complexes as biomimetic models for the enzyme tyrosinase.[97] Metal-selective bidentate, tridentate and tetradentate sulfur-containing ligands have also been prepared for the selective extraction of platinum(II) and palladium(II) in the presence of base metals,[98] while highly selective polydentate malonamide ligands have been developed to chelate silver(I) selectively.[99] In both of these studies, the chelating potential of the ligands was explored experimentally and by computer modelling methods. In an extension of this research, bidentate ligands containing amine and pyridyl groups have been developed for use in the formation of metal-selective molecularly-imprinted polymers (MIP's). The resulting MIP's showed clear selectivity for nickel(II) over iron(III).[100]

More recently, attention has been given by Sabbagh[101] to the design and synthesis of camphor-derived tridentate ligands to be used in ruthenium catalyst development. The chelating potential and catalytic possibilities of the targeted ruthenium complexes were assessed by computer modelling methods at the DFT level.

With the above experience in ligand design and synthesis and the clear need for further development of olefin metathesis catalysts as outlined in Sections 1.3.4.1-1.3.4.5, it was decided to extend the studies initiated by Sabbagh.[101] Consequently the present study has been concerned with the development of multidentate ligands for use in the construction of novel metathesis catalysts. More specifically, the aims have included:-

i) design, synthesis and characterisation of novel tridentate ligands, using Kemp's triacid (1,3,5-trimethyl-1,3,5-cyclohexanetricarboxylic acid)- and camphor-based molecular scaffolds;

ii) assessment of the chelating potential of the targeted ligands by calculations at the DFT level, using the Accelrys DMol^3 package; and

iii) application of ^{13}C NMR chemical shift prediction methods to support the assignments of experimental NMR data.

2. DISCUSSION

The discussion that follows gives a detailed account of the work that has been done in an attempt to design and synthesise novel tridentate ligands to be used in the development of metathesis catalysts. The synthesis and characterization of Kemp's triacid- and camphor-based compounds are discussed. The characterization of these compounds has been effected through the use of spectral, computational and x-ray crystallographic methods. Computational methods have also been used as a design tool in assessing the binding ability of the proposed multidentate ligands.

2.1. LIGAND DESIGN AND SYNTHESIS

Grubbs type metathesis catalysts are perhaps the most explored and optimised metathesis catalysts.[31] These explorations have led to commercial derivatives such as the Grubbs-Hoveyda type catalysts.[63] In our research group, detailed DFT theoretical studies on the metathesis mechanism involving Grubbs' catalyst[74] and the structures of ruthenium complexes with camphor-based tridentate ligands have been conducted.[101] In the present study, the intention was to design similar tridentate ligands that could replace the two chlorine and one phosphine ligand in Grubbs first- and second-generation catalysts (**Fig. 8**) to form tethered chelates. Ideally, a strong electron-donating ligand is needed to substitute a phosphine group in Grubbs' first-generation catalyst **4,** while a labile donor group is needed in the Grubbs' second-generation catalyst **12**. Our model is based on the fact that labile ligands readily promote initiation of catalyst **12**.[77] The tethered labile ligand would re-coordinate to the metal after the catalytic cycle and thus increase the chances of catalyst recovery. It is also known that chlorine atoms participate in the decomposition of Ru metathesis catalysts.[89] Thus, the substitution of the chloride ions with a chelating ligand might inhibit decomposition and prolong catalyst life-time. Kemp's triacid **43** and camphor **44** were both explored as ligand precursors in this study.

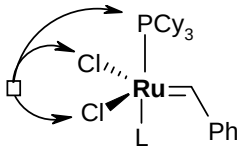

4: L = PCy_3

12: L = H_2IMes

Figure 8. Grubbs' first- and second-generation catalysts. Arrows show the intended chelation centres.

2.1.1. Kemp's triacid derivatives and analogues

Kemp's triacid has attractive characteristics that have been used in designing of chelating molecules, since the *cis*-tricarboxylic acid moieties can easily be modified into useful donor groups using classical transformations.[102] In this study, Kemp's triacid was explored as a precusor for the development of *cis*-tridentate ligands such as compound **45** (**Scheme 22**) which contains O- and N-donor groups. Preliminary assessment of the chelating potential of the target ligands was carried out by modelling the putative complexes, in which secondary and tertiary amines were used as N-donor groups. The DFT optimised geometries of complexes **49** and **50** (**Fig. 9**) show important similarities to typical Grubbs' type catalysts. These include the *trans*-arrangement of phosphine to N-donor ligands and a *cis*-orientation of the alkylidene moiety to the phosphine ligand. However, the angle between the O-donor ligands (135-138^o) deviates from the typical *trans*-orientation of the anionic chloride ligands. No significant difference was observed when the N-donor group was attached to the metal centre by a σ-bond (as in **49**) or when coordinated by lone pair electrons (as in **50; Figure 9**). Schiff base [79] and pyridinium[77] N-donor ligands, which have been used in ruthenium complexation, coordinate to the metal centre *via* the lone pair of electrons.

Trihalogenated analogues, such as compound **48,** were also targeted. Grubbs and co-workers reported that increasing the electron-withdrawing ability of alkoxides in 14-electron ruthenium alkylidene complex increases catalytic activity.[103] However, Krause *et al.* showed that an excessive increase of the electron-withdrawing ability of the ligands in 16-electron ruthenium alkylidene complexes decreases the activity of

the catalyst by reducing electron density around the Ru centre, thus preventing the formation of highly active 14-electron species (**Scheme 18**).[104] The electron-withdrawing ability of fluorinated systems have been assessed in our research group using DFT calculations and experimental data.[101] The findings were consistent with those of Krause *et al*[104] who found that electron-withdrawing ligands, such as fluorinated systems, enhanced the stability of ruthenium complexes.

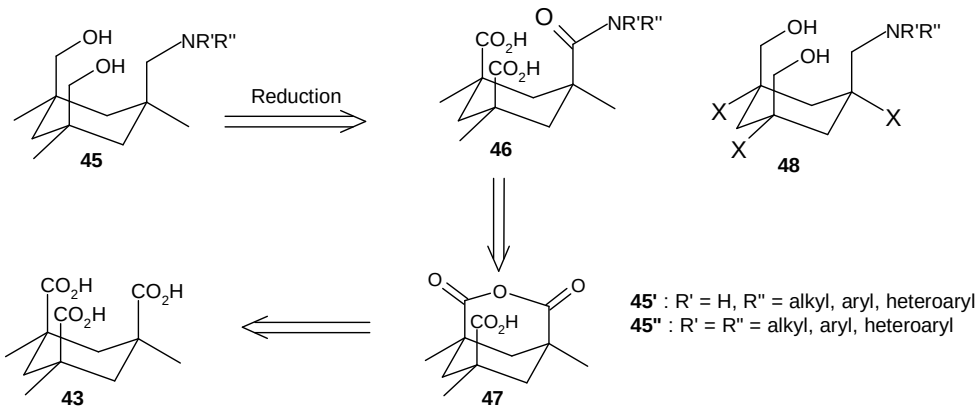

Scheme 22: Retro-synthetic approach to the tridentate ligand **45**

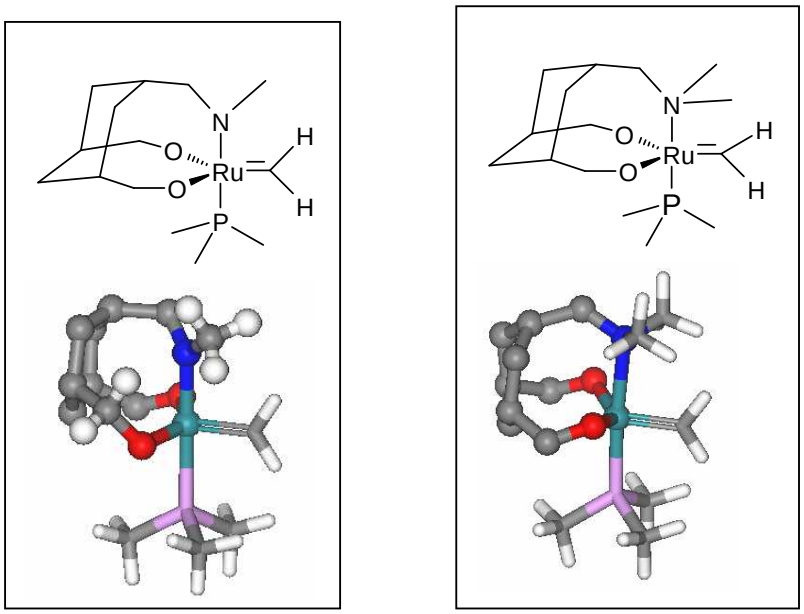

49 **50**

Figure 9. Dmol^3/GGA/PW91/DNP geometry-optimised structures of the putative catalysts **49** and **50** (H's omitted in ligand ring for clarity).

2.1.1.1. *Synthetic Approach*

Our synthetic approach followed Curran's[102] condensation of amines and acid anhydride **47** to form secondary amides**.** Thus, the acid anhydride **47** was prepared in 37% by dehydration of Kemp's tracid **43.** Condensation of anhydride **47** with phenethylamine hydrochloride, however, afforded 1,5,7-trimethyl-2,4-dioxo-3-phenethyl-3-azabicyclo[3.3.1]nonane-7-carboxylic acid **51** instead of the desired product **52** (**Scheme 23**). The ^{1}H NMR spectrum of the imide **51** (**Fig. 10**) shows the presence of only one acidic proton, and there is no secondary amide proton signal. The HMBC spectrum (**Fig. 11**) shows the correlation of the imide C=O groups with the enantiotopic 1- and 5-methyl groups. In the high resolution mass spectrum, a peak at *m/z* 343 corresponds to the molecular ion, which confirms $C_{20}H_{25}O_4N$ as the molecular formula. The formation of imides, such as imide **51**, from condensation of acid anhydrides **47** and amines has been reported previously.[105,106]

Preliminary synthesis of tertiary amides, such as compound **54,** from the acid chloride **53** was explored using Hansen's literature procedure [107] (**Scheme 23**). Thus, acid chloride **53** was synthesised in good yield from the reaction of Kemp's triacid **43** with thionyl chloride. However, when acid chloride **53** was reacted with pyrrolidine in the presence of pyridine using Hansen's procedure, no identifiable product could be isolated. Hansen describes the synthesis of tertiary amides, such as compound **55,** from heterocyclic amines and acid chloride **53** in 11-71% yield[107] (**Scheme 24**).

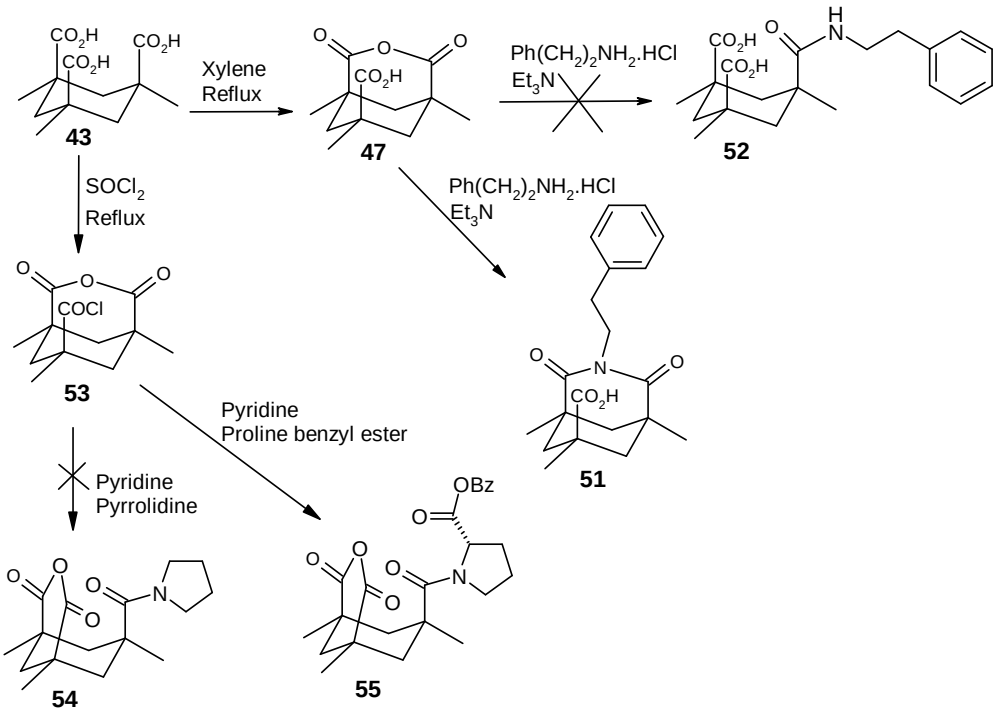

Scheme 23

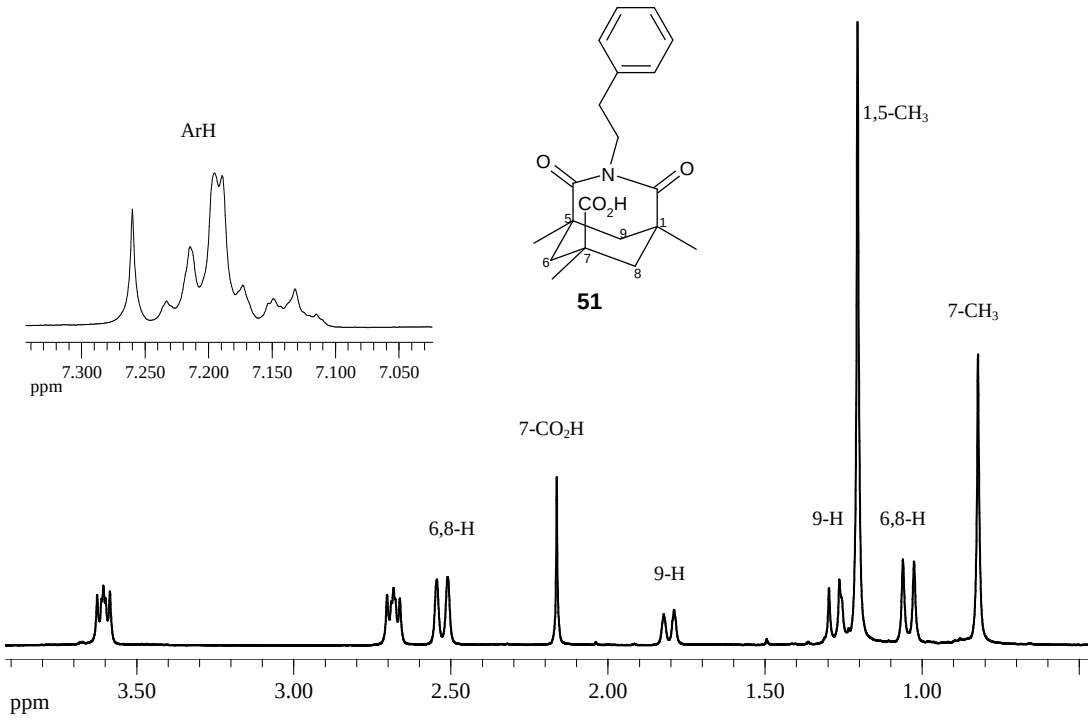

Figure 10. 400MHz ^{1}H NMR spectrum of imide **51** in $CDCl_3$.

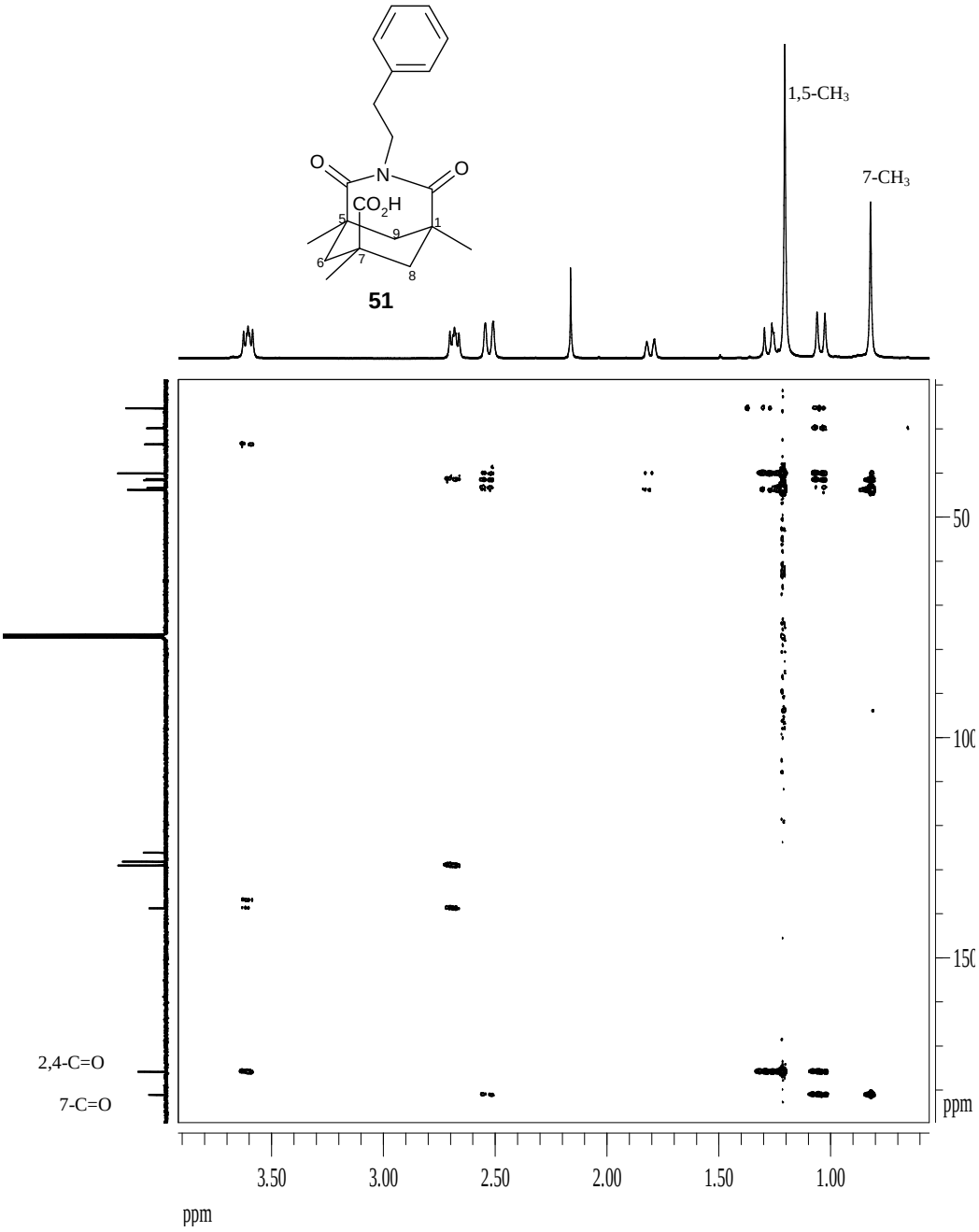

Figure 11. Partial 400MHz HMBC spectrum of imide **51** in $CDCl_3$. The aromatic signals are not shown.

Unfortunately, during the course of this study, Kemp's triacid became unavailable commercially. Consequently, attention was given to the synthesis of Kemp's triacid and halogenated analogues (**Scheme 24**). The triester **57**, a Kemp's triacid precursor, was prepared in 60% yield following a literature procedure,[108] but attempted α-

methylation using dimethyl sulphate and commercial or specially prepared LDA, proved unsuccessful. Attempts to α-halogenate **57** using Selectfluor/NaH or NBS/$Mg(ClO_4)_2$[109] were similarly unsuccessful. However, more promising results were obtained using NBS/NH_4OAc.[110] In this reaction, 40% of the starting material was recovered and trace amounts of trimethyl *r*-1,*c*-3-dibromocyclohexane-1,3,*t*-5-tricarboxylate **58** and monobrominated derivatives tentatively assigned as structures **59** and **60** were obtained by semi-preparative HPLC. No improvement was observed when reaction conditions were altered in an attempt to increase the yield and, ultimately, to access a tribrominated product.

The ^{1}HNMR spectrum of compound **58** shows the presence of one remaining α-H, resonating as a triplet at 2.87 ppm. The COSY NMR spectrum (**Fig. 12**)**,** shows that the remaining α-H is coupled to the enantiotopic 4- and 6-methylene protons with coupling constants of 3.4 and 13.0 Hz reflecting correlation with equatorial and axial protons, respectively. Two C=O signals were found in ^{13}C NMR spectrum and the relative correlations to 1-, 3- and 5-methoxy protons were evident in the HMBC spectrum (**Fig. 13**). However, the 2D NMR data did not clearly establish the orientation of the remaining α-H relative to the carboxylate groups. On the basis of the NMR prediction values, the dibromo analogue **58** was considered to be the most likely isomer. High resolution mass spectroscopy also confirmed $C_{12}H_{16}O_6Br_2$ as the molecular formula of the dibromo compound **58**.

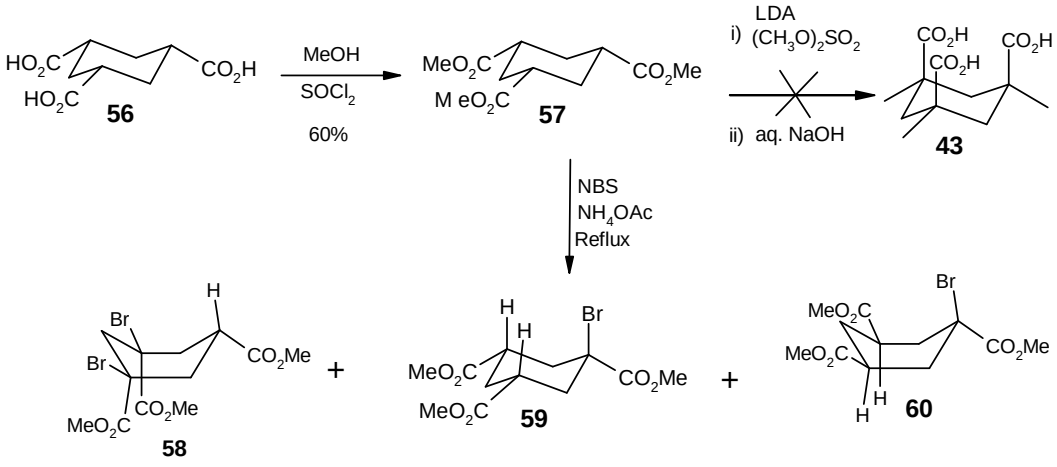

Scheme 24

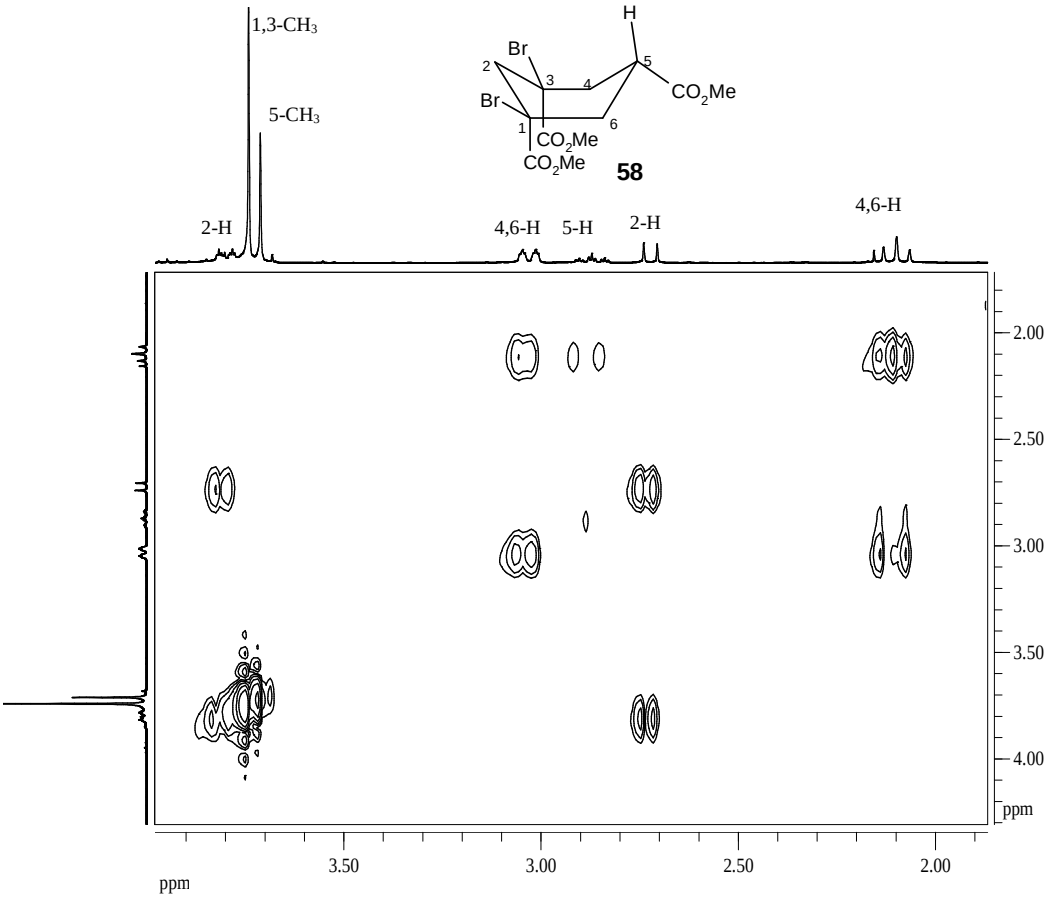

Figure 12. 400MHz COSY spectrum of trimethyl 1,3-dibromocyclohexane-1,3,5-tricarboxylate **58** in $CDCl_3$.

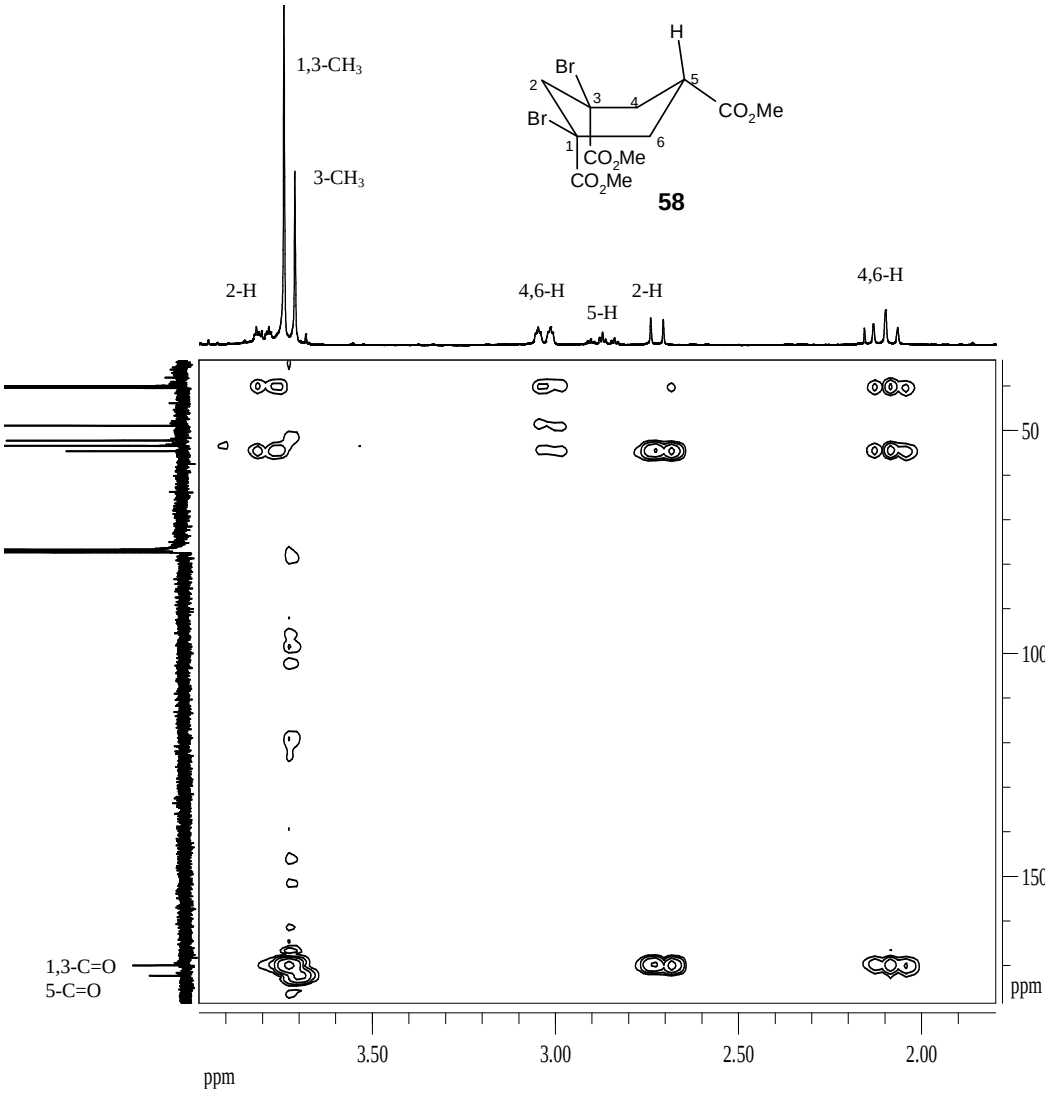

Figure 13. 400MHz HMBC spectrum of trimethyl 1,3-dibromocyclohexane-1,3,5-tricarboxylate **58** in $CDCl_3$.

Besides the dibrominated product, trace amounts of monobrominated products were also isolated by HPLC. Using NMR analysis in a similar manner, as for the dibrominated product **58,** and density functional theory (DFT) calculations, the monobrominated products were tentatively identified as trimethyl *r*-1-bromocyclohexane-1,*t*-3,*t*-5-tricarboxylate **59** and trimethyl *r*-1-bromocyclohexane-1,*c*-3,*c*-5-tricarboxylate **60**. The DFT geometry-optimised structures suggest that different conformations are favoured in compounds **59** and **60**. An integrated ^{1}H NMR spectrum of the crude material shows that the ratio of the two monobrominated products **59**:**60** is *ca.* 1:2. Other features observed in the ^{1}H NMR spectra of compounds **59** and **60** were:

i) the presence of two α-Hs in each spectrum (*i.e.* α to the carboxylate group); and

ii) the fact that the 2- and 6-methylene nuclei are relatively deshielded (δ 2.10 and 3.03 ppm) in compound **59** but relatively shielded (δ 1.80 and 2.65 ppm) in compound **60.**

The presence of two α-Hs in each compound immediately supports the formation of monobrominated products. Moreover, the relative deshielding of the 2- and 6-methylene nuclei in isomer **59** is probably due to the anisotropic effects of the carbonyl groups.[111] This also agrees with the DFT generated structure of compound **59** which places the 2- and 6-methylene groups in the carbonyl plane (**Fig. 14**).

The formation of the monobrominated products may be rationalised by Tanemura's[110] mechanism which, proposes that, during the NBS/NH_4OAc bromination of ketones, free acetic acid can catalyse the formation of an enol that is attacked, in turn, by an electrophile on either side of the double-bond enol plane (**Scheme 25**). In view of the various difficulties encountered with Kemp's triacid approach, attention was focused on use of D-(+)-camphor as a more promising scaffold for the construction of multidentate ligands.

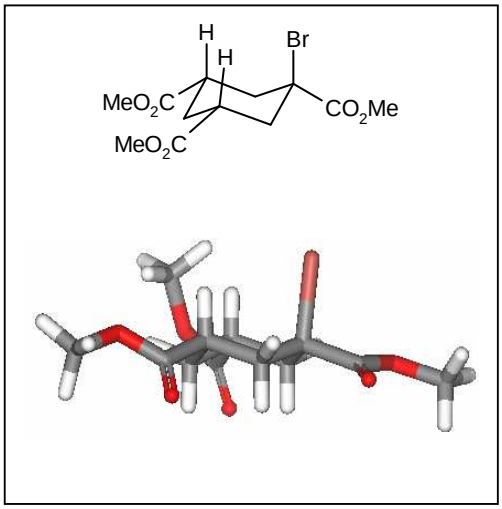

59

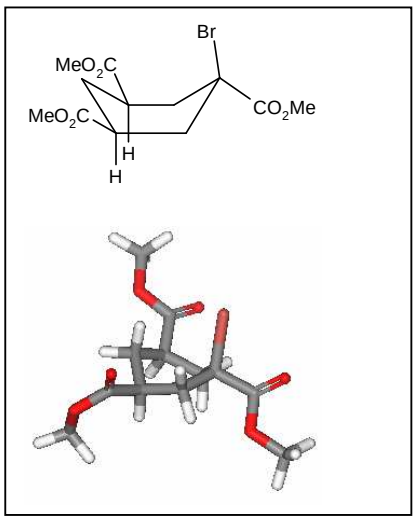

60

Figure 14. DMol^3/GGA/PW91/DNP geometry-optimised structures of the monobrominated products **59** and **60.**

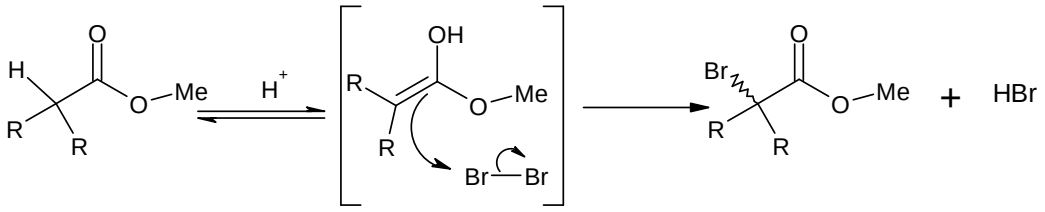

Scheme 25

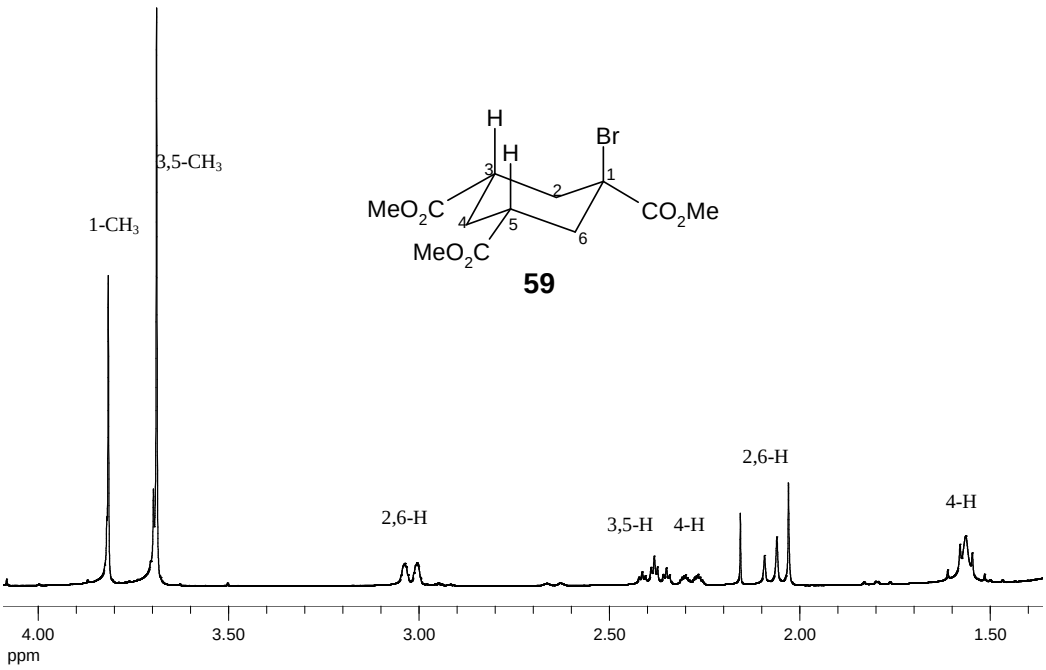

Figure 15. 400MHz ^{1}H NMR spectrum of trimethyl *r*-1-bromocyclohexane-1,*t*-3,*t*-5-tricarboxylate **59** in $CDCl_3$.

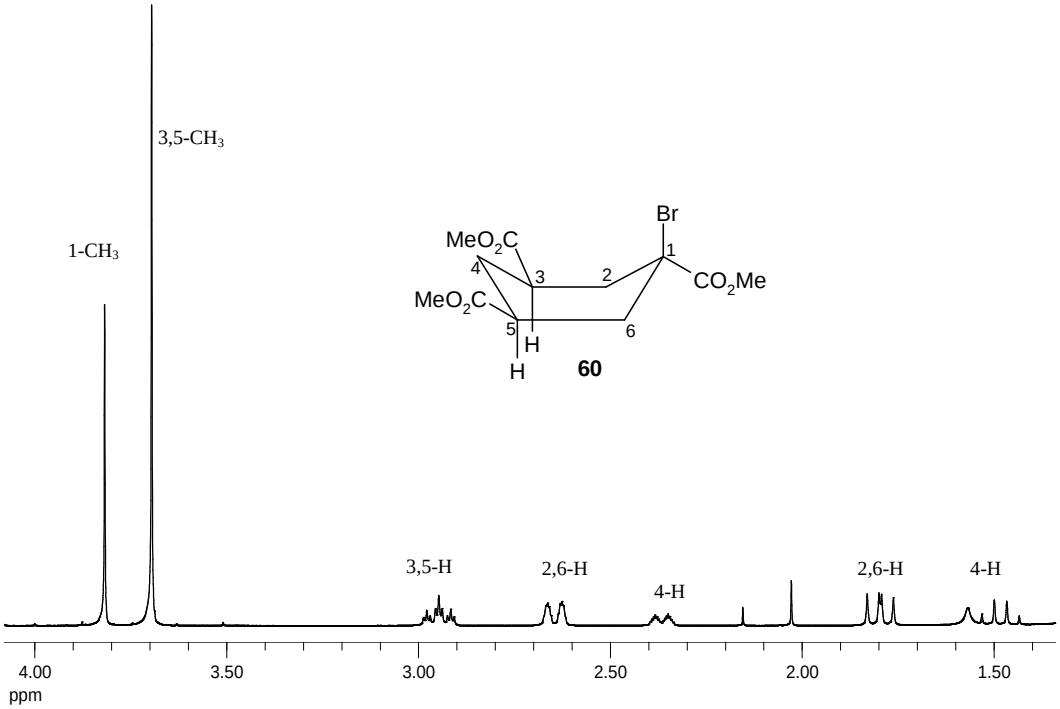

Figure 16. 400MHz ^{1}H NMR spectrum of trimethyl *r*-1-bromocyclohexane-1,*c*-3,*c*-5-tricarboxylate **60** in $CDCl_3$.

2.1.2. Camphor systems as ligand precursors

Camphor systems have been explored as asymmetric ligand precursor by other research groups.[112] The availability of camphor at low cost and its well-studied chemistry make camphor an ideal chiral substrate in asymmetric ligand design. In our laboratories, camphor systems have been explored in asymmetric synthesis. Recently, Sabbagh explored camphor systems in the design of the tridentate phosphine ligand **63**[101] (**Scheme 26**). In Sabbagh's study, however, problems were encountered, the major challenge being cleavage of the C(2)–C(3) bond in intermediate systems. Furthermore, an attempt to replace the 8-bromo substituent with a phosphine group failed. In the present study, the problems encountered by Sabbagh have been addressed and various approaches to camphor-derived tridentate ligands have been explored.

2.1.2.1. *Camphor-derived phosphine ligands*

Various ways that might be used to introduce a phosphine group (*i.e.* dicyclohexylphosphine or diphenylphosphine) at the C-8 position of camphor systems were investigated. The intention was to construct the tridentate ligands **62 - 65** (**Scheme 26**)**.** DFT geometry optimization of a proposed catalyst **66** formed from ligand **64** showed a typical *trans*-orientation of the phosphine ligands (**Fig. 17**). The bond lengths between phosphorous and ruthenium atoms are 2.36 Å for $RPPh_2$ and 2.55 Å for PCy_3. The difference in bond lengths indicates that PCy_3 is likely to disscociate in the catalytic cycle.

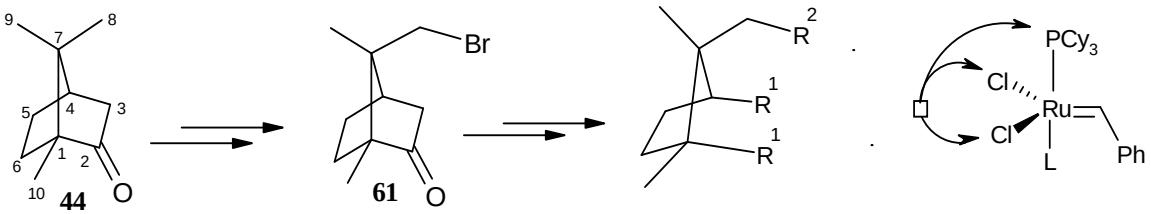

62: R_1 = COOH, R_2 = PPh_2
63: R_1 = COOH, R_2 = PCy_2
64: R_1 = CH_2OH, R_2 = PPh_2
65: R_1 = CH_2OH, R_2 = PCy_2

4: L = PCy_3
12: L = H_2IMes

Scheme 26

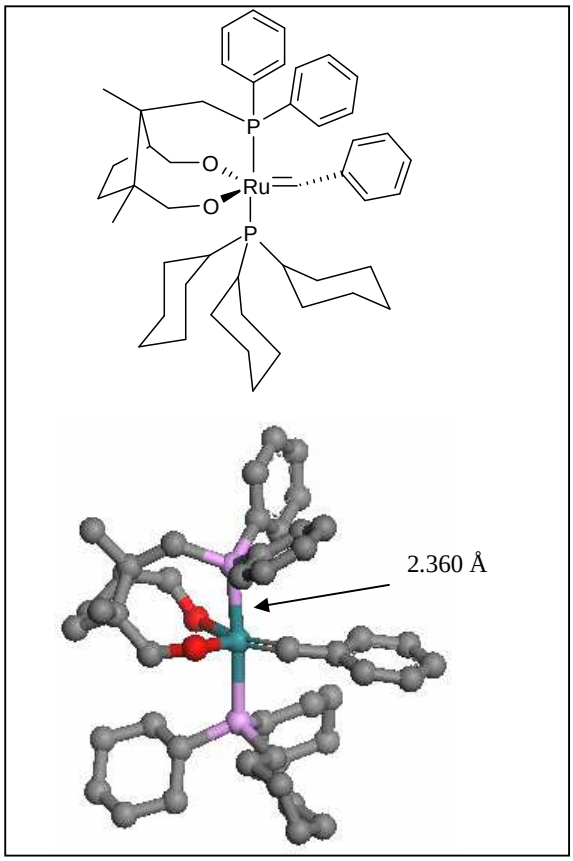

66

Figure 17. DMol^3/GGA/PW91/DNP geometry-optimised structure of the proposed catalyst **66** (H's are omitted for clarity).

2.1.2.1.1. *Synthesis of phosphine ligands*

Camphor derivatives are known to undergo a variety of intramolecular rearrangements in acidic medium.[113] Selective bromination of camphor at C-8 requires pre-functionalisation at C-3 to prevent certain intramolecular conversions that may lead to undesirable by-products.[114] In order to synthesise 8-bromocamphor **61**, Money's[114] literature procedure was followed. Commercial 3-bromocamphor **67** was treated with neat bromine to afford 3,3-dibrocamphor **68** in quantitative yield (**Scheme 27**). 8-Bromocamphor **61** was then synthesized in 38% yield by selective bromination of the intermediate **68** at C-8 position and subsequent Zn-catalysed reduction, permitting displacement of the Br atoms at C-3. Prior to the debromination

step, a sample was chromatographed and resulting fractions were subjected to NMR analysis, which revealed the presence of 3,3,8-tribromocamphor **69**, 3,3,8,10-tetrabromocamphor **70** and (-)-1,7-dibromo-4-dibromomethyl-3,3-dimethylnobornan-2-one **71** in 7:1:5 ratio. Moreover, the debrominated analogue of compound **71**, 3,3,4-trimethyl-1,7-dibromonorbornan-2-one **72** (*ca*. 6%) was formed in the subsequent debromination step. These camphor derivatives have been previously isolated and characterised by Money and co-workers.[113]

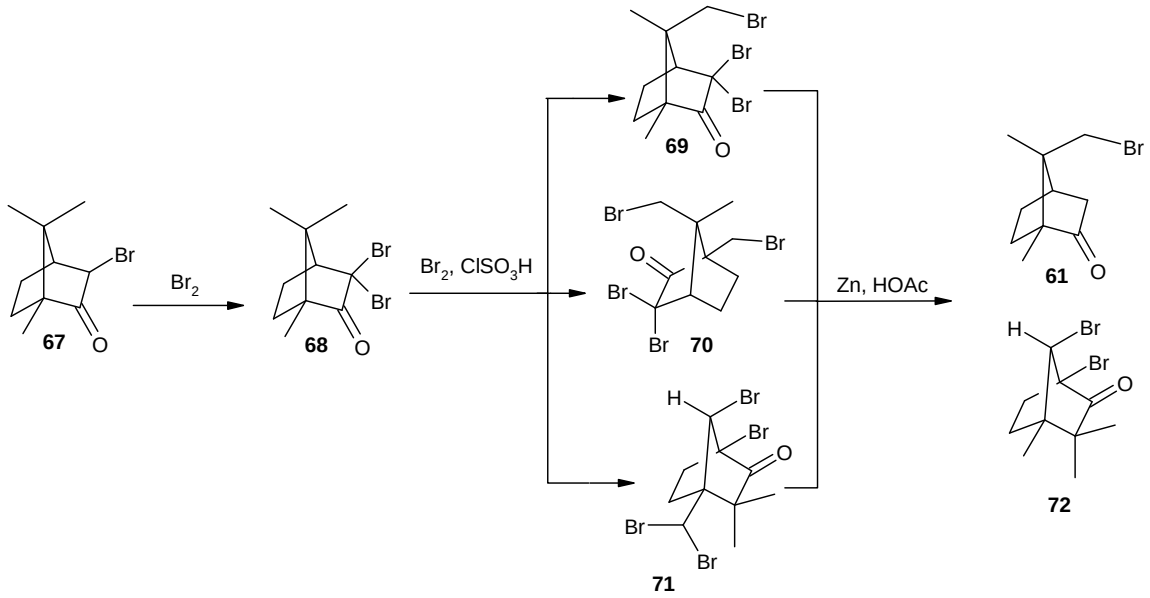

Scheme 27

The formation of brominated camphor derivatives such as compound **69, 70** and **71** has been rationalised by Money[114] in terms of the mechanistic sequence shown in **Scheme 28**. Money's postulate was based on the fact that protonation of camphor initiates a series of intramolecular rearrangements that can lead to a total change of stereochemistry, including the formation of enantiomeric systems. Monobromination of camphor at C-3 allows a 2,3-*exo*-methyl shift which leads to the formation of 9-brominated products (**76a**→**79**). However, the dibromination of camphor at C-3 *via* a 2,3-*endo*-methyl shift to the 8-brominated camphor derivative **69**. Money suggested that the bulky nature of bromine group at the 7-*syn* position (R^1) of carbocation **76b**,

exerts steric hindrance to *exo*-3,2-methyl shifts.[114] On the other hand, Antkowiak and Antkowiak [113] suggested that the *endo*-3,2-methyl shift is facilitated by anchimeric assistance by the 7-*syn*-bromine of **76b**. Computational results obtained in our research group suggest that both steric and anchimeric factors facilitate the otherwise unfavourable *endo*-3,2-methyl shift.[101] Moreover, torsional effects on the camphor framework were considered to be an additional factor facilitating the *endo*-3,2-methyl shift. Further bromination of intermediates **76b** and **80** leads to the formation of 3,3,8,10-tetrabromocamphor **70** and (-)-1,7-dibromo-4-dibromomethyl-3,3-dimethyl-norbornan-2-one **71** respectively.[113]

In order to facilitate the opening of the bond between C-2 and C-3 of the camphor skeleton and thus access the targeted ligand systems, 8-bromocamphor **61** was oxidised with selenium dioxide to form 8-bromocamphorquinone **88** in 83% yield (**Scheme 29**). 8-Bromocamphorquinone was first isolated as a bromination by-product by Antkowiak and Antkowiak,[113] and its synthesis *via* selenium dioxide oxidation was mentioned by the same authors but no procedure was given. The procedure used in this study was adapted from the one reported for the oxidation of 9-bromocamphor.[115] The displacement of Br by a phosphine group was not performed at this stage because the carbonyl groups in compound **88** are susceptible to phosphine attack.[112] In order to facilitate subsequent introduction of a phosphine moiety at C-8, the bromide was replaced by the better leaving group, iodide, to give 8-iodocamphorquinone **89** in 27% yield following treatment of 8-bromocamphorquinone **88** with potassium iodide in DMF (**Scheme 29**). Spectroscopic analysis permitted the characterisation of the iodo-derivative **89;** the presence of only two methyl signals in the ^{1}H NMR spectrum indicates the retention of a halogen substituent at C-8. As expected, the introduction of the less electronegative iodine resulted in shielding of the diastereotopic 8-methylene protons and of the C-8 nucleus itself. Thus, the ^{13}C NMR spectrum (**Fig. 18**) shows the signal for the 8-iodomethylene carbon resonating at 11.9 ppm whereas C-8 in 8-bromocamphorquinone resonates at 38.0 ppm; the HSQC and HMBC spectra were used to assign the signal for the 8-iodomethylene group. The HMBC spectrum showed a strong correlation of between C-8 and the quaternary carbon C-7. This evidence, together with the MS data, confirmed the formation of the iodo product **89**.

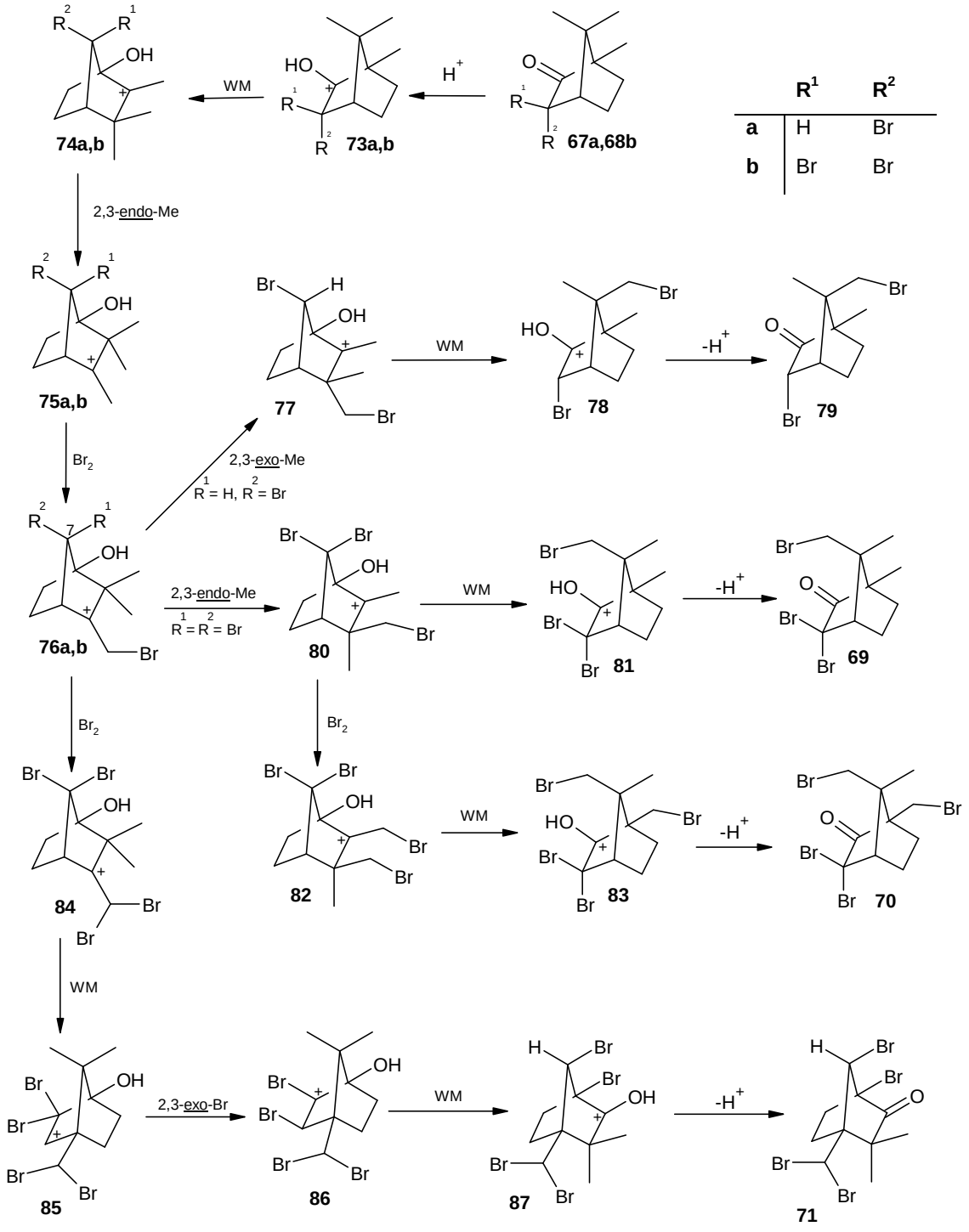

	R^1	R^2
a	H	Br
b	Br	Br

Scheme 28. The mechanistic sequence postulated by Money,[114] where WM = Wagner-Merwein, 2,3-*endo*-Me/Br = 2,3-*endo* methyl/bromo shift, 2,3-*exo*-Me/Br = 2,3-*exo* methyl/bromo shift.

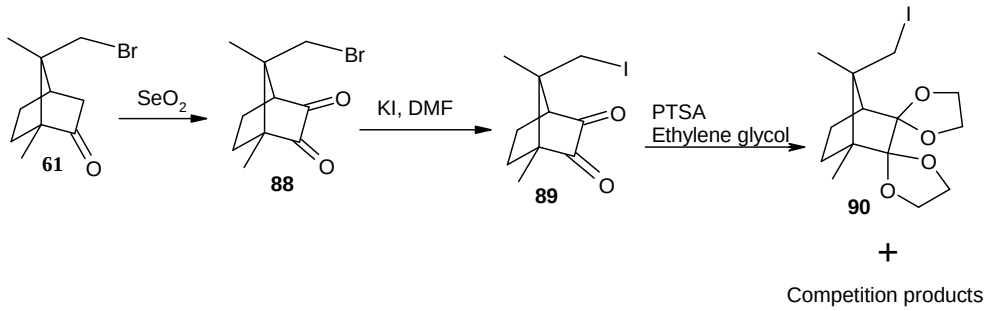

Scheme 29

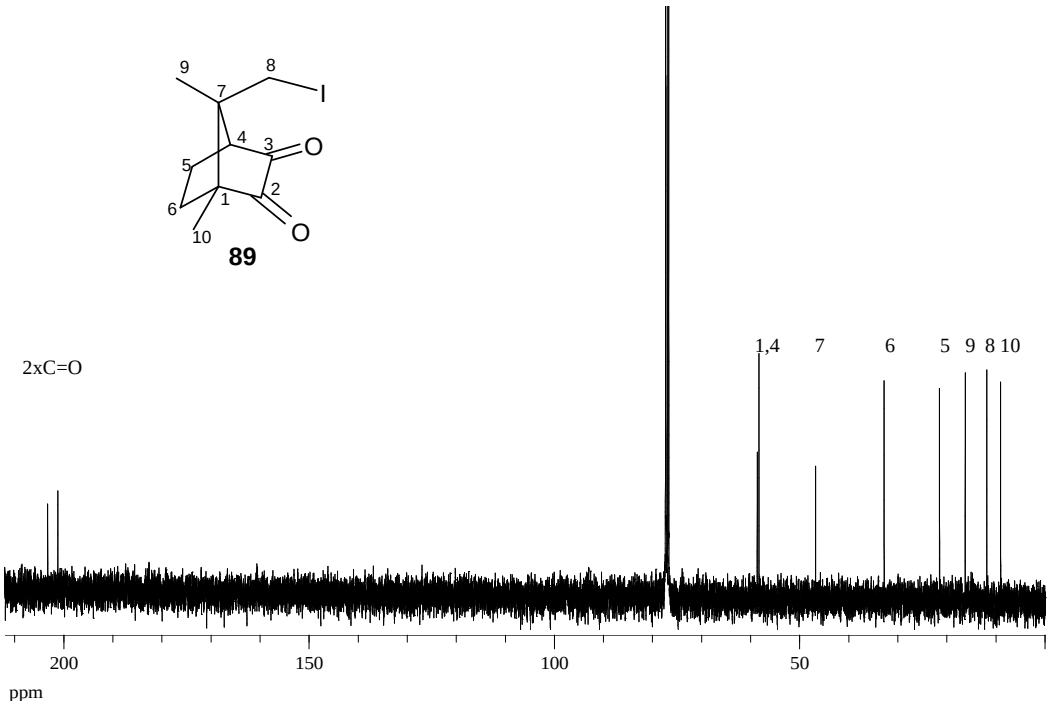

Figure 18. 100MHz ^{13}C NMR spectrum of 8-iodocamphorquinone **89** in $CDCl_3$.

Before attempting the introduction of a phosphine moiety into the 8-iodo diketone **89**, the carbonyl groups were protected by ketalisation using ethylene glycol in acidic medium following a procedure described by Komarov and co-workers (**Scheme 29**).[112] Spectroscopic analysis of the crude material recovered after the reaction indicated the presence of a mixture of compounds. Chromatographic separation and subsequent spectroscopic analysis permitted the isolation and characterisation of five different ketal products from the mixture. 8-Iodocamphorquinone bis(ethylene ketal) **90,** the desired product, was isolated from the mixture in 24% yield. The ^{1}H NMR spectrum (**Fig. 19**) shows the presence of two ketal groups resonating as overlapping

multiplets at *ca.* 4.0 ppm as well as remarkable chemical shift difference (*ca.* 1.2 ppm) between the diastereotopic 8-methylene protons – an observation which indicates that these nuclei experience significantly different magnetic environments. The ^{13}C and DEPT 135 NMR spectra reveal the presence of four secondary carbon signals at *ca*. 65 ppm, and these were assigned to the ketal groups. The ^{13}C NMR spectrum also shows the presence of two signals at 133.0 and 133.5 ppm that were assigned to C-3 and C-2 respectively; the assignment of these signals was facilitated by the HMBC spectrum (**Fig. 21**) which reveals a correlation between the 10-methyl protons and C-2 and between the 4-methine proton and C-3. Finally, single crystal x-ray analysis clearly confirmed the structure (**Fig. 20**) as the one indicated by the NMR analysis. Interestingly, the x-ray crystal structure reveals particular orientation of the 8-methylene hydrogens relative to the ketal groups. If a similar conformation is adopted in solution in $CDCl_3$, this could account for the significant chemical shift difference observed for these protons. Thus, the hydrogen pointing towards the ketal groups would be deshielded by the electronegative oxygens while the one pointing away would be shielded by the 9- and 10-methyl groups.

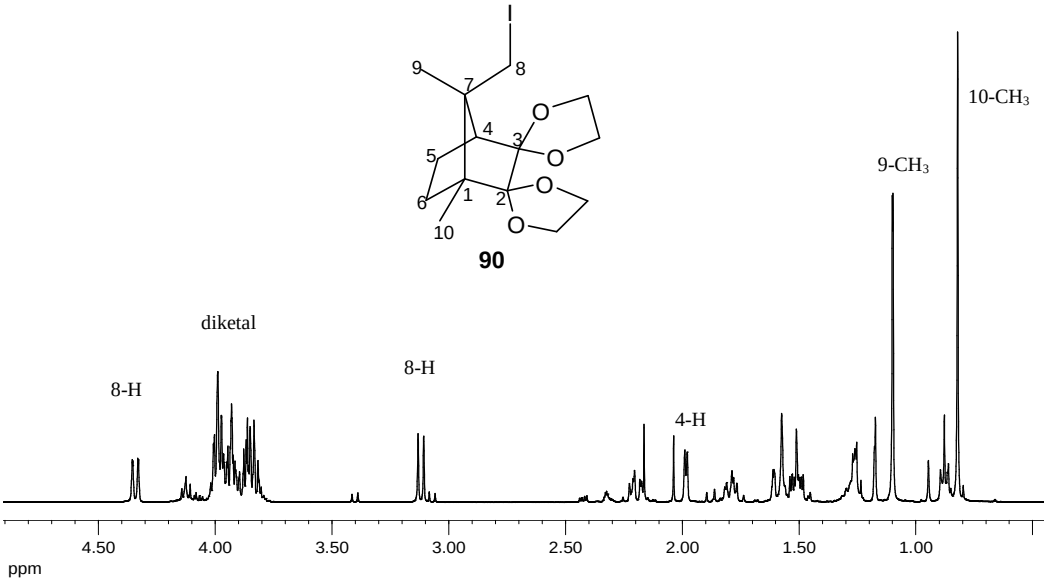

Figure 19. 400MHz ^1H NMR spectrum of 8-iodocamphorquinone bis[ethylene ketal] **90** in $CDCl_3$.

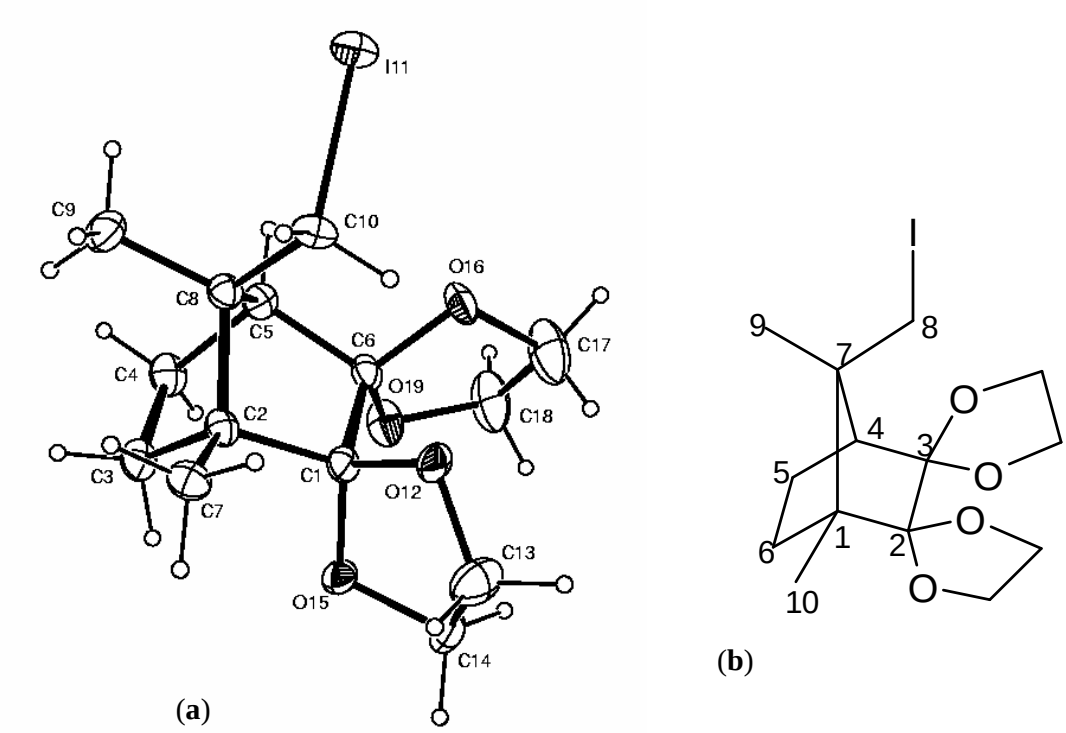

Figure 20. a) X-ray crystal structure of 8-iodocamphorquinone bis(ethylene ketal) **90**, showing the crystallographic numbering and **b**) the corresponding wire-frame structure showing the systematic numbering.

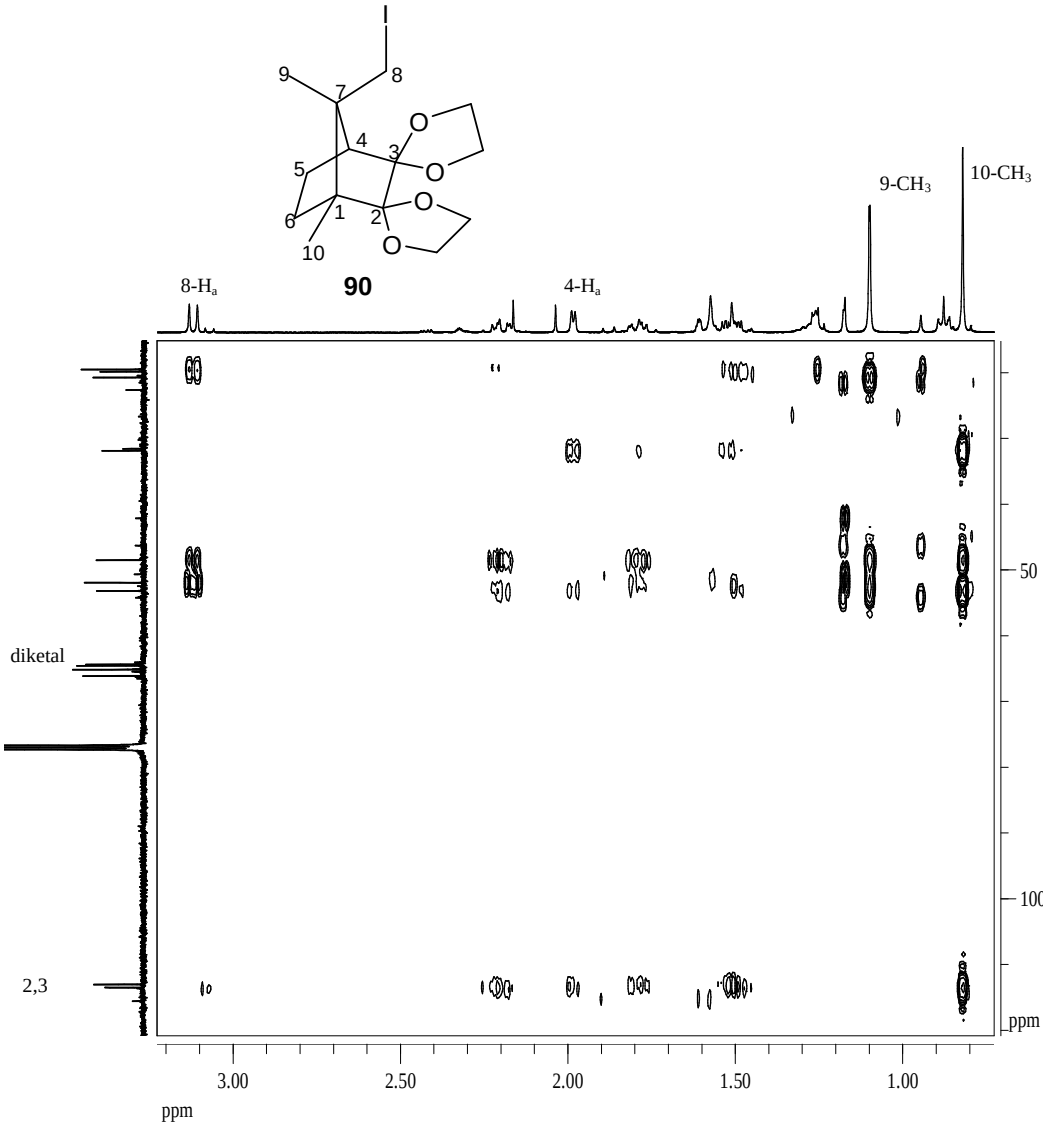

Figure 21. Partial 400MHz HMBC spectrum of 8-iodocamphorquinone bis[ethylene ketal] **90** in $CDCl_3$ (signals for the ketal nuclei and 8-H_b are not shown).

NMR analysis of one of the four remaining ketal products indicated the presence of an isomeric diketal isomer of compound **90**. The most obvious difference between the two isomers was the shifting of the diastereotopic 8-methylene proton signals relative to those of compound **90**. In ^{1}H NMR spectrum of diketal **90**, these protons resonate as doublets at 3.13 and 4.33 ppm (**Fig. 19**), while the corresponding protons in the isomer resonate at 3.42 and 3.92 ppm (**Fig. 22**). Apart from the chemical shift patterns of 8-iodomethylene protons, no major differences in the NMR spectra could be used to differentiate the structures of the isomers.

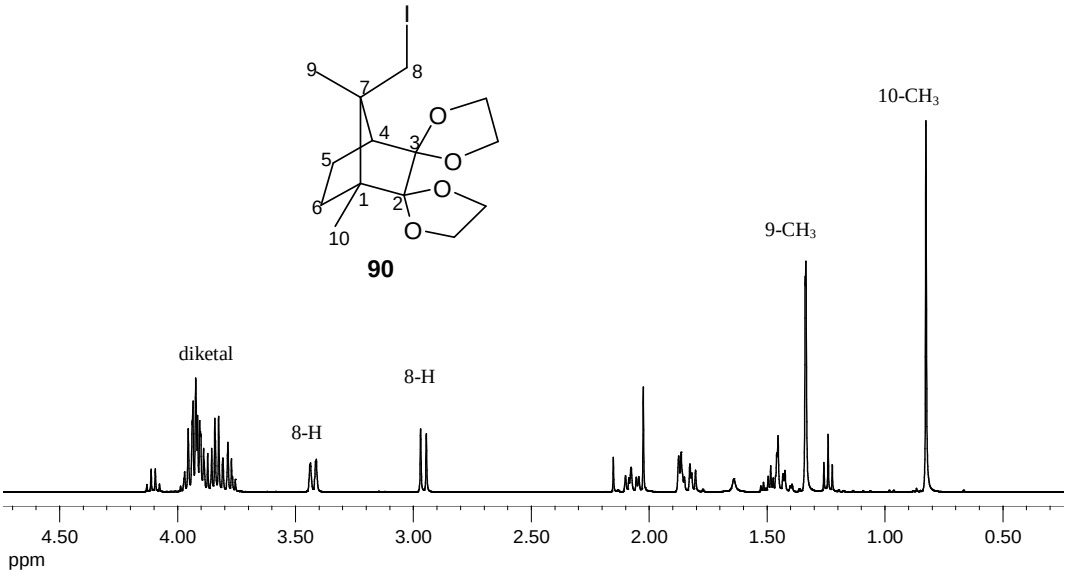

Figure 22. 400MHz ^{1}H NMR spectrum of the diketal isomer of compound **90** in $CDCl_3$.

Based on the mechanistic considerations, the isomeric diketal was initially thought to have a structure **91** (**Scheme 30**). The rationale was that either diketal could, in principle, be formed from the diketone **89** (**Scheme 30**). However, single crystal x-ray analysis unambiguously showed that the isomer was, in fact, 9-iodocamphorquinone bis(ethylene ketal) **92** (**Fig. 23**).

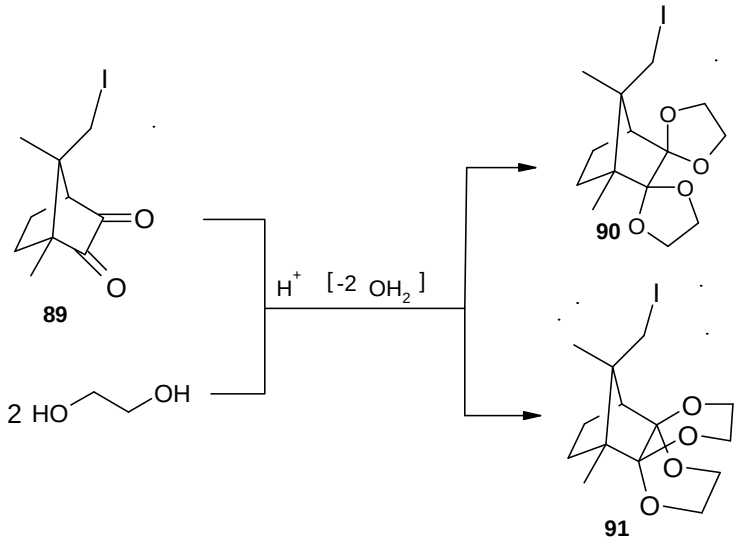

Scheme 30

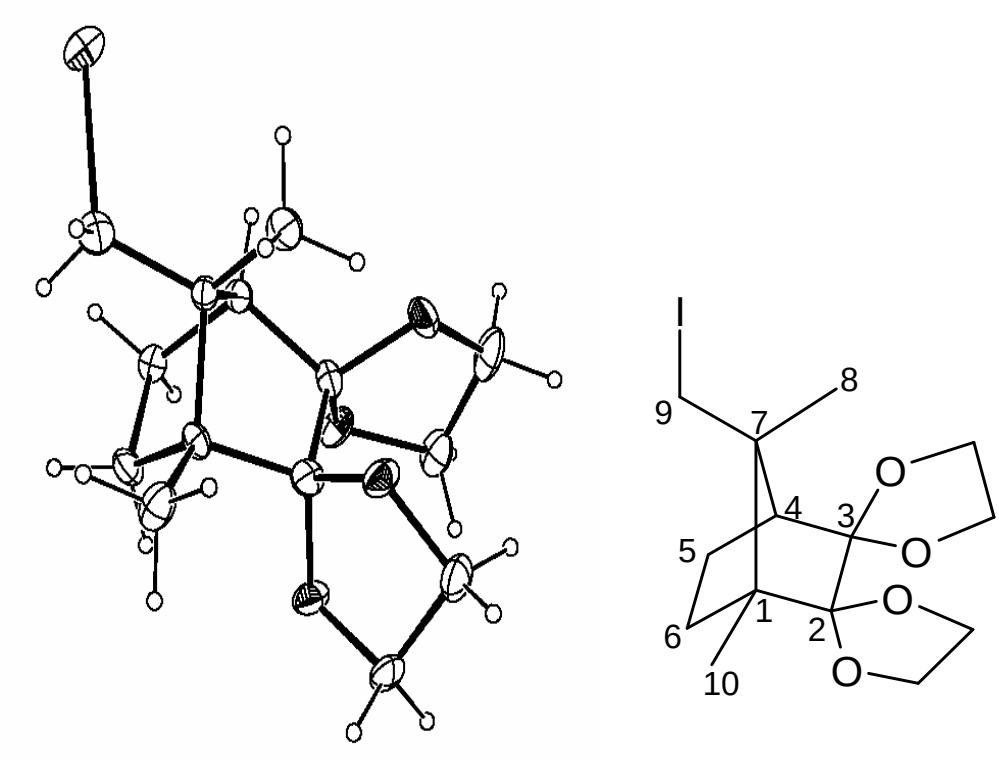

(a) **(b)**

Figure 23. a) X-ray crystal structure of 9-iodocamphorquinone ethylene diketal **92** and **b**) the corresponding wire-frame structure showing systematic numbering.

Our first hypothesis in attempting to explain the presence of the 9-iodomethyl diketal **92** was that its formation was, perhaps, due to a small quantity of 9-iodo-camphorquinone **93** present in the starting material. It was thought that the 9-iodo isomer **92** could have originated *via* compound **93**, following the sequence outlined in **Scheme 31**, from compound **79**, which might have formed during bromination of 3-bromocamphor **67** (see **Scheme 27** and **28**). Consequently, thorough purification steps were carried out using HPLC to obtain a pure starting material **89** to repeat the reaction. ^{1}H NMR analysis of the crude material collected after the repeated reaction showed similar results as the previous reaction *i.e.* both diketal isomers **90** and **92** were present (**Figs. 24** and **25**). The ^{1}H NMR spectrum of the pure starting material obtained after purification step is shown in **Fig. 25a** while **Fig. 25b** shows the ^{1}H NMR spectrum of the crude material obtained after the ketalization of pure diketone

89. The 9-iodo diketal **92** was clearly produced during the ketalization step (**Scheme 30** and **31**), and the first hypothesis was eliminated.

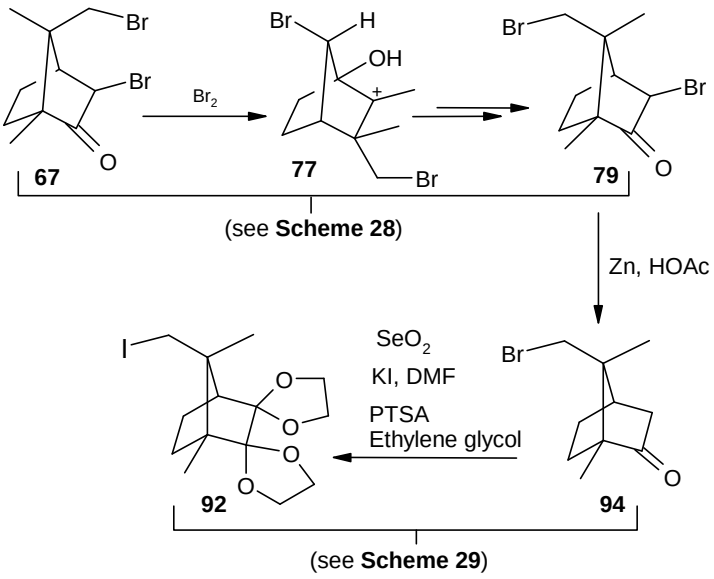

Scheme 31

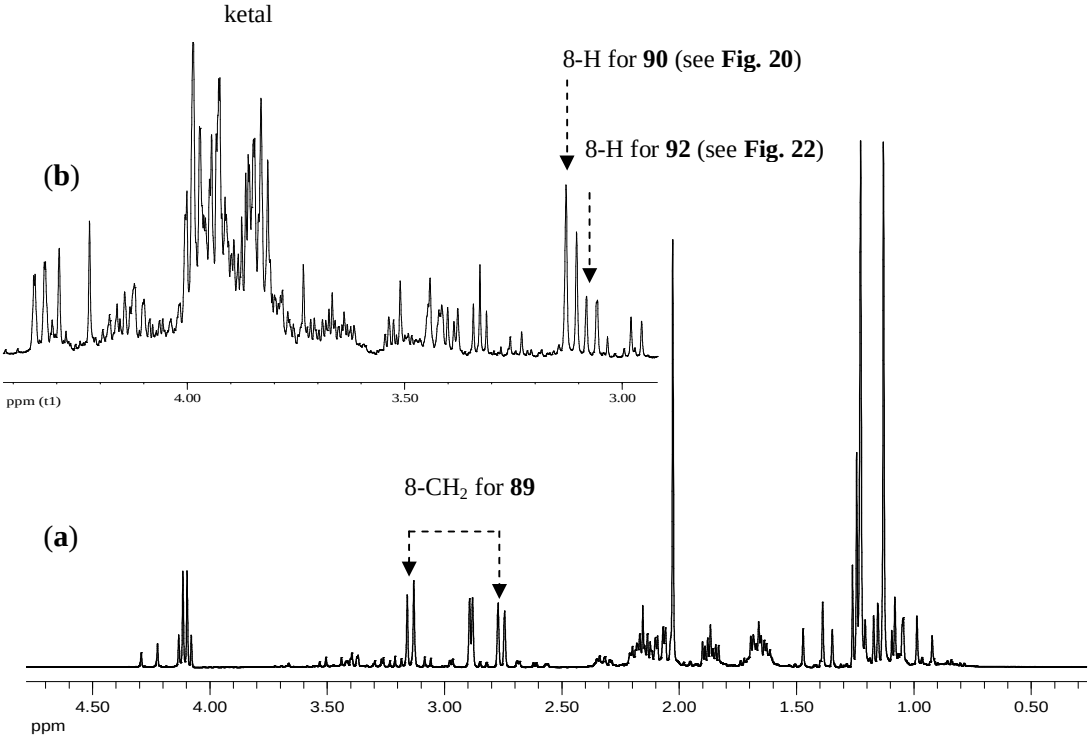

Figure 24. 400MHz ^{1}H NMR spectra of **a**) crude diketone **89** used for the initial ketalization and **b**) crude product containing diketals **90** and **92**, in $CDCl_3$.

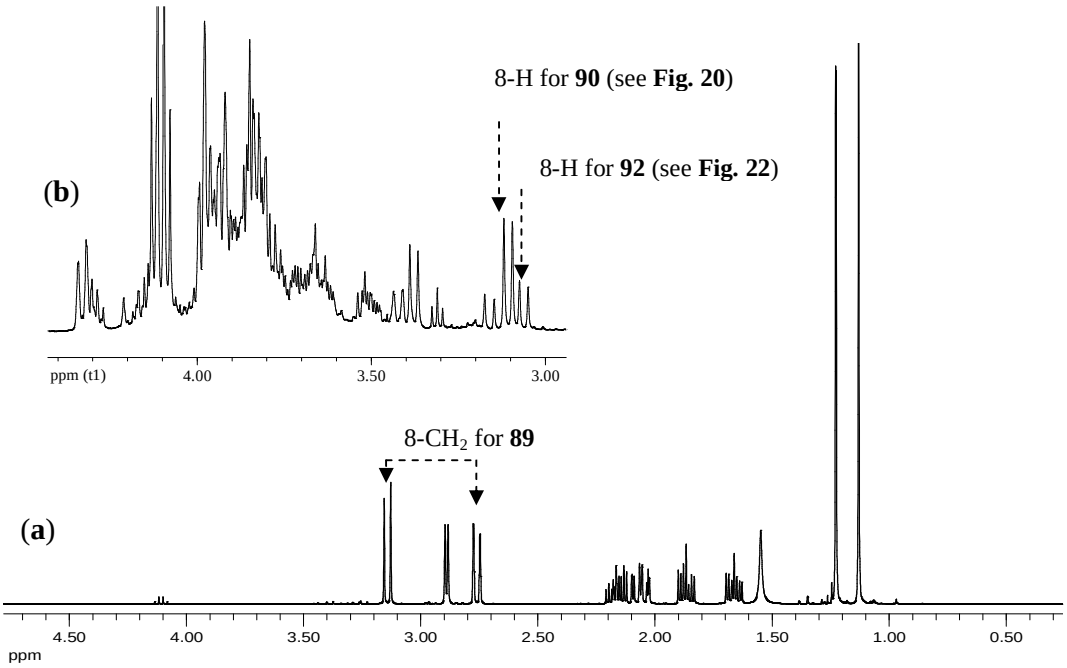

Figure 25. 400MHz ^{1}H NMR spectra of **a**) purified substrate, the diketone **89** and **b**) crude product containing diketals **90** and **92**, in $CDCl_3$.

The second hypothesis was that diketal **92** is produced during the acid-catalysed ketalization of 8-iodocamphorquinone **89**. It was thought that protonation of the substrate **89** would afford the cation **95** which could then rearranges to the 9-iodocamphorquinone cation **96,** following the intramolecular rearrangement sequence shown in **Scheme 28**. Possible pathways involved in such rearrangements have been determined using a fine-tuned version[116] of Jonson and Collins'[117] coset analysis. The coset analysis used is a computer assisted technique which determines all possible pathways between a given substituted bicyclo[2.2.1]heptyl cation and a designated isomeric norbonyl cation *via* common unimolecular rearrangements ("generator permutations"). The intermediate cations formed by a sequence of rearrangements are mapped into coset graphs which provide alternative pathways to isomeric norbonyl cation. The sequence of rearrangements from cation **95** to cation **96** was searched within a limit of 13 rearrangement steps, and two pathways were generated by the following "permutation operators":- Wagner-Meerwein rearrangements (WM), 2,3-

exo-methyl (23x), 2,3-*endo*-methyl (23e) and 6,2-hydride (62) shifts (**Scheme 32)**. The shortest pathway is detailed in **Scheme 33.**

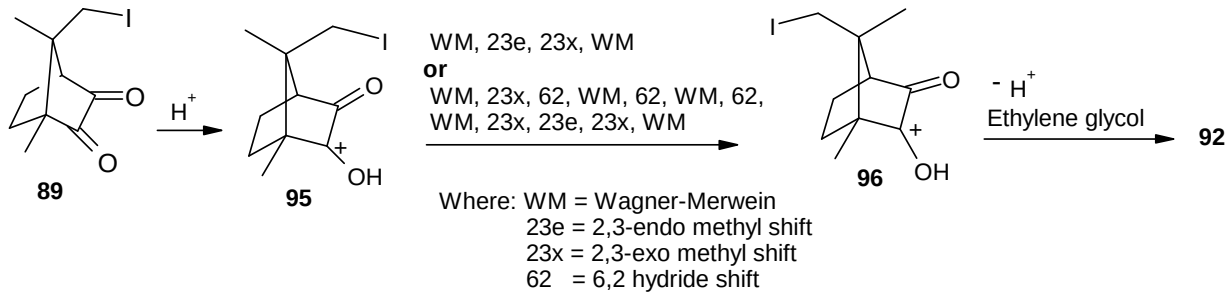

Scheme 32.

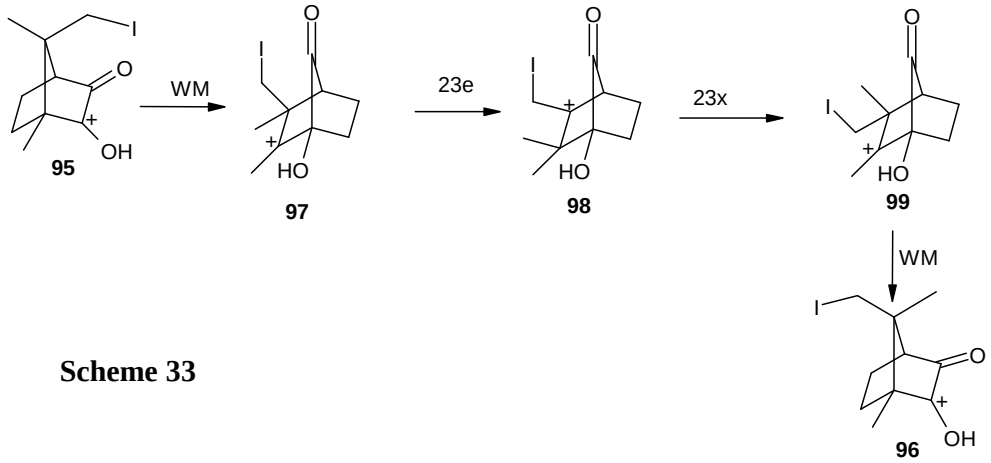

Scheme 33

The shorter pathway, depicted in **Scheme 33**, involves rearrangements commonly observed in norbornane systems. The longer pathway, however, involves unusual steps such as 6,2-hydride shifts. No conclusive results were obtained when the C-3 protonated analogue of cation **95** was used in the coset analysis. We therefore suggest that the 9-iodo diketal **92** forms as a ketalisation by-product *via* the shorter mechanistic sequence detailed in **Scheme 33**.

In addition to the diketals **90** and **91** discussed above, two monoketals were also isolated and characterised as 2,2-(ethylenedioxy)-8-iodocamphorquinone **100** and 3,3-(ethylenedioxy)-8-iodocamphorquinone **101** (**Fig. 25**). The ^{1}H NMR spectrum of monoketal **100** showed overlapping multiplets at 4.16 ppm integrating for four protons and corresponding to the ketal methylene groups, while the 4-methine proton resonates as a doublet at 2.23 ppm due to coupling with the equatorial 5-methylene nucleus. The ^{13}C NMR signal at 215.9 ppm was assigned to C-3 based on the

correlation with the 10-methyl and 4-methine protons illustrated in the HMBC spectrum (**Fig. 26**). The second monoketal **101** to be isolated was characterised similarly, the significant up-field shift of the 9-methyl signal (compared to the isomeric monoketal **100**) is attributed to the effect of ethylene ketal (**Fig. 27**). The same trend is observed on diketal **90**, the methyl signals are relatively shielded (0.82 and 1.10 ppm for 10- and 9-methyl, respectively) (**Fig. 19**) compared to corresponding protons in the diketone substrate **89** (1.13 and 1.23 ppm for 10- and 9-methyl, respectively). Trace amounts of the camphor ethylene diketal **102** were also isolated and characterised by NMR analysis. The diketal **102** has been previously synthesized in 68% yield in our research group following the carbonyl protection procedure described above.[118]

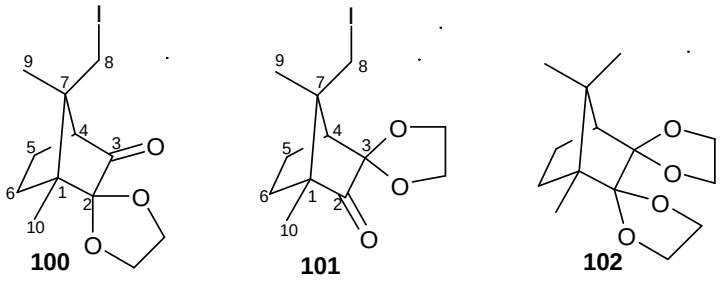

Figure 25.

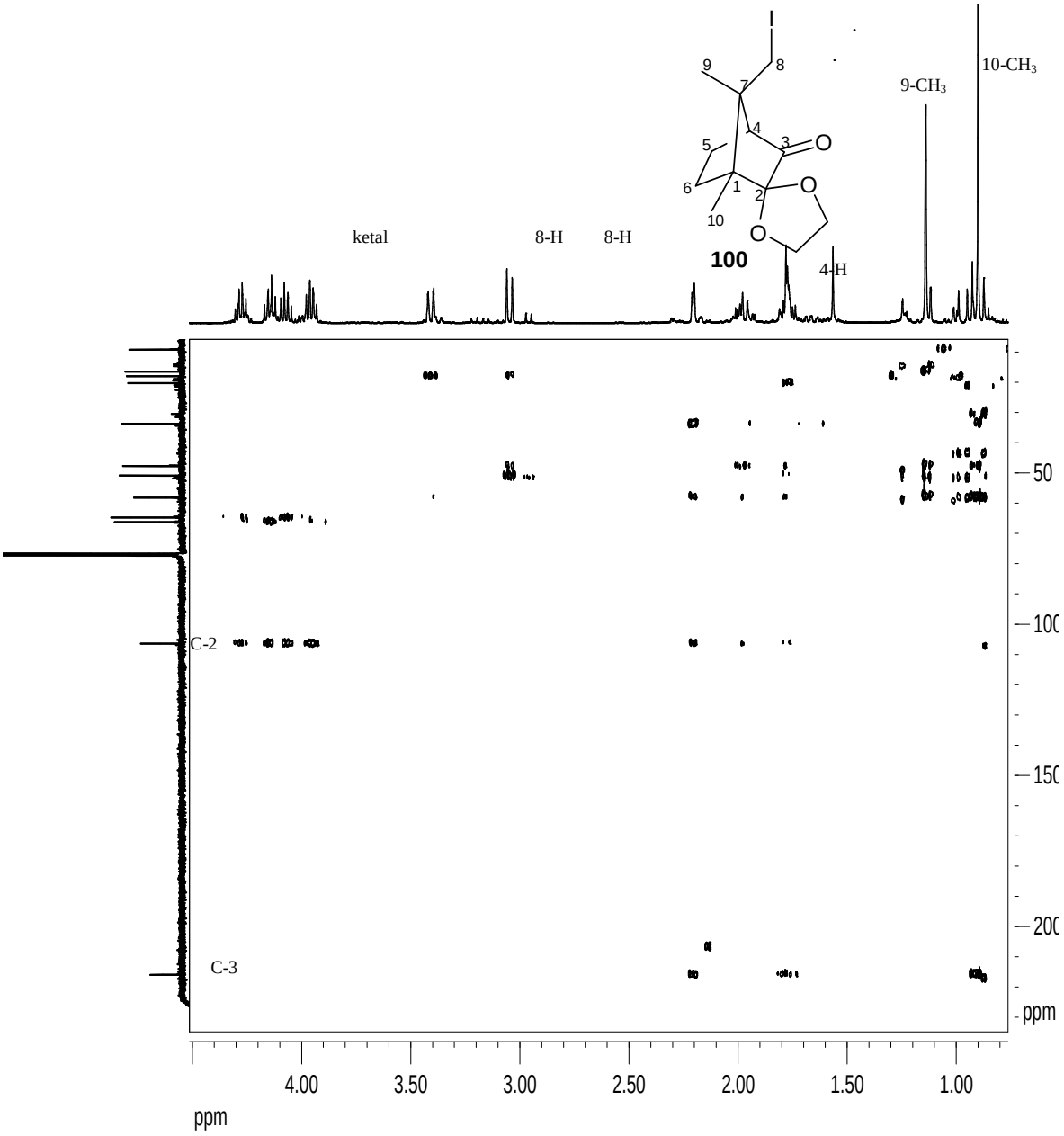

Figure 26. 400MHz HMBC spectrum of monoketal **100** in $CDCl_3$.

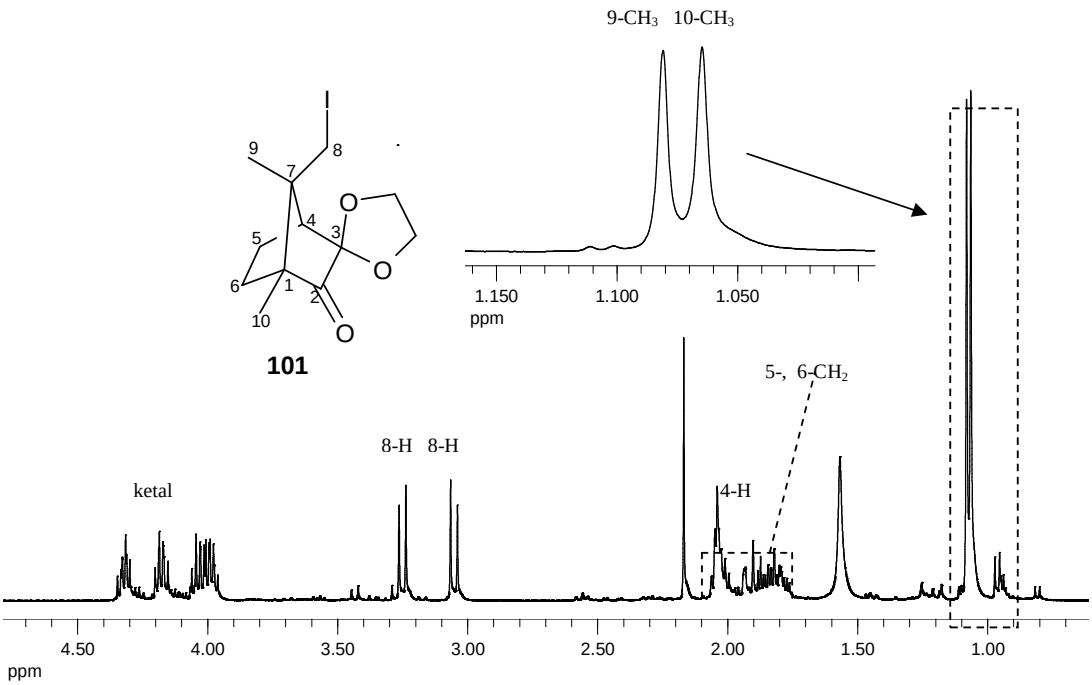

Figure 27. 400MHz ^{1}H NMR spectrum of monoketal **101** in $CDCl_3$.

In an attempt to replace the iodide with a phosphine group, 8-iodocamphorquinone bis(ethylene ketal) **90** was treated with specially prepared lithium dicyclohexylphosphine following a literature procedure developed for diphenylphosphine substitution.[119] From the ^{1}H NMR spectrum isolated after work-up, it was apparent that the desired product had not been formed since the cyclohexyl proton signals were not present.

Since ketalisation of both carbonyl groups in 8-iodocamphorquinone **89** leads to multiple products and a low yield of the desired diketal **90** (see page 20), phosphinated camphor analogues were approached *via* 8-bromocamphor ethylene ketal **103** (**Scheme 34**). Following a literature procedure,[119,120] a solution of 8-bromocamphor **61,** ethylene glycol and PTSA in benzene was boiled for 5 days to give the ketal **103** in 46% yield, while treatment of 8-bromocamphor **61** with ethylene glycol in the presence of TMSCl for 7 hours at room temperature afforded the same product in 40% yield. The monoketal **103** was first synthesised by Money and co-workers to facilitate displacement of bromide in 8-bromocamphor **61**.[120] In our study, displacement of bromide by diphenylphosphine proceeded smoothly to form the

diphenylphosphine analogue **104**, which was further oxidised to afford 8-(diphenylphosphinoyl)camphor ethylene ketal **105** in 70% yield. The oxidation of the monoketal **104** was conducted to facilitate separation. Hydrolytic deprotection of the carbonyl group in the phosphinoxide **105** yielded 8-(diphenylphosphinoyl)camphor **106** in quantitative yield. All of the diphenylphosphine compounds (**104-106)** discussed above had been previously synthesised by Komarov and co-workers[119] in excellent yields, but our attempt to displace bromide in compound **103** with dicyclohexylphosphine, following the same approach was unsuccessful (**Scheme 34**).

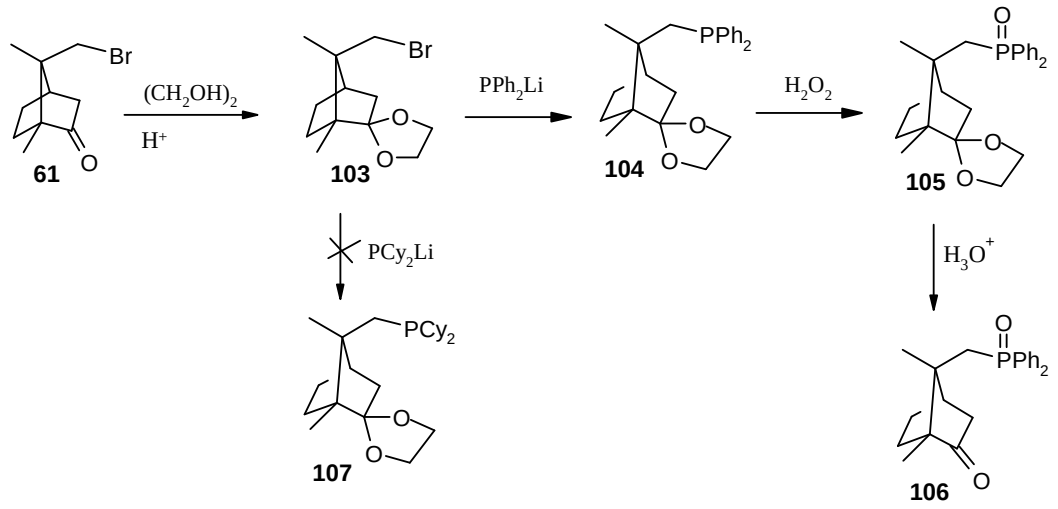

Scheme 34

In order to facilitate ring-opening of the phosphine oxide **106**, 8-(diphenylphosphinoyl)camphorquinone **108** was synthesised in 41% yield by oxidation of the monoketone **106** with selenium dioxide (**Scheme 35**), following a literature procedure developed for the synthesis of 9-bromocamphorquinone.[115] Infrared analysis of the diketone **108** revealed the presence of only one C=O stretching band at 1753 cm^{-1} presumably due to overlap of the C=O bands. However, assignment of the structure of the novel diketone **108** was achieved based on 1- and 2D-NMR and MS data.

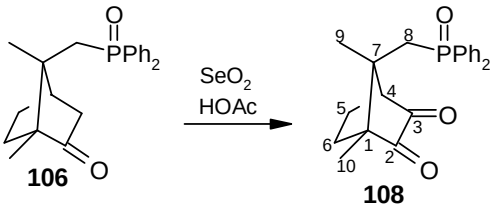

Scheme 35

Thus, the presence of the diastereotopic 8-methylene protons in ^{1}H NMR spectrum of compound **108** (**Fig. 28**) was supported by the signals at 1.6 and 2.4 ppm. The 4-methine proton is deshielded by the adjacent C=O group at C-3 and resonates as a doublet at *ca.* 2.9 ppm due to coupling with the equatorial 5-methylene proton. In the ^{13}C NMR spectrum (**Fig. 29**) relative magnitude of the $J_{P\text{-}C}$ coupling constants were used to assign the signals corresponding to carbons 1, 7, 8, and 9. For instance, $J_{P\text{-}C(8)}$ (69.4 Hz) is *ca.* 6 times larger than $J_{P\text{-}C(7)}$ (11.7 Hz), while the three bond $J_{P\text{-}C}$ couplings for C-1 and C-9 are comparable (4.1 and 2.3 Hz, respectively). These signal assignment were supported by HMQC and HMBC NMR data, while the two carbonyl carbon signals in the ^{13}C NMR spectrum were assigned on the basis of the HMBC correlations with the 10-methyl, 5- and 6-methylene and 4-methine nuclei. The 10-methyl HMBC correlation clearly identifies the C-2 carbonyl signal while a correlation with the 4-methine proton permits assignment of the C-3 carbonyl (**Fig. 30**).

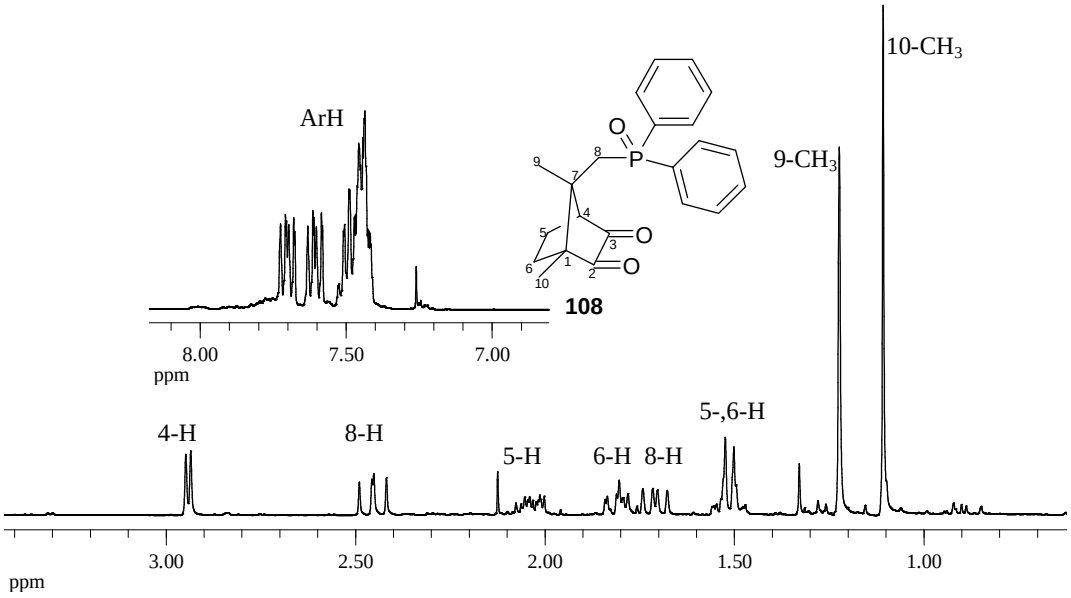

Figure 28. 400MHz ^{1}H NMR spectrum of diketone **108** in $CDCl_3$.

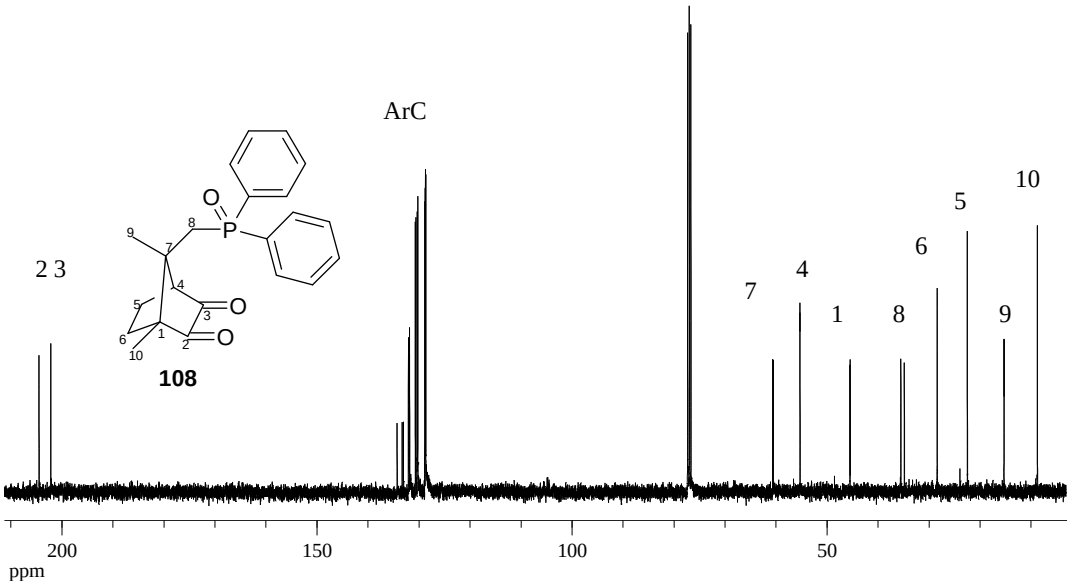

(a)

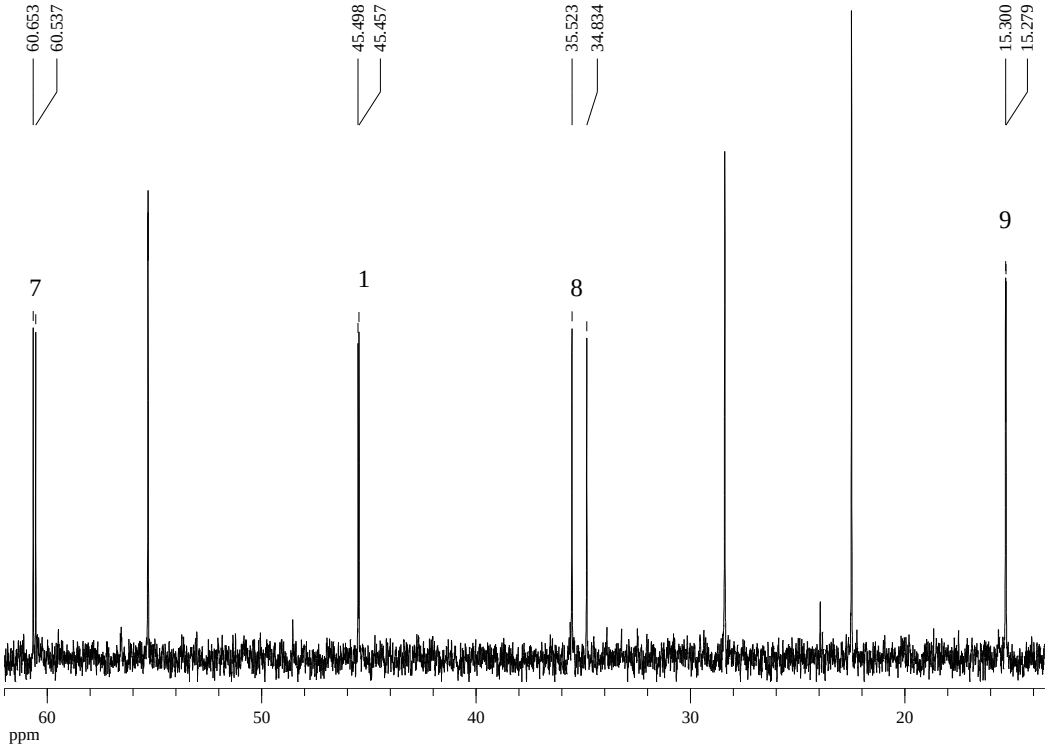

(b)

Figure 29. (a) 100MHz ^{13}C NMR spectrum of diketone **108** in $CDCl_3$. **(b)** Partial expansion of the 100MHz ^{13}C spectrum in **(a)**.

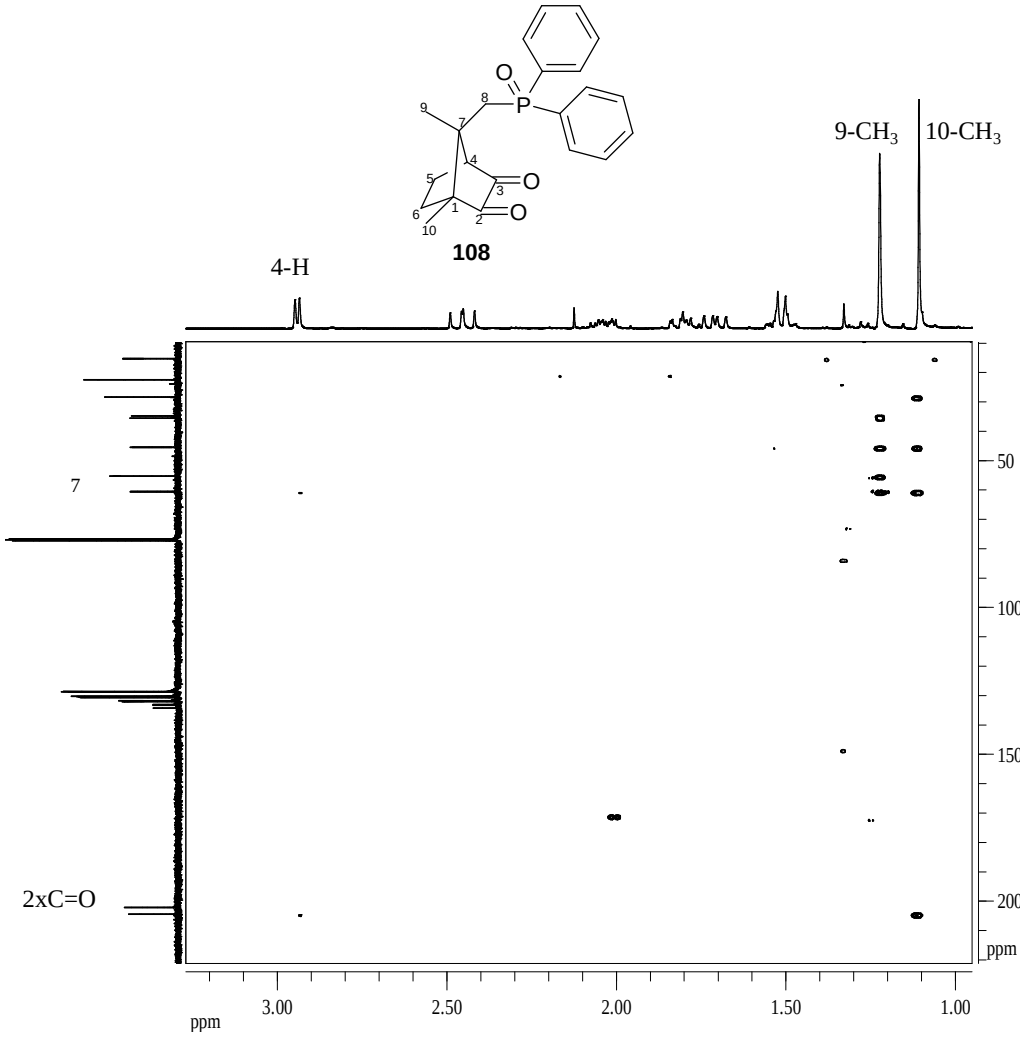

Figure 30. Partial 400MHz HMBC spectrum of diketone **108** in $CDCl_3$.

Preparation of the diacid **109** and the diol **111** was achieved *via* ring–opening of the phosphine oxide **106** and diketone **108** (**Schemes 36** and **38**). Boiling a solution of the phosphine oxide **106** in the presence of $FeSO_4.7H_2O$ and aqueous HNO_3[121] afforded the crude diacid **109** in 75% yield after 3 days, while treatment of the diketone **108** (obtained by the SeO_2 oxidation of the monoketone **106**) with aqueous NaOCl at room temperature[122] afforded the crude diacid **109** in 73% yield after 3 days. In both reactions, the formation of minor by-products was detected by NMR analysis. Purification could not be achieved since the crude material was an insoluble solid with a high melting point (*ca.* 300°C). Samples of the diacid **109** were prepared for NMR analysis by warming the material in DMSO-d_6 followed by filtration. In the ^{13}C

NMR spectrum, the carboxylic carbonyl carbons were identified by their characteristic chemical shifts at 175.2 and 177.0 ppm. The overlapping multiplets corresponding to the phenyl carbons were also evident at *ca.* 129 ppm and confirmed retention of diphenylphosphine oxide group. In the ^{1}H NMR spectrum, signals corresponding to two methyl groups and the phenyl protons were detected. The presence of the carboxyl acid groups was also confirmed by IR analysis which showed a broad COOH band at 3650-2792 cm^{-1} and a C=O stretching band at 1691 cm^{-1}. High resolution MS revealed a peak at *m/z* = 400 which is consistent to the molecular formula ($C_{22}H_{25}O_5P$) of the diacid **109.**

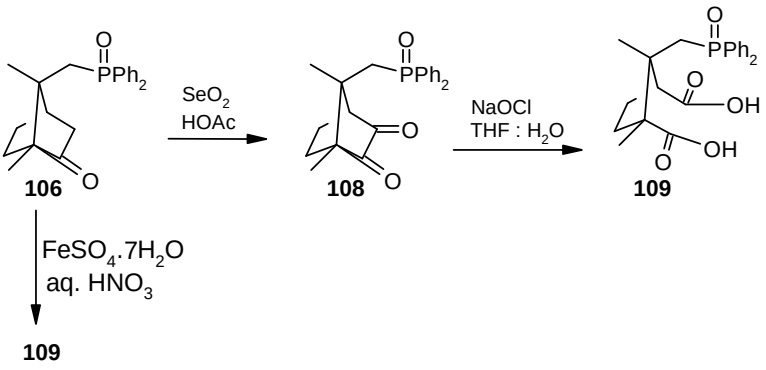

Scheme 36

The bis(hydroxymethyl) analogue **111** of the diacid **109** was prepared *via* reductive ring-opening of the acid anhydride **109** (**Scheme 37**). The acid anhydride **110** was prepared in 45% yield by H_2O_2 oxidation of diketone **107** following the Komarov procedure for the preparation of 9-bromocamphoric anhydride. Characterisation of compound **110** was effected by NMR, IR and high resolution MS analysis.

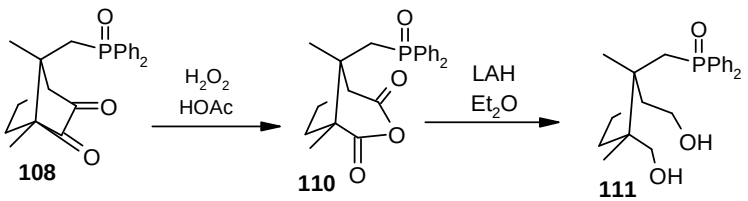

Scheme 37

Reduction of acid anhydride **110** by lithium aluminium anhydride (LAH) in ether proceeded for 1 hour to afford 2-(diphenylphosphinoylmethyl)-1,3-bis-(hydroxymethyl)-1,2-dimethylcyclopentane **111** in 63% yield. The ^{1}H and ^{13}C NMR spectra (**Fig. 32-33**) show the following crucial signals:

i) a broad singlet at 5.01 ppm in the ^{1}H NMR spectrum, which integrates for one proton;

ii) multiplets in the ^{1}H NMR spectrum at *ca.* 3.4 and 3.7 ppm which integrate for four protons; and

iii) two signals at 63.1 and 68.3 ppm in the ^{13}C.NMR spectrum which correspond to the hydroxymethyl carbons.

The broad singlet at 5.01 ppm is consistent with the presence of a hydroxyl group, but a second OH signal was not detected. The ^{1}H NMR multiplets at 2.55 and 3.38 ppm and two the ^{13}C NMR signals at 63.1 and 68.3 ppm were, on the basis of the DEPT 135, HSQC and HMBC spectra (**Fig. 34** and **35**), assigned to the two hydroxymethyl groups. The 6-methylene protons resonate as multiplets on ^{1}H NMR spectrum (**Fig. 32**) while the corresponding carbon signals resonate as a doublet due to neighbouring phosphorus as shown in HSQC spectrum (**Fig. 34**). The 6-methylene protons were further assigned on the basis of HMBC correlation with C-1, C-2 and C-3 nuclei (**Fig. 35**). In the ^{31}P NMR spectrum, a relatively deshielded singlet at 29.3 ppm was detected, confirming the presence of a phosphine oxide moiety. The presence of hydroxyl groups was supported by IR analysis which showed a broad absorption band at 3609-3017 cm^{-1}. The molecular formula of compound **111** was also confirmed by high resolution MS analysis of the molecular ion at m/z = 372.

Crystals of the bis(hydroxymethyl) analogue **111** were obtained by recrystalisation from chloroform. Single crystal X-ray analysis clearly confirmed the structure (**Fig. 31**) as the one indicated by the spectral analysis. Furthermore, the crystallographic data revealed the intramolecular hydrogen bond [O(10)-H···O(14)] which gives rise to an 8-membered ring (**Fig. 31a**).

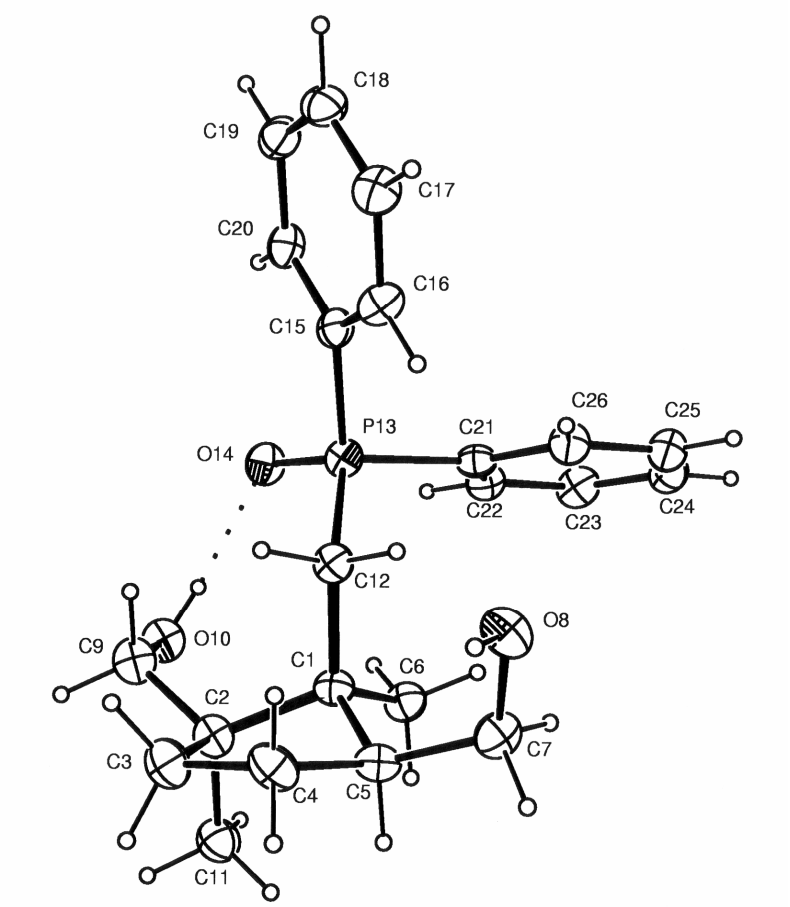

(a)

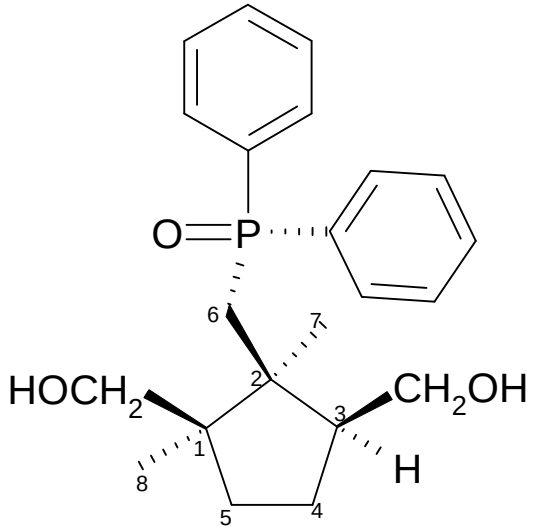

(b)

Figure 31. a) X-ray crystal structure of (1*R*,2*S*,3*S*)-(+)-2-(diphenylphosphinoylmethyl)-1,3-bis(hydroxymethyl)1,2-dimethyl-cyclopentane **111**, showing the crystallographic numbering and **b**) the corresponding wire-frame structure showing the systematic numbering.

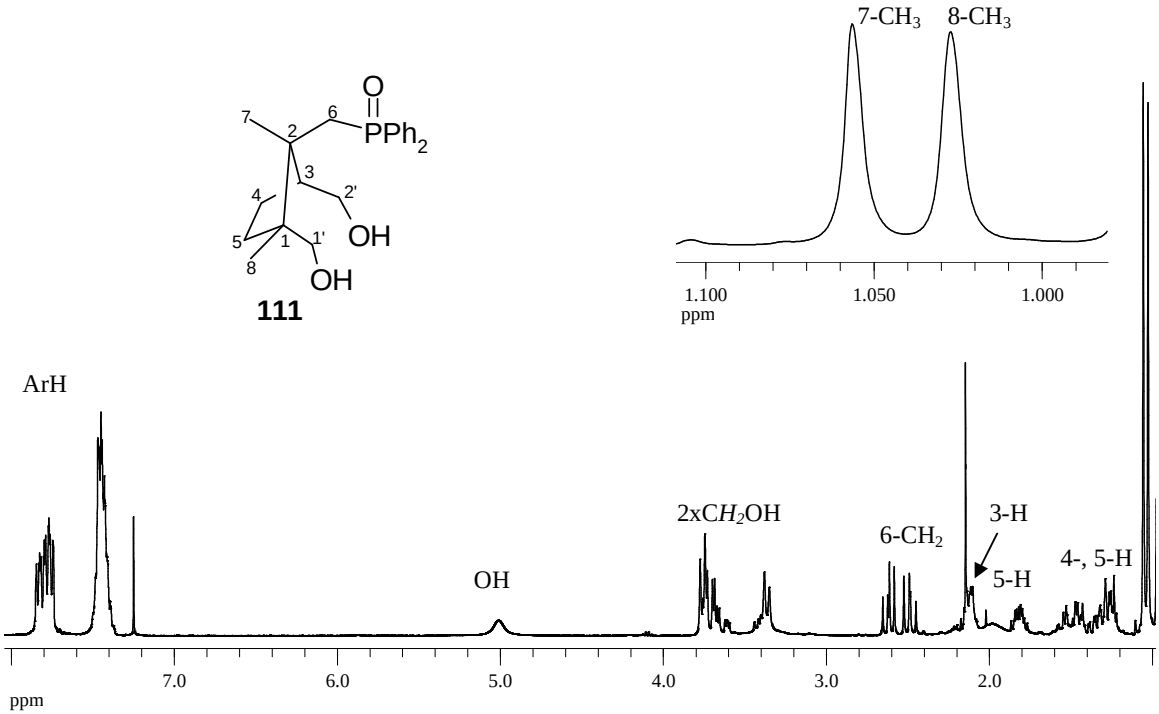

111

Figure 32. 400MHz ^{1}H NMR spectrum of compound **111** in $CDCl_3$.

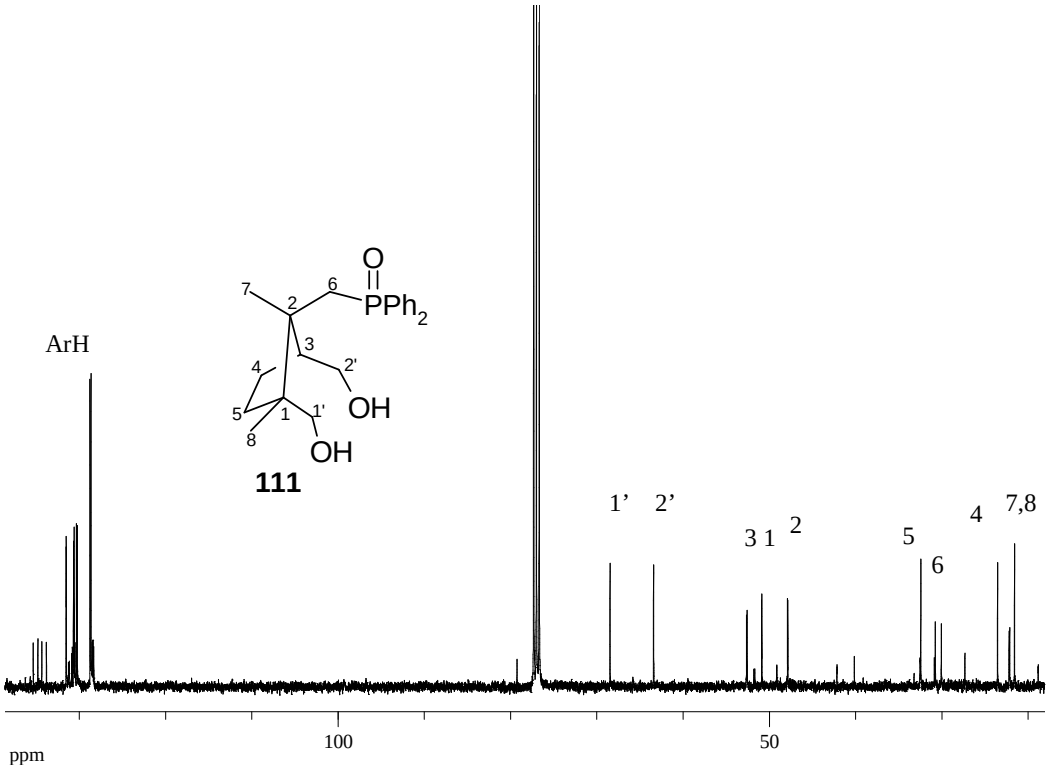

111

Figure 33. 100MHz ^{13}C NMR spectrum of compound **111** in $CDCl_3$.

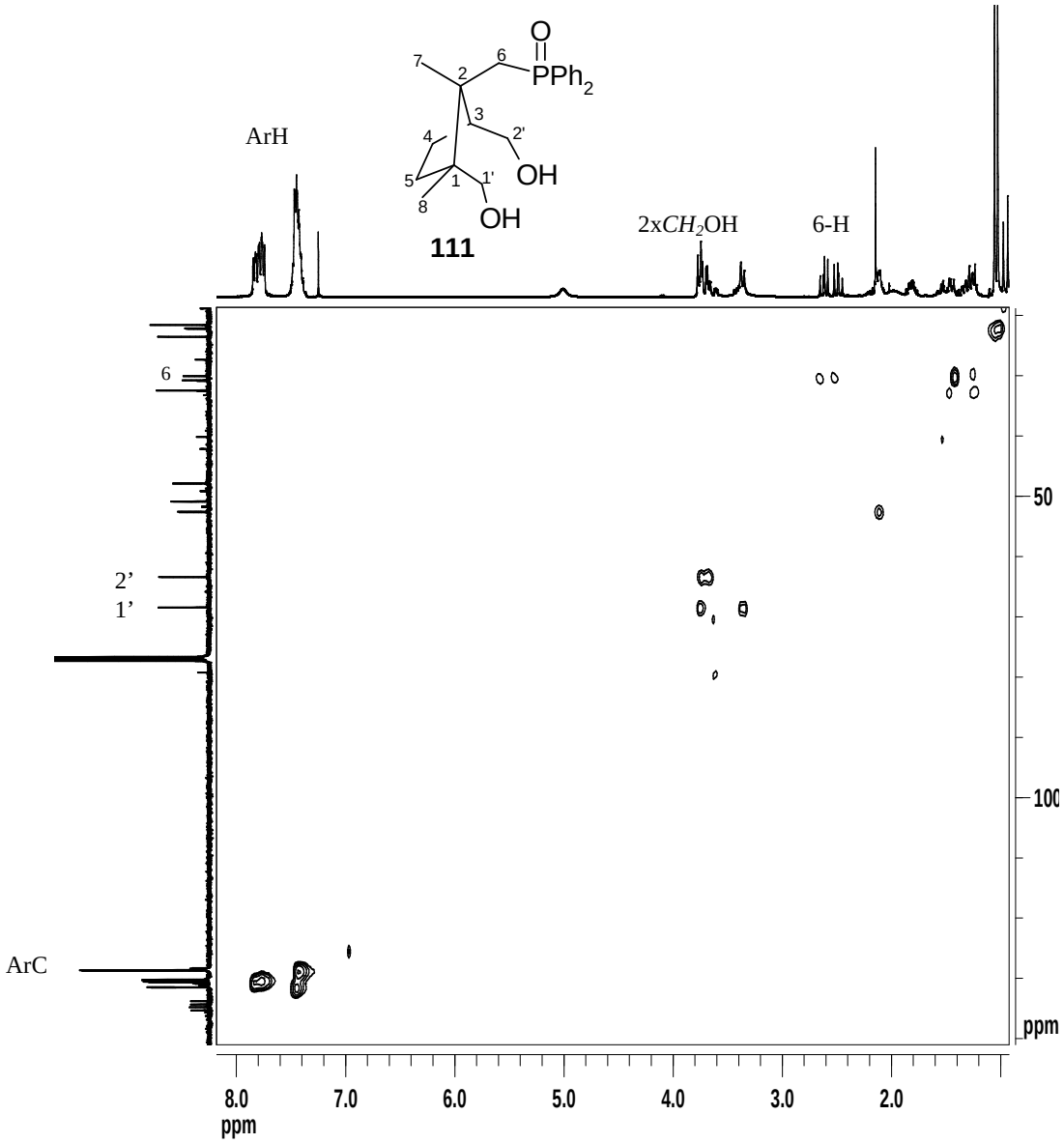

Figure 34. 400MHz HSQC spectrum of compound **111** in $CDCl_3$.

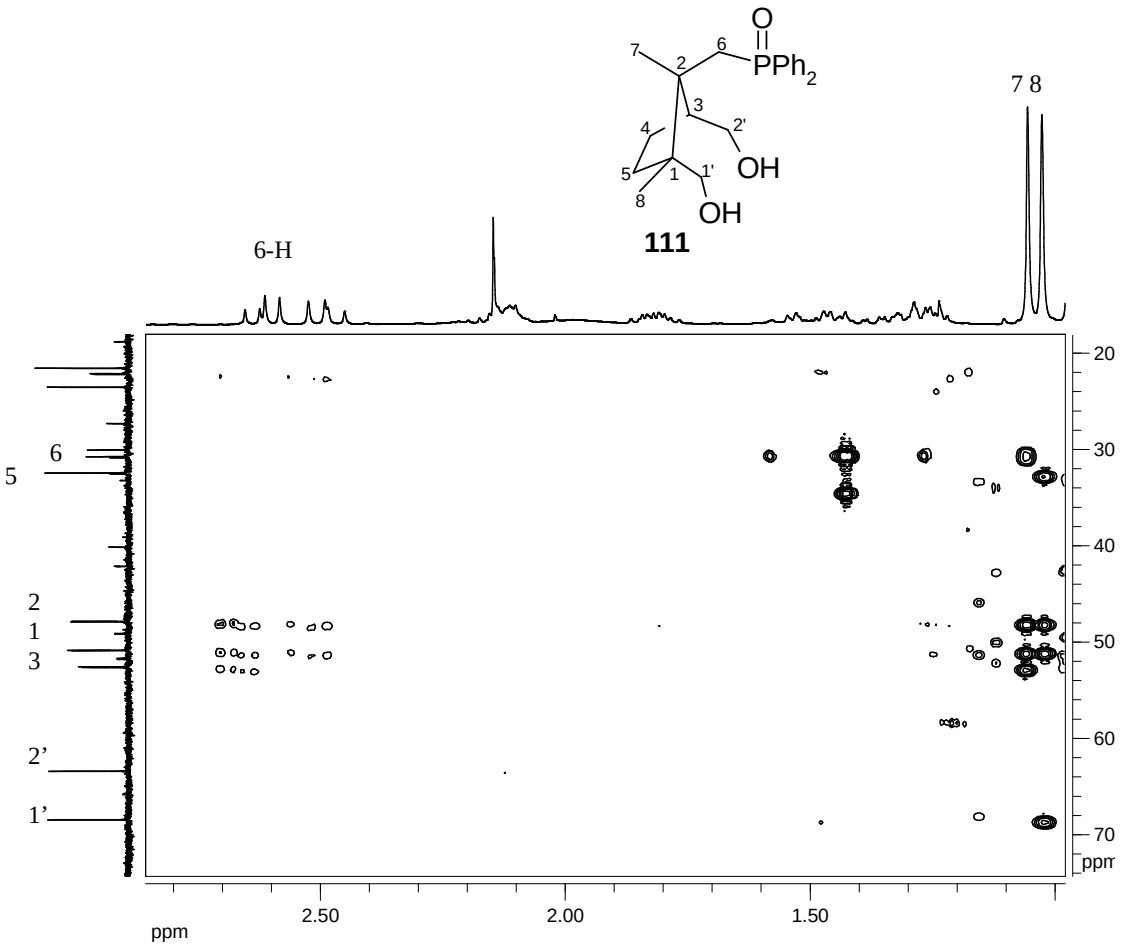

Figure 35. Partial 400MHz HMBC spectrum of compound **111** in $CDCl_3$ (phenyl group signals are not shown).

The last step in the synthesis of the target phosphine ligands **62** and **64** was, in each case, the reduction of the phosphine oxides to the corresponding trivalent phosphorus groups in compounds **109** and **111** (**Scheme 38**). In the first attempt to reduce the phosphine oxide group, a suspension of the diacid **109** was treated with $SiHCl_3$ in the presence of Et_3N ($SiHCl_3/Et_3N$).[119] However, no identifiable product appeared to form and the isoluble white material was collected. The same procedure was applied to the diol **109** but, again, similar insoluble material was collected (**Scheme 38**). Other reducing agents that were used in an attempt to reduce the diol **111** were $LiAlH_4/MeI$,[123] $SiHCl_3/PPh_3$[124] and Cl_6Si_2[125] (**Scheme 38**). In each case only starting material was recovered. Time constraints did not permit further methods to be investigated, but it is expected that future studies will explore the use of catalytic reduction methods.

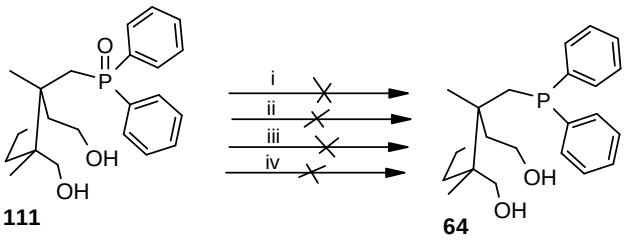

111 **64**

Scheme 38. Reagents i) $SiHCl_3$, Et_3N, reflux; ii) $LiAlH_4$, MeI, reflux; iii) $SiHCl_3$, PPh_3, reflux; iv) Cl_3Si_2.

2.1.2.2. *Camphor-derived pyridinyl ligands*

The construction of tridentate camphor-derived pyridinyl ligands was also attempted in the present study. Pyridinyl ligands have been used previously to substitute a phosphine ligand in the Grubbs' second generation catalyst **12**.[77,91] The resulting complexes exhibited increased initiation rates,[77] but the catalysts readily decomposed.[78] Chelating ligands containing a pyridine moiety, *e.g.* **112** (**Scheme 39**), could be used to form complexes such as **113** (**Fig. 36**), which might be expected to resist decomposition. The DFT-optimised geometry of the complex **113**, however, deviates significantly from the typical *trans*-arrangement of the dissociating ligand to the NHC ligand (N-Ru-NHC angle = 135°) (**Fig. 36**). Similar geometry was obtained when the R group (R = CH_2 in complex **113**) was increased to R = CH_2CH_2. However, the requirement of a *trans*-arrangement is not clear since catalytically active catalysts with a *cis*-orientation of dissociating ligand have been reported.[91]

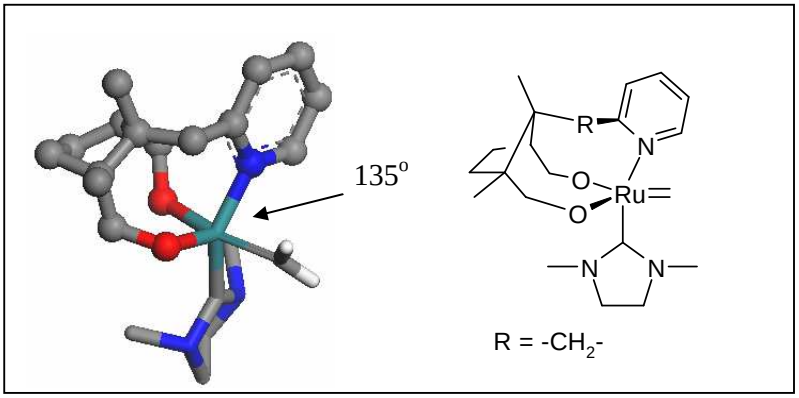

113

Figure 36. Dmol^3/GGA/PW91/DNP geometry-optimised structure of the putative catalyst **113** (H's omitted for clarity).

2.1.2.2.1. *Synthesis*

Attempted coupling of 8-bromocamphoric anhydride **114** with 2-bromopyridine **115** in the presence of Zn in DMSO proved unsuccessful (**Scheme 39**); only starting materials were recovered at the end of the reaction. Introduction of a pyridine moiety was also attempted by substituting the bromine in 8-bromocamphorquinone **87** by 2-aminopyridine **117** (**Scheme 40a**). Unfortunately the reaction afforded the isomeric hemi-aminals **118** and **119** instead of the desired 8-(2-pyridylamino)camphorquinone **120**.

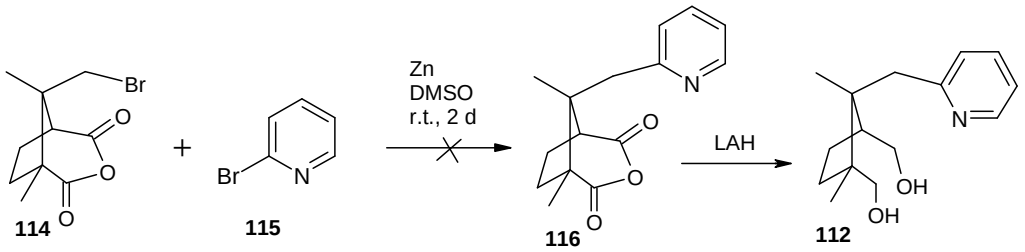

Scheme 39

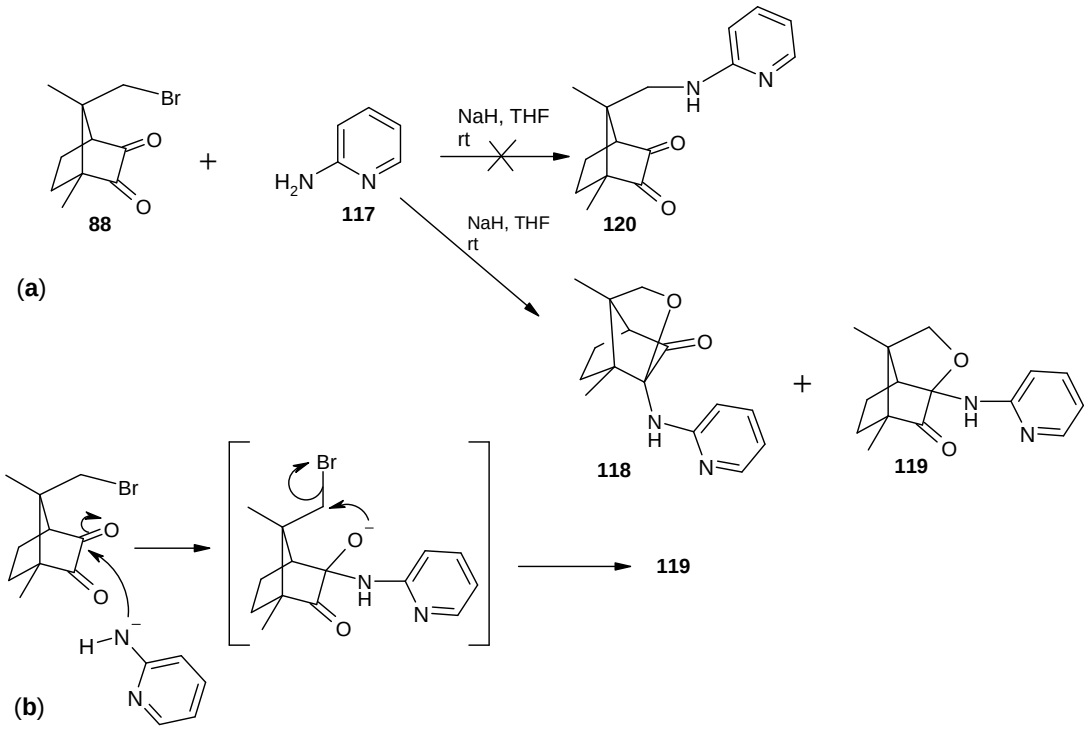

Scheme 40

The ^{1}H NMR spectrum (**Fig. 37**) of the tricyclic compound **118** shows the aromatic protons (resonating at 6.70 - 8.06 ppm) integrating for four protons and an amine

proton signal resonating at 5.21 ppm. The diastereotopic 5-methylene and the 1-methine protons were identified by their splitting patterns. The 10- and 11-methyl protons resonated in their characteristically high-field chemical shift region (*ca*. 1.0 ppm). In the ^{13}C NMR spectrum (**Fig. 38**), only one carbonyl signal is evident and this was assigned as C-2 on the basis of the HMBC spectrum (**Fig. 39**) which indicated correlation to the 1-methine proton. The other carbons were also assigned based on their HMBC and HSQC correlations. The presence of a secondary amine was supported by a strong IR stretching band at 1602 cm^{-1}. Similar spectroscopic features were observed for the isomeric product **119**.

The tricyclic compounds **118** and **119** are presumably formed *via* nucleophilic attack of the pyridylamino anion at the C-2 and C-3 carbonyl carbons in 8-bromocamphorquinone **88** followed by intramolecular displacement of bromide ion to form a cyclic ether (**Scheme 40b**). A similar tricyclic compound was formed by Komarov and co-workers in the reaction of 8-bromocamphor **61** and Ph_2PLi.[119] Since the carbonyl groups in camphorquinone proved to be vulnerable to nucleophilic attack, the protected camphor derivative **103** was used as a substrate to react with 2-aminopyridine **115** (**Scheme 41**). This reaction also failed with unconverted substrate being collected after boiling the mixture under reflux for 24 hours. The use of a palladium catalyst, complemented by a bis-phosphine ligand, could well facilitate the carbon-nitrogen bond formation,[126] and will be explored in future studies.

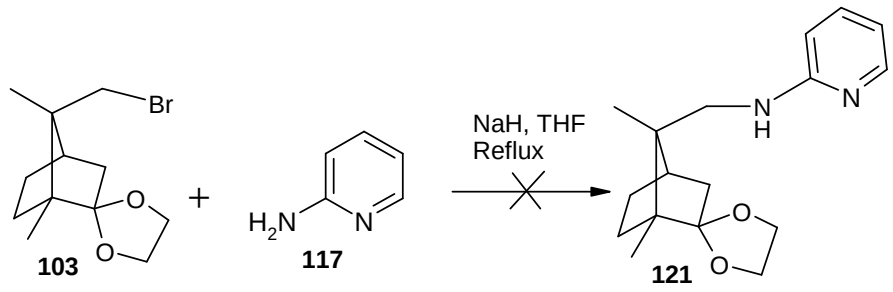

Scheme 41

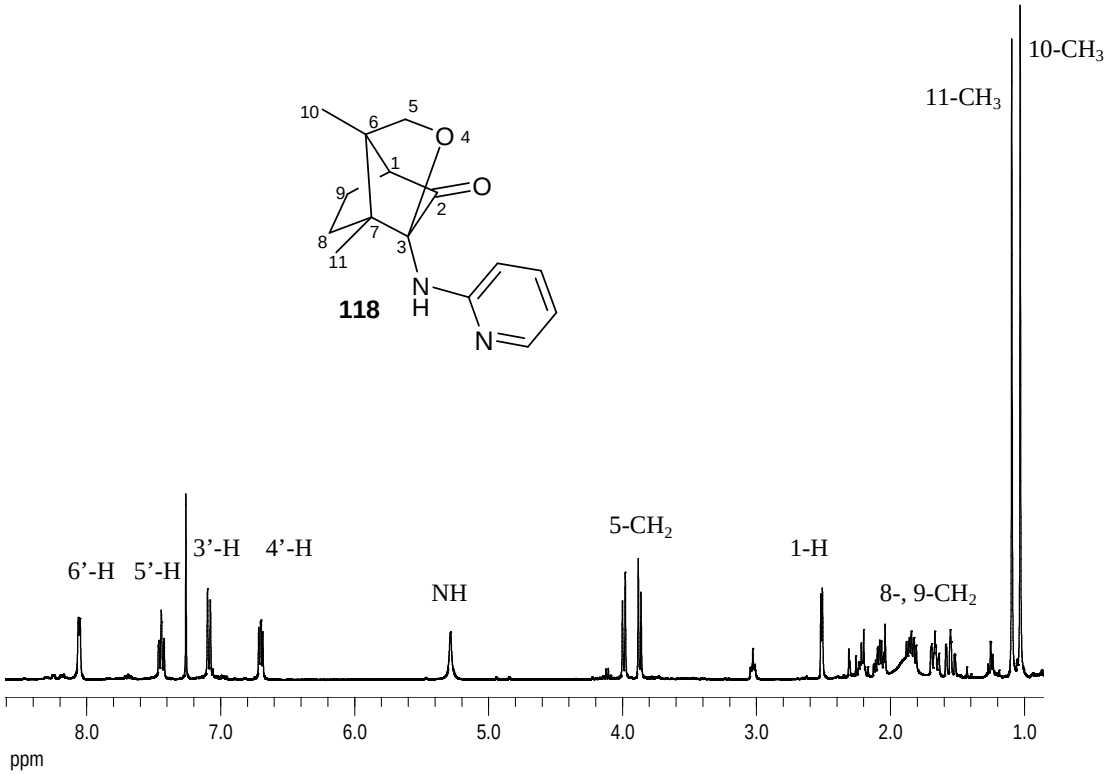

Figure 37. 400MHz ^{1}H NMR spectrum of compound **118** in $CDCl_3$.

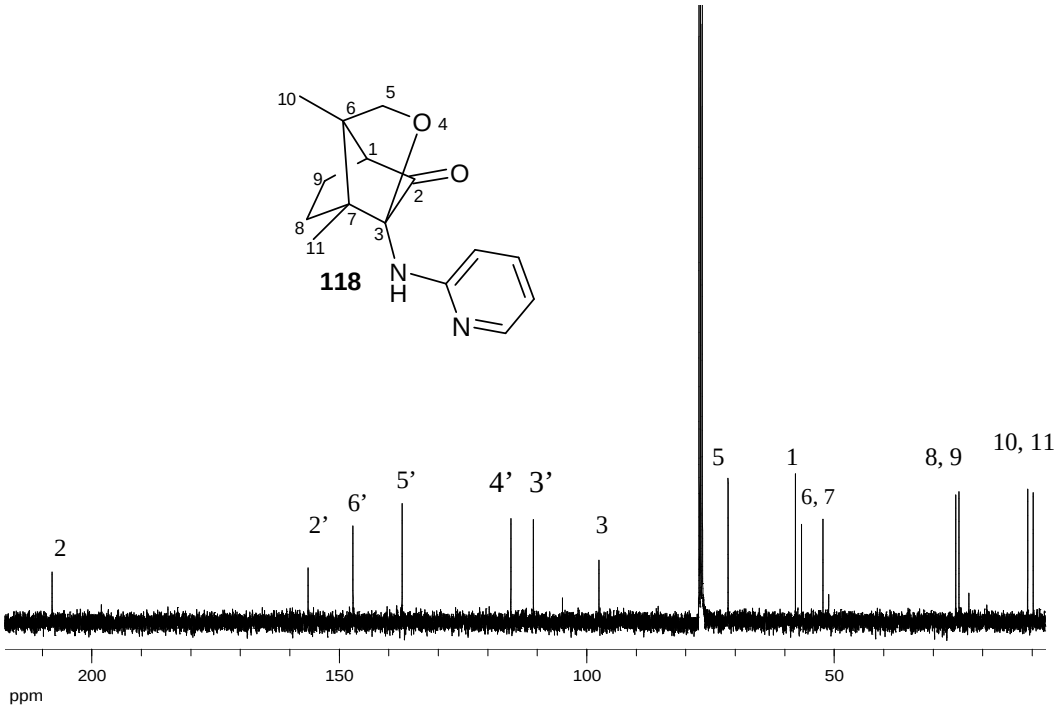

Figure 38. 100MHz ^{13}C NMR spectrum of compound **118** in $CDCl_3$.

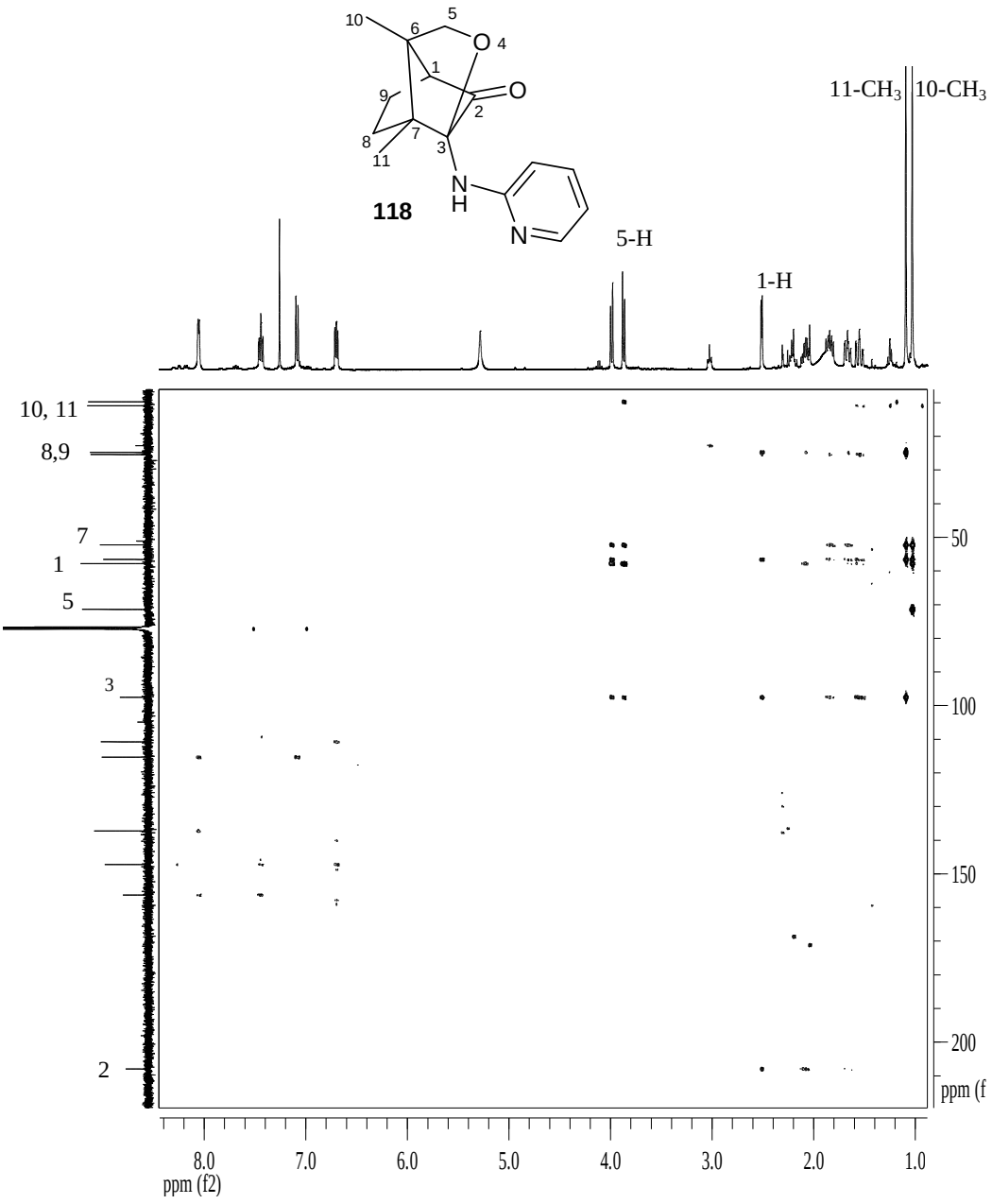

Figure 39. 400MHz HMBC spectrum of compound **118** in $CDCl_3$.

2.1.2.3. *Camphor-derived* N-*heterocyclic carbene (NHC) ligands*

Various NHC ligands have been used to enhance the activity of Ru-based olefin metathesis catalysts.[54] Moreover, chiral bidentate NHC ligands have been reported to improve the catalytic selectivity of such catalysts.[86] In this study, the development of a chiral tridentate NHC ligand **124** to be used in a Ru-based catalyst **125** was approached as illustrated by the retrosynthetic analysis detailed in **Scheme 42**. Numerous attempts to displace the bromide ion in 8-bromocamphoric anhydride **113** or 8-bromocamphoquinone **86** by 1-phenylimidazole **122** using reported[127] or modified methods proved unsuccessful. Another attempted approach to the development of a chiral tridentate NHC ligand, *viz.*, the ligand **129** is outlined by the retrosynthetic analysis detailed in **Scheme 43**. Preliminary assessment of the chelating potential of ligand **129** was carried out by DFT analysis of the truncated complex **131.** The geometry-optimised structure showed reasonable features indicating a *trans*-orientation of the dissociating ligand (L) relative to the NHC ligand (**Fig. 40**).

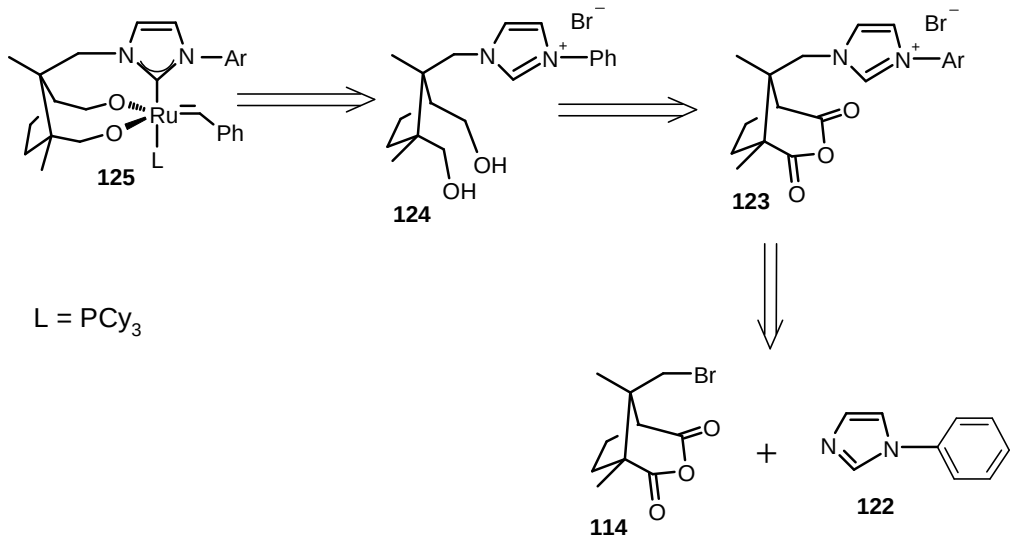

Scheme 42

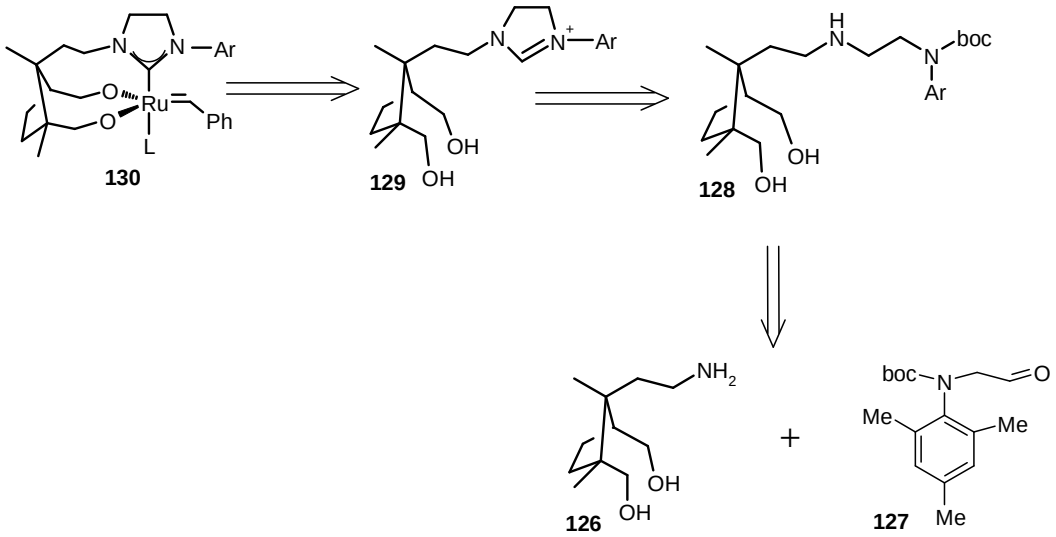

Scheme 43

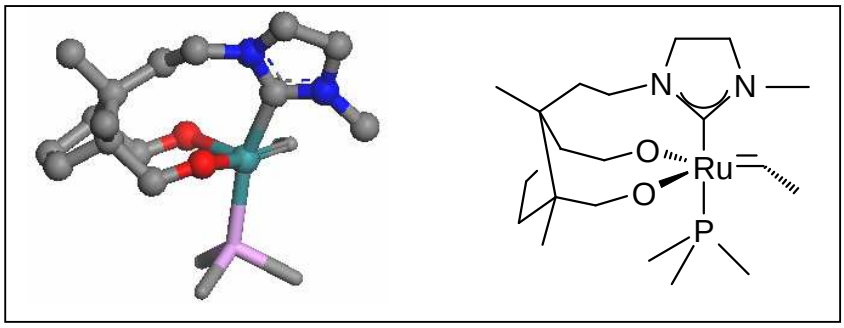

131

Figure 40. Dmol[3]/GGA/PW91/DNP geometry-optimised structure of a truncated model of a putative catalyst **131.** (H's are omitted for clarity).

2.1.2.3.1. *Synthesis*

The synthesis of primary amine **126** was approached *via* 8-cyanocamphor ethylene ketal prepared **132** following the Kuo and Money literature procedure (**Scheme 44**).[120] 8-Cyanocamphor ethylene ketal **131** was obtained in 69% yield which is comparable with the literature range of 54-92%. Deprotection of 8-cyanocamphor ethylene ketal with hydrochloric acid in acetone afforded crude material that proved to contain a considerable amount of impurities as judged by the ^{1}H NMR spectrum. However, the ^{13}C NMR spectrum (**Fig. 41**) of the crude material showed the presence of 8-cyanocamphor **133** as a major component with the nitrile carbon resonating at

118 ppm and carbonyl carbon at 217 ppm. The presence of the nitrile group in the crude material was confirmed by an IR absorption band at 2241 cm^{-1}.

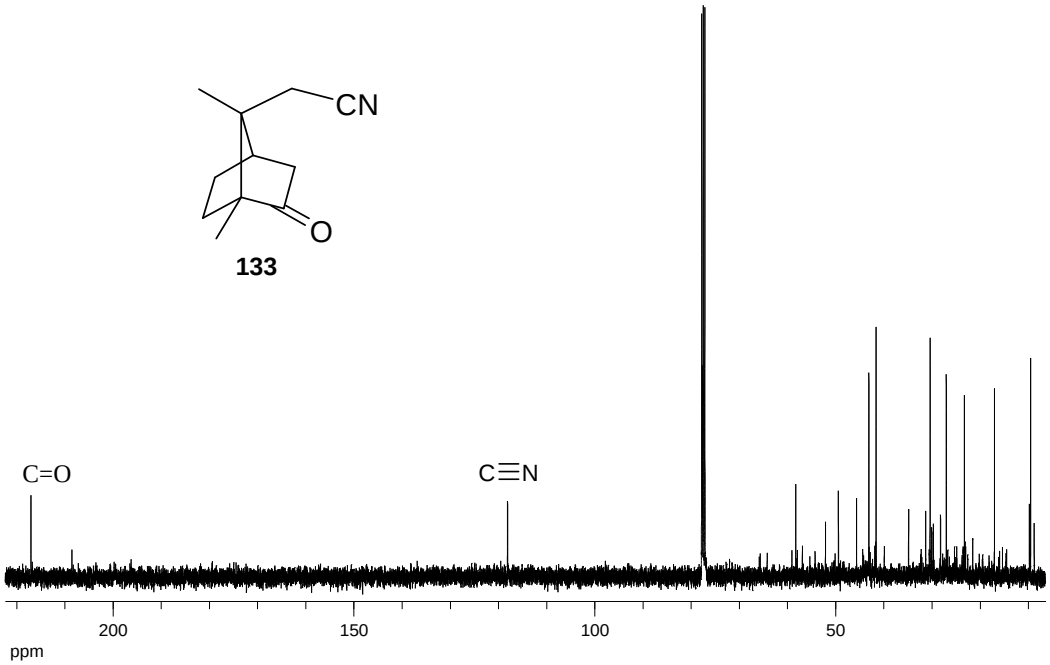

133

Figure 41. 100MHz ^{13}C NMR spectrum of crude compound **133** in $CDCl_3$.

Attempts to isolate 8-cyanocamphor **133** by chromatography on silica gel resulted in loss of the nitrile. The crude 8-cyanocamphor **133** was therefore oxidised using selenium dioxide to 8-cyanocamphorquinone **134**, which could be isolated by gravity column chromatography. Although the nitrile and two carbonyl groups were detected in the ^{13}C NMR spectrum, various impurities were also detected. Further purification by HPLC resulted in loss of the 8-cyano group as camphorquinone **135** was collected as a major fraction (**Scheme 44**). Given the difficulties experienced in working with the nitrile derivatives, future work is expected to involve early reduction of the nitrile to a primary amine which can be protected prior to further structural elaboration.

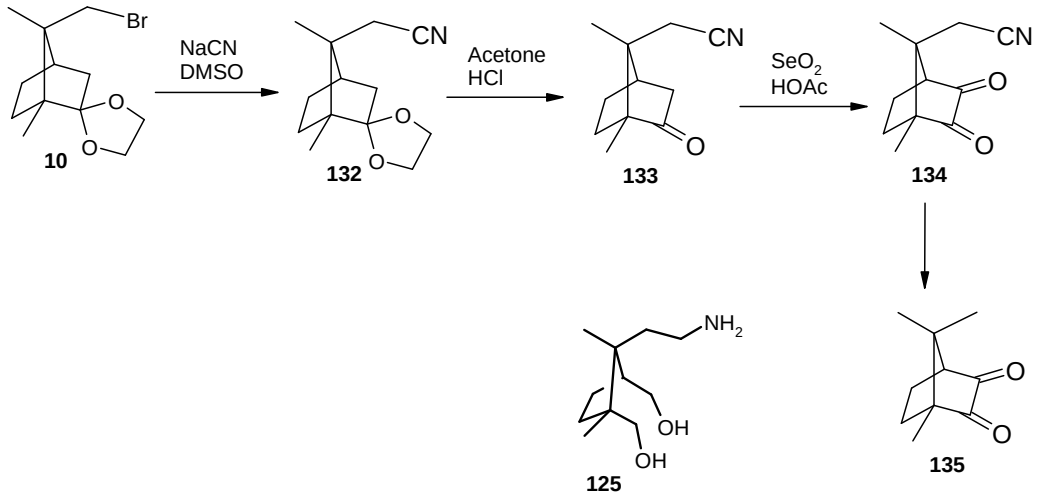
Br
NaCN
DMSO
CN
Acetone
HCl
CN
SeO_2
HOAc
CN
O
O
O
O
O
O
10
132
133
134
NH_2
OH
OH
O
O
125
135

Scheme 44

2.2. PRELIMINARY RUTHENIUM COMPLEXATION STUDIES

Unsuccessful attempts to reduce the ligand precursor **111** to the corresponding tridentate ligand **64** led to the decision to explore the chelating ability of compound **111** itself in displacing the Cl ions in Grubbs' first-generation catalyst **4**. It was assumed that the hydroxyl groups could bind in a bidentate fashion and DMSO has been shown to bind ruthenium through oxygen, raising the possibility of coordination through the phosphine oxide oxygen.[128] Following a method reported by Sanford *et al.*[103] the hydroxyl groups in compound **111** were activated using potassium hydride (KH) in benzene under inert conditions. The resulting suspension was then treated with the Grubbs' 1st-generation catalyst **4** as described by Sanford *et al.* (**Scheme 45**). During the reaction, a colour change from purple to dark red was observed, consistent with the colour changes described by Sanford *et al.* (purple to brownish red). However, after the reaction none of the 14-electron ruthenium alkylidene **136** could be identified by ^{1}H NMR spectroscopy. Moreover, the alkylidene proton, which usually resonates far downfield (at *ca.* 16.0 ppm), was clearly not present.

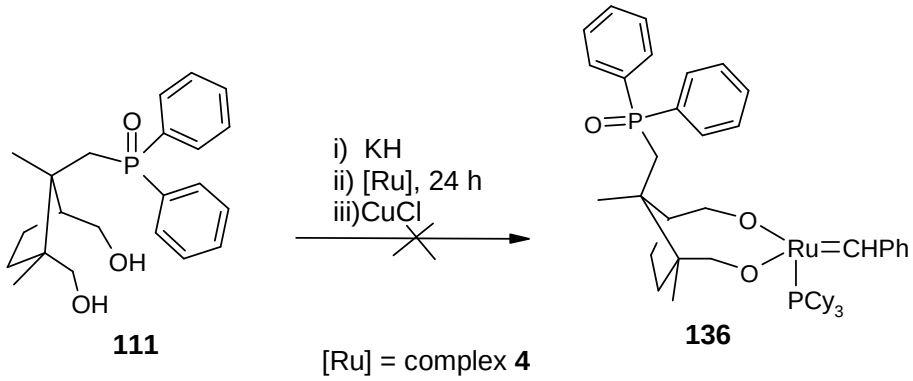

111 **136**

[Ru] = complex **4**

Scheme 45

2.3. APPLICATION OF NMR SHIFT PREDICTION PROGRAMMES

Four sets of isomers (compounds **59** and **60; 90** and **92; 100** and **101;** and **118** and **119**) have been synthesised in the present study. NMR structure elucidation of these isomers was not always straightforward due to the structural similarities. In fact, in the case of the 8- and 9-iodo derivatives **90** and **92**, X-ray crystal analysis was needed to establish the identity of the isomers. It was decided to assess the reliability of three different NMR prediction programmes, *viz.*, ChemWindow,[129] and the MODGRAPH neural network and HOSE (Hierachially Ordered Spherical description of Environment)[130] methods, to predict the ^{13}C chemical shifts of the isomers **90** and **92**, **118** and **119** and of two other compounds, **51** and **58**. MODGRAPH prediction methods have been used previously to provide useful information on ^{1}H NMR chemical shifts of molecules containing ester groups.[130b]

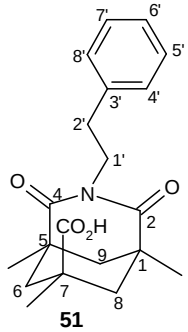

51

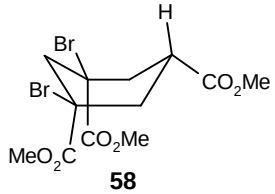

58

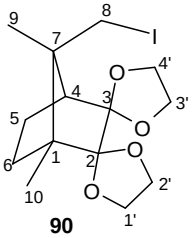

90

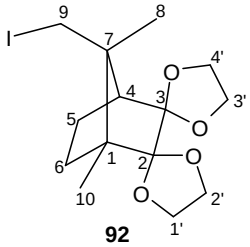

92

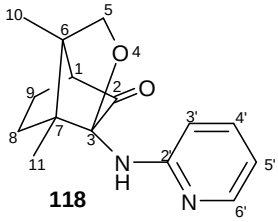

118

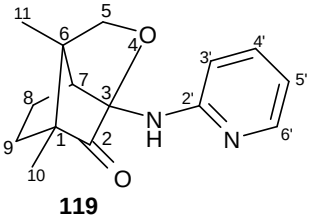

119

The predicted ^{13}C NMR chemical shifts in **Tables 3 - 8** show that, except for compound **58** (**Table 4**), the MODGRAPH neural network (column C), could not predict all the ^{13}C chemical shifts of the selected compounds. The omitted chemical shifts are mainly those of highly substituted and quaternary carbons. Apart from this short-coming, the predicted values appear to correlate well with the experimental chemical shifts (column **A**). It is also worth noting that the prediction programmes correctly predict the chemical shifts for symmetrical compounds such as **51** and **58,**

but they all failed to predict the lack of symmetry in the diketal ketal groups in compounds **90** and **92**. The 1'-, 2'-, 3'- and 4'-methylene carbons, in all cases, were predicted as pairs of chemically equivalent atoms. The experimental ^{13}C NMR chemical shifts for isomers **90** and **92** are very similar and the same trends are observed in the predicted data, thus precluding differentiation by the NMR prediction programmes. However, the differences between isomers **118** and **119** could be detected by the prediction methods. For instance, the relative shielding patterns of the C-11 nucleus in compound **118** and the isomeric C-10 nucleus in compound **119** (**Tables 7 and 8**) could be predicted reasonably by two of the three methods.

In order to assess the accuracy of the prediction programmes, the experimental ^{13}C NMR chemical shifts were used to compare the predicted data using root mean square (rms) errors (observed – predicted). The accuracy of the chemical shifts is given by the smallest possible rms error. Since some of the ^{13}C chemical shifts were omitted by the MODGRAPH neural network in column **C** of **Table 3** and **Tables 5-8**, only the predicted values were used to calculate the rms error in these cases. The rms error of the prediction programmes range from 5 to 15 ppm and the HOSE NMR prediction method appears to give the lowest rms values most consistently. These NMR prediction programmes should clearly be used with caution in predicting shifts for new compounds since the rms errors tend to be quite large.

Table 3: Experimental (100MHz) and predicted ^{13}C NMR chemical shift data* (δ/ppm) for 1,5,7-trimethyl-2,4-dioxo-3-phenethyl-3-azabicyclo[3.3.1]nonane-7-carboxylic acid **51** in $CDCl_3$.

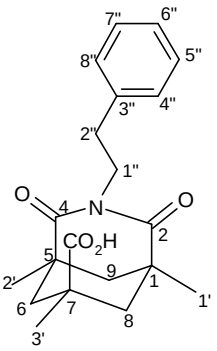

Nucleus	A	B	C	D
C-1	41.3	30.5	40.5	45.3
C-2	181.1	176.5		168.7
C-4	181.1	176.5		168.7
C-5	41.3	30.5	40.5	45.3
C-6	33.5	41.4	46.9	44.7
C-7	40.1	25.4		47.0
C-8	33.5	44.1	46.9	44.7
C-9	41.4	38.5	46.2	28.5
C-1'	25.3	21.0	24.7	23.7
C-2'	25.3	21.0	24.7	23.7
C-3'	29.8	20.0	23.9	13.7
C-4'	175.9	181.0	180.8	182.4
C-1"	43.9	44.4	45.6	46.9
C-2"	43.4	34.5	35.6	34.5
C-3"	138.7	140.2	138.5	139.2
C-4"	128.2	127.9	129.1	128.7
C-5"	129.0	128.4	129.1	128.8
C-6"	126.2	125.7	126.5	126.5
C-7"	129.0	128.4	129.1	128.9
C-8"	128.2	127.9	129.1	128.7
RMS error		6.8	6.3	7.8

* A: Experimental data; B: ChemWindow predictions; C: MODGRAPH neural network predictions; D: MODGRAPH HOSE predictions

Table 4: Experimental (100MHz) and predicted ^{13}C NMR chemical shift data* (δ/ppm) for trimethyl *cis*-1,3-dibromocyclohexane-1,3,5-tricarboxylate **58** in $CDCl_3$.

Nucleus	**A**	**B**	**C**	**D**
C-1	54.6	41.9	67.0	67.1
C-2	48.9	41.7	46.5	29.2
C-3	54.6	41.9	67.0	67.1
C-4	40.0	33.5	39.4	29.2
C-5	40.4	29.8	37.4	42.5
C-6	40.0	33.5	39.4	29.2
1-C=O	170	176.0	173.5	175.7
3-C=O	170	176.0	173.5	175.7
5-C=O	171.9	176.0	176.5	174.7
1-$CO_2\mathit{C}H_3$	53.4	50.0	52.6	52.1
3-$CO_2\mathit{C}H_3$	53.4	50.0	52.6	52.1
5-$CO_2\mathit{C}H_3$	52.2	50.7	52.2	51.6
RMS error		7.6	5.5	9.2

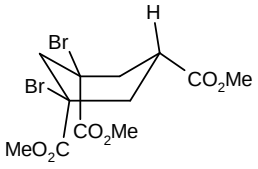

* A: Experimental data; B: ChemWindow predictions; C: MODGRAPH neural network predictions; D: MODGRAPH HOSE predictions

Table 5: Experimental (100MHz) and predicted ^{13}C NMR chemical shift data* (δ/ppm) for 8-iodocamphorquinone bis(ethylene ketal) **90** in $CDCl_3$.

Nucleus	**A**	**B**	**C**	**D**
C-1	53.7	45.8	49.4	46.8
C-2	116	124.1		108.3
C-3	113	114.2	122.8	108.3
C-4	52.6	41.7	55.8	46.9
C-5	29.1	10.2	21.8	25.9
C-6	20.6	20.6	35.0	30.6
C-7	48.5	33.9	50.6	45.9
C-8	18.5	18.8	16.9	17.4
C-9	18.8	10.5	13.6	15.5
C-10	10.1	7.0	12.6	17.3
C-1’	64.4	71.8	65.0	64.5
C-2’	64.6	71.8	65.0	64.5
C-3’	65.0	72.1	65.1	66.0
C-4’	66.0	72.1	65.1	66.0
RMS error		8.8	5.5	5.0

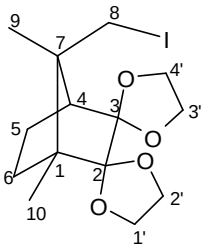

* A: Experimental data; B: ChemWindow predictions; C: MODGRAPH neural network predictions; D: MODGRAPH HOSE predictions

Table 6: Experimental (100MHz) and predicted ^{13}C NMR chemical shift data* (δ/ppm) for 9-iodocamphorquinone bis(ethylene ketal) **92** in $CDCl_3$.

Nucleus	**A**	**B**	**C**	**D**
C-1	53.2	45.8	49.4	46.8
C-2	114	124.1		108.3
C-3	113	114.2	122.3	108.3
C-4	51.9	41.7	55.8	46.9
C-5	31.9	10.2	21.8	25.9
C-6	19.8	20.6	35.0	30.6
C-7	48.5	33.9	50.6	45.9
C-8	20.7	10.5	13.6	15.5
C-9	19.5	18.8	16.9	17.4
C-10	9.89	7.0	12.6	17.3
C-1’	64.2	71.8	65.0	64.5
C-2’	64.6	71.8	65.0	64.5
C-3’	65.2	72.1	65.1	66.0
C-4’	66	72.1	65.1	66.0
RMS error		9.5	6.1	5.1

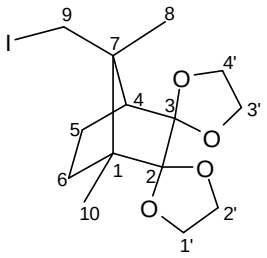

* A: Experimental data; B: ChemWindow predictions; C: MODGRAPH neural network predictions; D: MODGRAPH HOSE predictions

Table 7: Experimental (100MHz) and predicted ^{13}C NMR chemical shift data* (δ/ppm) for 6,7-dimethyl-3-(2-pyridylamino)-4-oxatricyclo[4.3.0.$0^{3,7}$]-2-nonanone **118** in $CDCl_3$.

Nucleus	**A**	**B**	**C**	**D**
C-1	57.8	48.1		47.9
C-2	208	211.3		212.3
C-3	97.5	116.0		89.6
C-5	71.4	68.2		66.7
C-6	56.6	33.6		46.9
C-7	52.3	52.7		46.9
C-8	24.8	21.5	30.9	36.0
C-9	25.4	16.2	24.1	34.2
C-10	10.9	15.2	10.7	18.3
C-11	9.79	7.9	9.0	15.5
C-2’	156.3	161.1	152.4	155.9
C-3’	110.8	108.9	112.9	112.9
C-4’	115.3	138.0	140.0	136.5
C-5’	137.3	113.0	114.9	117.5
C-6’	147.2	148.9	149.0	147.6
RMS error		12.3	11.4	10.0

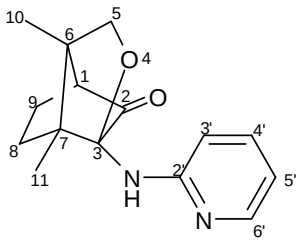

* A: Experimental data; B: ChemWindow predictions; C: MODGRAPH neural network predictions; D: MODGRAPH HOSE predictions

Table 8: Experimental (100MHz) and predicted ^{13}C NMR chemical shift data* (δ/ppm) for 1,6-dimethyl-3-(2-pyridylamino)-4-oxatricyclo[4.3.0.$0^{3,7}$]-2-nonanone **119** in $CDCl_3$

Nucleus	**A**	**B**	**C**	**D**
C-1	53.1	53.7		53.9
C-2	209.1	213.9		212.3
C-3	95.3	106.1		89.6
C-5	69.1	68.2		66.7
C-6	57.0	41.9		46.9
C-7	50.5	12.7		44.7
C-8	16.9	11.1	18.3	36.0
C-9	34.2	26.6	31.7	34.2
C-10	11.03	13.0	11.1	19.2
C-11	8.21	12.7	11.8	18.3
C-2’	156.1	161.1	153.2	155.9
C-3’	137.4	108.9	111.8	112.9
C-4’	110.0	138.0	139.6	136.5
C-5’	115.2	113.0	114.5	117.5
C-6’	148.2	148.9	149.1	147.6
RMS error		15.4	13.2	11.6

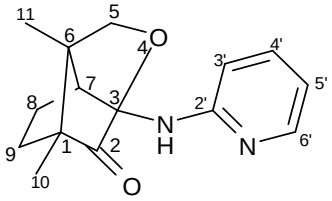

2.4. CONCLUDING REMARKS

The present study has been concerned with the development of novel tridentate ligands for use in the formation of potential metathesis catalysts and has extended significantly the previous approaches towards camphor-derived multidentate ligands.[101] The project has required the application of various synthetic, chromatographic, spectroscopic and computational methods. DFT calculations using the Accelrys DMol^3 package have been used as a design tool to assess the binding potential of the intended tridentate ligands. Such calculations have been shown

* A: Experimental data; B: ChemWindow predictions; C: MODGRAPH neural network predictions; D: MODGRAPH HOSE predictions

previously to be a reliable tool in assessing the structural geometry of ruthenium complexes.[74]

A series of novel compounds have been prepared and the formation of the 8- and 9-iodocamphor diketals **90** and **92** in the same reaction has illustrated the rearrangement potential of camphor framework – a major complicating factor in the synthetic elaboration of such systems. The mechanistic implications for the formation of diketal **92** were explored using a coset analysis, which has indicated a usual mechanistic sequence for the rearrangement. The successful formation of the 8-diphosphinoyl ligands **109** and **111** has involved the introduction of a phosphine group at the C-8 position and ring-opening of the bicyclic camphor system between C-2 and C-3 – critical steps towards the construction of the target ligands. The formation of the tricyclic compounds **118** and **119** *via* intramolecular cyclization reflects the sluggishness of intermolecular S_N^2 displacement at the neopentyl-like 8-, 9-, or 10-positions of the camphor system.

NMR analysis proved insufficient to unambiguously differentiate and establish the structures of the diketal isomers **90** and **92**, but the structures of both diketals were established by single crystal x-ray analysis. ^{13}C NMR chemical shift prediction programmes were explored to predict the chemical shifts in selected compounds. While, prediction programmes correlated reasonable with the experimental data, they failed to differentiate the chemical shifts of the diketal isomers **90** and **92**.

This study has clearly provided a solid foundation for future work on camphor-derived ligands and this is expected to include:-

i) the investigation of alternative ways to reduce phosphine oxide derivatives **109** and **111**;
ii) completion of the synthetic approach to pyridinium ligands; and
iii) the use of the resulting ligands in complexation studies.

3. EXPERIMENTAL

3.1. COMPUTATIONAL

3.1.1. Density Functional Calculations

Density functional calculations were conducted using the Accelrys DMol^3 DFT code in MaterialsStudio (version 2.2)[131] on LINUX-based Pentium IV PC's. All calculations involved used of the generalised gradient approximation (GGA) functional by Perdew and Wang (PW91)[132] and the 'double numerical plus polarization' (DNP) basis set: a polarized split valence basis set of numeric atomic functions which are exact solutions to the Kohn-Sham equations for the atoms.[133]

Convergence criteria for geometry optimizations were the threshold values: $2x10^{-5}$ Hartree, 0.004 Hartree/Å, 0.005 Å and $1x10^{-5}$ Hartree for energy, force, displacement and self consistent field (SCF) density, respectively. All calculations employed a method based on Pulay's[134] direct version of iterative subspace (DIIS) technique to accelerate SCF convergence, using a small electron thermal smearing value of 0.005 Hartree.

3.2. SYNTHESIS

3.2.1. General

Melting points were determined using a Kofler hot-stage apparatus, and are uncorrected. All NMR spectra were recorded on a Bruker AMX400 spectrometer for solutions in $CDCl_3$ or DMSO-d_6, and referenced using solvent signals (δ_H: 7.26 ppm for $CDCl_3$ and 2.50ppm for DMSO-d_6; δ_C: 77.0 ppm for $CDCl_3$ and 39.4 ppm for DMSO-d_6). An H_3PO_4 solution in DMSO-d_6 was used as an external standard for ^{31}P-NMR measurements. IR spectra were recorded on a Perkin-Elmer FT-IR Spectrum 2000 spectrometer using KBr discs or thin films on CsI discs. Low-resolution mass spectra were recorded on a Finnegan Mat GCQ spectrometer and high-resolution mass spectra were obtained by the University of the Witswatersrand Mass Spectrometry Service. Optical rotations were recorded on a Perkin-Elmer 141

polarimeter and samples were analysed as solutions in specified solvents in concentrations given as grams per 100mL.

Thin layer chromatography (TLC) was performed on Merck pre-coated TLC plates; visualisation was achieved by iodine vapour or under UV light. Flash chromatography was conducted using Merck silica gel 60 (particle sizes 0.040-0.063mm) and radial chromatography was effected on chromatotron plates coated with silica gel 60 PF_{254} and visualised under UV light. HPLC analyses were carried out using a Spectra-Physics P100 pump fitted with a Whatman Partsil 10 Magnum 6 normal phase column and a Waters R1410 differential refractometer detector.

Methods described by Perrin and Armerego[135] were used to dry solvents; Et_2O, THF and toluene were dried over Na wire and benzophenone, and distilled under N_2; benzene was pre-dried over CaH_2 and then distilled from molecular sieves (4Å) under N_2; both DMF and DMSO were dried over molecular sieves (4Å) and then distilled under reduced pressure.

3.2.2. Synthesis of Kemp's Triacid Derivatives and Analogues

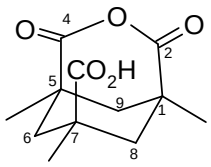

47

r-*1*,c-*5*,c-*7*-*Trimethyl-2,4-dioxo-3-oxabicyclo[3.3.1]nonane-7-carboxylic acid*[105] 47

A suspension of Kemp's triacid **43** (0.780 g, 3.02 mmol) in xylene (60 mL) was boiled under reflux in a flask fitted with a Dean-Stark trap, containing 5Å molecular sieves. After 18 hours the reaction mixture was cooled to room temperature and the solvent evaporated *in vacuo* to afford *r*-1,*c*-5,*c*-7-trimethyl-2,4-dioxo-3-oxabicyclo[3.3.1]-nonane-7-carboxylic acid **47** as white powder (0.270g, 37%), m.p. 207-210°C (lit.,[105] 252-254°C); ν_{max}(thin film)/cm^{-1} 3290-2787 (OH), 1769 and 1701 (C=O); δ_H (400MHz; DMSO-d_6) 1.13 (3H, s, 7-CH_3), 1.20 (6H, s, 1- and 5-CH_3), 1.35 (2H, d, J = 13.8Hz, 6- and 8-H_a), 1.43 (1H, d, J = 13.1 Hz, 9-H_a), 2.16 (1H, d, J = 13.1 Hz, 9-H_b) and 2.42 (2H, d, J = 13.6 Hz, 6- and 8-H_b); δ_C (100MHz; DMSO-d_6) 24.4 (7-CH_3), 29.7 (1- and 5-CH_3), 40.3 (C-7), 41.0 (C-9), 41.9 (C-1 and C-5), 44.0 (C-6 and C-8), 172.5 and 176.0 (C=O).

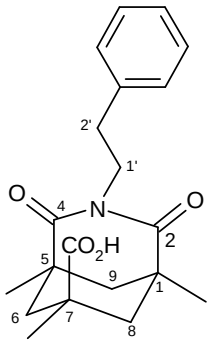

51

r-*1*,c-*5*,c-*7*-*Trimethyl-2,4-dioxo-3-phenethyl-3-azabicyclo[3.3.1]nonane-7-carboxylic acid* 51

Triethylamine (0.304 mL, 2.17 mmol) was added to a suspension of the acid anhydride **47** (200 mg, 0.830 mmol) and phenethylamine hydrochloride (160 mg, 0.996 mmol) in dichloromethane (2 mL) at 22°C. The resulting solution was stirred for 16h, then diluted with dichloromethane and washed sequentially with HCl (1N; 3

x 10 mL), brine (10 mL) and water (10 mL). The organic layer was separated and dried (anhydrous $MgSO_4$), and the solvent was evaporated *in vacuo* to afford an oily residue. The residue was crystallised from CH_2Cl_2-Et_2O (1:1) to afford r-*1*,c-*5*,c-*7*-*trimethyl-2,4-dioxo-3-phenethyl-3-azabicyclo[3.3.1]nonane-7-carboxylic acid* **51** as white crystals (94 mg, 36 %), m.p. 189-194^oC (Found $\mathbf{M}^+$: 343.18133. $C_{20}H_{25}O_4N$ requires *M*, 343.17836); ν_{max}(thin film)/cm^{-1} 3690-3081 (OH) and 1701 (C=O); δ_H (400MHz; $CDCl_3$) 0.82 (3H, s, 7-CH_3), 1.04 (2H, d, *J* = 14.3 Hz, 6- and 8-H_a), 1.21 (6H, s, 1- and 5-CH_3), 1.28 (1H, d, *J* = 13.3 Hz, 9-H_a), 1.81 (1H, d, *J* = 13.2 Hz, 9-H_b), 2.16 (1H, s, CO_2H), 2.53 (2H, d, *J* = 13.7 Hz, 6- and 8-H_b), 2.68 (2H, m, 2'-H), 3.61 (2H, m, 3'-H) and 7.19 (5H, m, ArH); δ_C (100MHz; $CDCl_3$) 25.3 (3- and 5-CH_3), 29.8 (1-CH_3), 33.5 (C-2 and C-6), 40.1 (C-1), 41.4 (C-4), 41.6 (C-3 and C-5), 43.4 (CH_2Ar), 43.9 (NCH_2), 126.2, 128.2, 129.0 and 138.7 (ArC), 175.9 (CO_2H) and 181.1 (2xNCO); *m/z* 343 (M^+, 40%) and 106 (100).

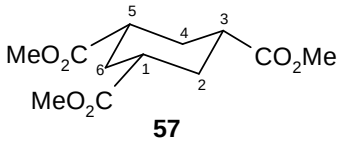

57

***Trimethyl cyclohexane*-r-*1*,c-*3*,c-*5*-*tricarboxylate*[108] 57**

A solution of cyclohexane-1,3,5-tricarboxylic acid **56** (2.16 g, 10.0 mmol) in dry methanol (50 mL) was added dropwise to thionyl chloride (3.34 mL) under argon. The stirred reaction mixture was boiled under reflux for 16 hrs. The resulting mixture was cooled to room temperature, and water (50 mL) was carefully added while cooling the flask in an ice bath. The aqueous solution was extracted with ethyl acetate (2 x 50 mL). The combined organic solutions and washings were dried (anhydrous Na_2SO_4) and concentrated *in vacuo* to afford trimethyl cyclohexane-*r*-1,*c*-3,*c*-*5*-tricarboxylate **57** as white crystals (1.56g, 60%), m.p. 40-43^oC (lit.[108] m.p. 48-49^oC); ν_{max} (thin film)/cm^{-1} 1743 (C=O); δ_H (400MHz; $CDCl_3$) 1.47 (3H, q, *J* = 12.8Hz, 2-, 4- and 6-H_a) 2.21 (3H, d, *J* = 12.6Hz, 2-, 4- and 6-H_b), 2.34 (3H, tt, *J* = 3.4 and 12.5Hz, 1-, 3- and 5-H) and 3.62 (9H, s, 3xOCH_3); δ_C (100MHz; $CDCl_3$) 30.3 (C-2, C-4 and C-6), 41.6 (C-1, C-3 and C-5), 51.7 (CO_2CH_3) and 174 (CO_2CH_3).

***Attempted synthesis of trimethyl cis,cis-1,3,5-trimethylcyclohexane-1,3,5-tricarboxylate (Kemp's triacid precursor).*[108]**

Method A.

A solution of triester **57** (300 mg, 1.16 mmol) in Et_2O (3 mL) was added drop-wise to a solution of LDA [prepared by the addition of BuLi (1.6 M, 2.5 mL) to a solution of diisopropylamine (1 mL) in Et_2O] at 0^oC under argon. The resulting solution was stirred for 2 hours at 0^oC, then dimethyl sulphate (0.8 mL) was added to the reaction mixture, and stirring was continued overnight at room temperature. The organic solution was washed sequentially with water (10 mL), aq. HCl (1 M, 5 mL), brine (10 mL) and water (10 mL). The organic extracts were dried (anhydrous Na_2SO_4) and concentrated *in vacuo*. The residue was crystallised from pentane-Et_2O.

Method B.

A similar procedure to that described for *Method A* was followed, using a solution of commercial LDA (2.5 M, 1.5 mL), triester **57** and dimethyl sulphate (0.8 mL). In both methods no crystals were formed in crystallisation step, moreover, no new methyl signals were observed in the ^1H NMR spectrum of the crude material collected after work-up.

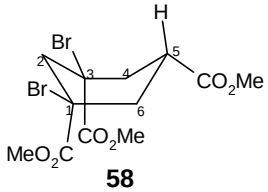

58

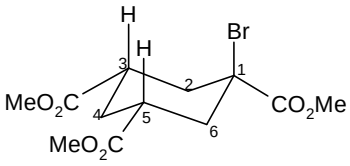

59

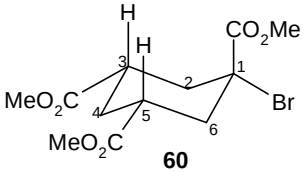

60

***Trimethyl* r-*1*,c-*3*-*dibromocyclohexane*-*1,3*,t-*5*-*tricarboxylate* 58, *trimethyl* r-*1*-*bromocyclohexane*-*1*,t-*3*,t-*5*-*tricarboxylate* 59 and *trimethyl* r-*1*-*bromocyclohexane*-*1*,c-*3*,c-*5*-*tricarboxylate* 60**

Ammonium acetate (23.2 mg, 0.300 mmol) was added to a mixture of trimethyl cyclohexane-1,3,5-tricaboxylate **57** (250 mg, 0.968 mmol) and NBS (534 mg, 3.00 mmol) in CCl_4 (5.00 mL). The resulting mixture was boiled under reflux. After 5 h., the reaction mixture was cooled to room temperature, diluted with CCl_4 (5 mL) and filtered. The filter cake was washed with a small amount of CCl_4. The filtrate and washings were washed with water, dried (anhydrous $MgSO_4$) and concentrated *in*

vacuo. The crude residue was first passed through a short pad of silica gel (elution with ethyl acetate) and then separated by radial chromatography [elution with hexane-ethyl acetate (4:1)] to afford trimethyl cyclohexane-1,3,5-tricaboxylate **57** as white crystals (100mg, 40 %) and a mixture, which was chromatographed further [HPLC on Partisil 10; elution with hexane:ethyl acetate (4:1)] to afford three fractions.
i) *Trimethyl* r-*1,*c-*3-dibromocyclohexane-1,3,*t-*5-tricarboxylate* **58,** as white paste (Found $\mathbf{M}^+$: 415.92941. $C_{12}H_{16}O_6{}^{79}Br^{81}Br$ requires *M,* 415.92931); ν_{max}(thin film)/cm^{-1} 1739 (C=O); δ_H (400MHz; $CDCl_3$) 2.10 (2H, m, 4- and 6-H_a), 2.71 (1H, d, *J* = 13.7Hz, 2-H_a), 2.87 (1H, tt, *J* = 3.4 and 13.0Hz, 5-H), 3.03 (2H, m, 4- and 6-H_b), 3.71 (3H, s, 5-CO_2CH_3), 3.74 (6H, s, 2xCO_2CH_3) and 3.82 (1H, m, 2-H_b); δ_C (100MHz; $CDCl_3$) 40.0 (C-4 and C-6), 40.4 (C-5), 48.9 (C-2), 52.2 (5-CO_2*C*H_3), 53.4 (2xCO_2*C*H_3), 54.6 (2xCBr), 170.0 and 171.9 (C=O); *m/z* 417 ($M^+(Br_2)^{81}$, 54.2%) and 303 (100).

b) Ttrimethyl r-*1-bromocyclohexane-1,*t-*3,*t-*5-tricarboxylate* **59** as a colourless oil (trace amount); δ_H (400MHz; $CDCl_3$) 1.58 (1H, m, 4-H_a), 2.06 (2H, t, *J* = 12.1 Hz, 2- and 6-H_a) 2.29 (1H, m, 4-H_b), 2.38 (2H, tt, 3.4 and 5.8Hz, 3- and 5-H) 3.03 (2H, m, 2- and 6-H_b), 3.70 (6H, s, 2xCO_2CH_3) and 3.83 (3H, s, 1-CO_2CH_3); δ_C (100MHz; $CDCl_3$) 29.9 (C-4), 40.0 (C-2 and C-6), 41.0 (C-3 and C-5), 52.1 (2xCO_2*C*H_3), 53.4 (1-CO_2*C*H_3), 56.1 (C-1), 170 and 173 (C=O).

c) Trimethyl r-*1-bromocyclohexane-1,*c-*3,*c-*5-tricarboxylate* **60** as **a** colourless oil (trace amount); δ_H (400MHz; $CDCl_3$) 1.49 (1H, m, 4-H_a), 1.79 (2H, d, *J* = 12.3Hz, 2- and 6-H_a), 2.37 (1H, m, 4-H_b) 2.65 (2H, m, 2- and 6-H_b), 2.95 (2H, tt, *J* = 3.5 and 5.5Hz, 3- and 5-H), 3.71 (6H, s, 2xCO_2CH_3) and 3.83 (3H, s, 1- CO_2CH_3); δ_C (100MHz; $CDCl_3$) 30.3 (C-4), 37.9 (C-2 and C-6), 38.8 (C-3 and C-5), 52.0 (2xCO_2*C*H_3), 53.3 (1-CO_2*C*H_3), 61.7 (C-1), 171 and 174 (C=O).

***Attempted α-fluorination of triester* 57**

A solution of triester **57** (1.00 g, 4.00 mmol) in dry THF (15 mL) was added drop-wise to sodium hydride (117 mg, 4.88 mmol) under argon. The suspension was stirred for 1 h at room temperature, then [1-(chloromethyl)-4-fluoro-1,4-diazoniabicyclo[2.2.2]-octanebis(tetrafluoroborate)] (Selectfluor™) (1.42 g,

4.00 mmol) was added to the reaction mixture. The resulting suspension was stirred overnight at room temperature. The reaction was quenched with water (10 mL) followed by extraction with ethyl acetate (2 x 20 mL). The combined organic extracts were washed sequentially with water (20 mL), a saturated aqueous solution of $NaHCO_3$ (20 mL), brine (20 mL), and water (20 mL) and then dried (anhydrous $MgSO_4$). The solvent was removed *in vacuo* to afford an inseparable mixture of unknown compounds.

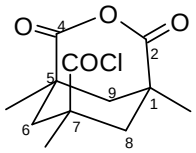

53

r-*7-(Chloroformyl)*-t-*1,*t-*5,7-trimethyl-2,4-dioxo-3-oxabicyclo[3.3.1]nonane*[136] 53

A mixture of Kemp's triacid **43** (1.00 g, 3.88 mmol) and $SOCl_2$ (20 mL, 0.27mol) was boiled for 8 h in a flask fitted with a condenser and a drying tube containing anhydrous $CaCl_2$. The reaction mixture was distilled, and the resulting brown solid was recrystallised from dry toluene to afford *r*-7-(chloroformyl)-*t*-1,*t*-5,7-trimethyl-2,4-dioxo-3-oxabicyclo[3.3.1]nonane **53,** as white crystals (613 mg, 64%), m.p. 215-225°C (lit.[136] 255-260°C); δ_H (400MHz; DMSO-d_6) 1.13 (3H, s, 7-CH_3), 1.20 (6H, s, 1- and 5-CH_3), 1.37 (2H, d, J = 14.0Hz, 6- and 8-H_a), 1.43 (1H, d, J = 13.2Hz, 9-H_a), 2.14 (1H, d, J = 13.2Hz, 9-H_b) and 2.40 (2H, d, J = 13.2Hz, 6- and 8-H_b); δ_C (100MHz; DMSO-d_6) 24.5 (1- and 5-CH_3), 29.8 (7-CH_3), 39.5 (C-6 and C-8), 40.2 (C-7), 41.1 (C-1 and C-5), 43.1 (C-9), 171.7 and 176.2 (C=O).

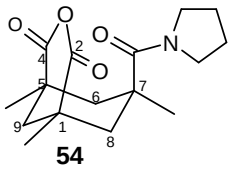

54

***Attempted synthesis of* r-*1,*c-*5,*c-*7-trimethyl*-t-*7-(1-pyrrolidinylcarbonyl)-3-oxabicyclo[3.3.1]nonane-2,4-dione*[107] 54**

Dry pyridine (6.8 mL) was added to a suspension of acid chloride **53** (620 mg, 2.52 mmol) in dry acetonitrile (50 mL) under argon. The mixture was cooled to -40°C and then pyrrolidine (5.0 mL, 60 mmol) was added and the resulting mixture stirred at

room temperature for 16 h. The solvent was removed under reduced pressure to afford a crude product which was chromatographed [flash chromatography, elution hexane-ethyl acetate (9: 1)] to afford a fraction with no identifiable product.

3.2.3. Synthesis of Camphor Derivatives

3.2.3.1. Synthesis of halogenated camphor derivatives

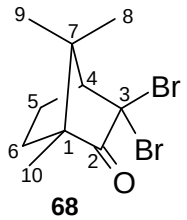

68

***(1*R*,4*S*)-(+)-3,3-Dibromocamphor*[137] 68**

A mixture of (+)-3-bromocamphor **67** (27.5 g, 0.119 mmol) and bromine (9.00 mL, 0.175 mol) was heated at 50^{o}C for 24 hours in the dark in a round-bottomed flask fitted with a condenser. The reaction mixture was cooled to room temperature before it was diluted with diethyl ether (100 ml) and water (100 ml). Excess bromine was removed by the addition of sodium metabisulphite. The aqueous layer was extracted with diethyl ether and the combined organic solutions were dried (anhydrous $MgSO_4$). The solvent was evaporated *in vacuo* to afford (1*R*,4*S*)-(+)-3,3-dibromocamphor **68,** as colourless crystals (35.29 g, 95.7%), m.p. 57-60 ^{o}C (lit.[137], 60^{o}C); $[\alpha]_D^{30}$ = 35.3^{o} (*c* 1.05, $CHCl_3$) {lit.[137] $[\alpha]^{26}$ = 37.1^{o} (*c* 1.67, EtOH}; δ_H (400MHz, $CDCl_3$) 1.02 (s, 3H, 10-CH_3), 1.11 (s, 3H, 9-CH_3), 1.24 (s, 3H, 8-CH_3), 1.64 (2H, m, 6-CH_2), 2.05 (1H, m, 5-H_a), 2.31 (1H, m, 5-H_b) and 2.81 (1H, d, *J* = 4.0Hz, 4-H); δ_C (100MHz; $CDCl_3$) 10.3 (C-10), 22.5 (C-9), 24.0 (C-8), 29.0 (C-6), 29.1 (C-5), 46.1 (C-1), 57.7 (C-7), 59.5 (C-4), 63.4 (C-3) and 206 (C-2).

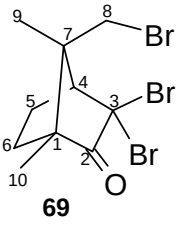

69

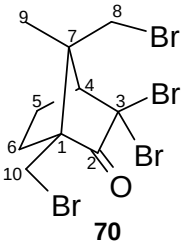

70

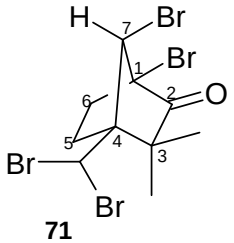

71

***(1*R*,4*S*,7*S*)-(+)-3,3,8-Tribromocamphor*[114] 69*, *(1*S*,4*S*,7*S*)-(+)-3,3,8,10-tetrabromocamphor* 70 and *(1*S*,4*R*,7*R*)-(-)-1,7-dibromo-4-dibromomethyl-3,3-dimethylnorbornan-2-one* 71**

(+)-3,3-Dibromocamphor **68** (8.62 g, 0.280 mmol) was dissolved in a cooled solution of bromine (2.25 mL) in chlorosulphonic acid (12.5 mL). The reaction mixture was stirred for 5 hours at room temperature, and then carefully added to ice water (*ca.* 100mL). The excess acid was neutralised with sodium hydrogen carbonate and the excess Br_2 destroyed with sodium bisulphite. The resulting aqueous mixture was extracted with diethyl ether (3 x 100 mL) and the combined organic extracts were dried (anhydrous $MgSO_4$). The solvent was removed *in vacuo* to afford a viscous dark-brown oil (9.70 g), which was used in the next step without further purification.

However, in order to obtain an analytical sample, the crude product (1.00 g) was eluted through a short pad of silica using using hexane-ethyl acetate (9:1). Further chromatography [HPLC on Partsil 10; elution with hexane-ethyl acetate (19:1)] afforded three fractions.

i) (1*R*,4*S*,7*S*)-(+)-3,3,8-Tribromocamphor **69**, as a pale-yellow oil, $[\alpha]_D^{22} = +70.5^o$ (*c* 1.2, $CHCl_3$) {lit.[113] $[\alpha]_D = +71.5^o$ (*c* 1.00, $CHCl_3$)}; δ_H (400MHz, $CDCl_3$) 1.03 (3H, s, 10-CH_3), 1.29 (3H, s, 9-CH_3), 1.78 (2H, m, 6-CH_3), 2.05 (1H, m, 5-H_a), 2.36 (1H, m, 5-H_b), 3.08 (1H, d, *J* = 4.1Hz, 4-H), 3.30 (1H, d, *J* = 11.0Hz, 8-H_a) 3.71 (1H, d, *J* = 11.0Hz, 8-H_b); δ_C (100MHz, $CDCl_3$) 10.3 (C-10), 20.2 (C-9), 28.4 (C-5), 31.1 (C-6), 41.1 (C-8), 50.8 (C-3), 56.6 (C-4), 57.5 (C-7), 61.0 (C-1) and 205.5 (C-2).

ii) (1*S*,4*S*,7*S*)-(+)-3,3,8,10-Tetrabromocamphor **70**, a brown oil; $[\alpha]_D^{22} = 22.2^o$ (*c* 0.21, $CHCl_3$) {lit.[113] $[\alpha] = +55.9^o$ (*c* 1.00 $CHCl_3$); δ_H (400MHz, $CDCl_3$) 1.42 (3H, s, 9-CH_3), 1.90 (2H, m, 6-CH_2), 2.12 (1H, m, 5-H_a), 2.43 (1H, m, 5-H_b), 3.13 (1H, d, *J* = 3.6Hz, 4-H), 3.38 (1H, d, *J* = 11.5Hz, 8-H_a), 3.47 (1H, d, *J* = 11.0Hz, 10-H_a), 3.56

(1H, d, *J* = 11.5Hz, 8-H_b), 3.77 (1H, d, *J* = 11.0Hz, 10-H_b); δ_C (100 MHz, $CDCl_3$) 21.6 (C-9), 29.9 (C-10), 28.0 (C-5), 29.3 (C-6), 40,3 (C-8), 52.0 (C-7), 57.3 (C-4), 59.3 (C-1), 60.3 (C-3) and 202.2 (C-2); *m/z* 468 (M^+, 1.6%), 279 (100).

iii) (1*S*,4*R*,7*R*)-(-)-1,7-Dibromo-4-dibromometyl-3,3-dimethylnobornan-2-one **71,** as white crystals, m.p. 123-127°C (lit.[137] 127-127.5°C) (Found $\mathbf{M}^+$: 467.75619. $C_{10}H_{12}O^{79}Br_2{}^{81}Br_2$ requires *M*, 467.75619), δ_H (400MHz, $CDCl_3$) 1.42 (3H, s, 3-CH_3), 1.56 (3H, s, 3-CH_3) 2.30 (2H, m, 6-H), 2.42 (2H, m, 5-H), 4.43 (1H, s, 7-H), 6.08 (1H, s, $CHBr_2$); δ_C (100MHz, $CDCl_3$) 22.0 (3-CH_3), 26.1 (6-CH_2), 26.5 (3-CH_3), 32.4 (5-CH_2) 46.4 (7-CH), 50.0 (3-C), 56.2 (1-C), 63.5 ($CHBr_2$), 69.6 (4-C) and 208.0 (C=O); *m/z* 468 (M^+, 17.8%) and 317 (100);

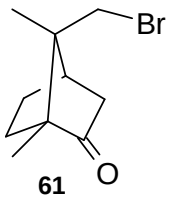

61

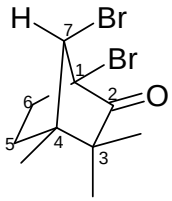

72

***(1*R*,4*S*,7*S*)-(+)-8-Bromocamphor*[114] 61 and *(1*S*,4*R*,7*R*)-(-)-3,3,4-trimethyl-1,7-dibromonorbornan-2-one* 72**

Zinc dust (4.4 g) was added cautiously to a cooled (ice-bath) solution of crude 3,3,8-tribromocamphor **69** (19.0 g, 48.8 mmol) in glacial acid (100 mL). The resulting suspension was stirred at room temperature for 1 hour. After the zinc salt had settled, the organic solution was decanted and the salt washed with Et_2O (3x100 mL). The combined organic solutions were washed with water (10 x 50 mL) and dried (anhydrous $MgSO_4$). Removal of the solvent *in vacuo* afforded a brown oil which was chromatographed [flash chromatography on silica; elution with hexane-ethyl acetate (9: 1)] to afford two fractions.

i) (1*R*,4*S*,7*S*)-(+)-8-Bromocamphor **61,** as pale yellow oil (7.65 g, 38%). An analytical sample was obtained by further chromatography [HPLC on Partsil 10; elution with hexane-ethyl acetate (19:1)] to afford (+)-8-bromocamphor **61** as white crystals, m.p. 69-75°C (lit.,[137] 83-85°C); $[\alpha]_D{}^{22}$ = 74.2° (*c* 1.0, $CHCl_3$) {lit.,[137] $[\alpha]_D{}^{25}$ = 76.7° (*c* 1.24,

$CHCl_3$)}; δ_H (400MHz; $CDCl_3$) 0.91 (3H, s, 10-CH_3), 1.13 (3H, d, *J* = 0.82Hz, 9-CH_3), 1.38 (1H, m, 6-H_a), 1.56 (1H, m, 5-H_a), 1.81 (1H, m, 5-H_b), 1.91 (1H, m, 6-H_b) 1.95 (1H, d, *J* = 18.4Hz, 3-H_a), 2.39 (1H, m, 3-H_b), 2.44 (1H, t, *J* = 4.4Hz, 4-H), 3.10 (1H, dd, *J* = 0.93, 10.9Hz, 8-H_a) and 3.16 (1H, d, *J* = 10.9Hz, 8-H_b); δ_C (100MHz; $CDCl_3$) 9.4 (C-10), 15.6 (C-9), 26.3 (C-6), 31.8 (C-5), 39.5 (C-8), 41.1 (C-4), 42.4 (C-3), 51.5 (C-1), 58.2 (C-7) and 217.8 (C-2); *m/z* 232 (M^+,100).

ii) (1*S*,4*R*,7*R*)-(-)-3,3,4-Trimethyl-1,7-dibromonorbornan-2-one **72** (6% - based on sample from the HPLC), m.p. 116-120°C (lit.,[137] 123-124°C); δ_H (400MHz; $CDCl_3$) 1.08, 1.23 and 1.39 (9H, 3 x s, 3 x CH_3), 1.71 (1H, m, 5-H_a), 2.11 (2H, m, 5-H_b and 6-H_a), 2.31 (1H, m, 6-H_b) and 4.22 (1H, s, 7-H); (100MHz; $CDCl_3$) 15.8 (C-8), 23.4 (C-10), 24.6 (C-9), 31.9 (C-5), 33.5 (C-6), 47.5 (C-4), 47.9 (C-3), 65.2 (C-7), 71.6 (C-1) and 210.7 (C-2); *m/z* 308 (M^+, 41%) and 161 (100).

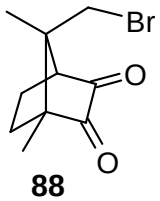

88

***(1*R*,4*R*,7*S*)-(-)-8-Bromocamphorquinone* 87**

8-Bromocamphor **61** (4.10 g, 17.7 mmol) was dissolved in glacial acetic acid (25 mL). Selenium dioxide (6.30 g, 56.0 mmol) was added and the resulting suspension was boiled under reflux for 12 hours with stirring. After cooling to room temperature, the black residue was filtered off and washed with methanol. The yellow filtrate and the washings were combined. The volatile organics were evaporated *in vacuo* at *ca.* 50°C. The residue was dissolved in ethyl acetate and washed sequentially with water, saturated aqueous $NaHCO_3$ and water. The aqueous phase was rendered slightly alkaline and extracted repeatedly with ethyl acetate. The organic extracts were combined and dried (anhydrous Na_2SO_4) and solvent evaporated *in vacuo*. The residue was chromatographed [flash chromatography; elution hexane-ethyl acetate (3: 1)] to afford (1*S*,4*R*,7*S*)-(-)-8-bromocamphorquinone **88,** as a yellow powder (3.62g, 83%), m.p. 80-85°C (lit.,[113] 95-96°C) (Found **M**$^+$: 246.00488. $C_{10}H_{13}O_2{}^{81}Br$

requires *M*, 246.00784); ν_{max} (thin film)/cm^{-1} 1758 and 1750 (C=O); $[\alpha]_D^{22}$ = -70.9° (*c* 1.1, $CHCl_3$) {lit.[113] = -79.3° (*c* 1.00, $CHCl_3$)}; δ_H (400MHz, $CDCl_3$) 1.13 (3H, s, 10-CH_3), 1.24 (3H, s, 9-CH_3), 1.67 (1H, m, 5-H_a), 1.78 (1H, m, 6-H_a), 2.03 (1H, m, 6-H_b), 2.16 (1H, m, 5-H_b), 2.97 (1H, s, 4-H), 2.99 (1H, d, *J* 8.8 Hz, 8-H_a) and 3.31 (1H, d, *J* 8.8 Hz, 8-H_b); δ_C (100MHz, $CDCl_3$) 9.2 (C-10), 14.4 (C-9), 21.9 (C-5), 31.7 (C-6), 38.0 (C-8), 47.7 (C-7), 56.3 (C-4), 59.3 (C-1), 201.2 (C-3) and 203.0 (C-2).

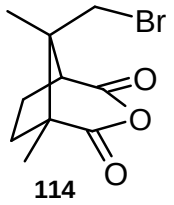

114

***(1*R*,4S,7S)-(+)-8-Bromocamphoric anhydride* 114**

A aqueous H_2O_2 (30%; 15.0 mL) was added to a solution of 8-bromocamphor **61** (0.700 g, 2.86 mmol) in glacial acetic acid (30 mL) in round-bottomed flask. The resulting solution was stirred for 24 hours at room temperature and then added to water (50 mL). The aqueous mixture was extracted with diethyl ether (3 x 50mL). The combined organic extracts were washed with water (10 x 50.0mL), and concentrated *in vacuo*. Water (20 mL) was added to the residue to precipitate the product which was filtered off and dried under reduced pressure to afford (1*R*,4*S*,7*S*)-(+)-8-bromocamphoric anhydride **114,** as a white powder (0.564g, 76%), m.p. 130-135°C (lit.[101], 132-136°C); ν_{max}(thin film)/cm^{-1} 1808 and 1768 (C=O); $[\alpha]_D^{22}$ = 16° (1.3, $CHCl_3$) {lit.[101] = +34.2° (*c* 0.19, $CHCl_3$)}; δ_H (400MHz, $CDCl_3$) 1.20 (3H, s, 9-CH_3), 1.29 (3H, s, 10-CH_3), 1.98 (1H, m, 6-H_a), 2.14 (1H, m, 5-H_a) 2.25 (1H, m, 5-H_b), 2.28 (1H, m, 6-H_b), 3.15 (1H, d, *J* = 6.8Hz, 4-H), 3.29 (1H, d, *J* = 20.0Hz, 8-H_a) and 3.32 (1H, d, *J* = 20.0Hz, 8-H_b); δ_C (100MHz, $CDCl_3$) 14.2 (C-10), 17.1 (C-9), 23.6 (C-6) 34.8 (C-5), 38.0 (C-8), 48.1 (C-1), 52.1 (C-4), 53.3 (C-7), 169.0 (C-3) and 172.1 (C-2).

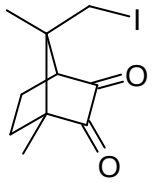

89

***(1*R*,4*S*,7*S*)-(-)-8-Iodocamphorquinone* 89**

A solution of 8-bromocamphorquinone **89** (4.00 g, 16.3 mmol) and KI (13.5 g) in DMF (50 mL) was stirred under argon at 110°C overnight. The mixture was then cooled to room temperature, diluted with water (200 mL) and extracted with diethyl ether (2 x 100 mL). The organic extracts were combined, washed with water (3 x 100 mL), dried (anhydrous Na_2SO_4) and concentrated *in vacuo*. The residue was chromatographed [flash chromatography; elution with hexane-ethyl acetate (3:1)] to afford *(1*R,*4*S,*7*S*)-8-iodocamphorquinone* **89,** as yellow crystals (1.50 g, 27.3%), m.p. 78-85°C (Found $\mathbf{M}^+$: 291.99603. $C_{10}H_{13}O_2I$ requires *M*, 291.99603); $[\alpha]_D^{22}$ = -76.5° (*c* 1.1, $CHCl_3$), ν_{max}(thin film)/cm^{-1} 1754 (C=O); δ_H (400MHz; $CDCl_3$) 1.13 (3H, s, 10-CH_3), 1.23 (3H, d, *J* = 1.0Hz, 9-CH_3), 1.66 (1H, m, 5-H_a), 1.87 (1H, m, 6-H_a), 2.10 (2H, m, 5-H_b and 6-H_b), 2.76 (1H, dd, *J* = 1.0, 11.1Hz, 8-H_a), 2.89 (1H, d, *J* = 5.1Hz, 4-H), 3.14 (1H, d, *J* = 11.1Hz, 8-H_b); δ_C (100MHz; $CDCl_3$) 9.02 (C-10), 11.9 (C-8), 16.3 (C-9), 21.5 (C-5), 32.7 (C-6), 46.8 (C-7), 58.3 (C-4), 58.6 (C-1), 201.2 and 203.3 (C=O); *m/z* 292 (100%).

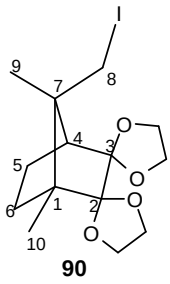

90

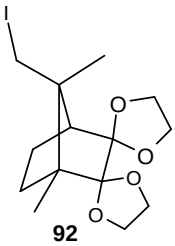

92

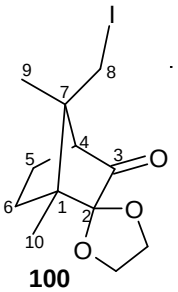

100

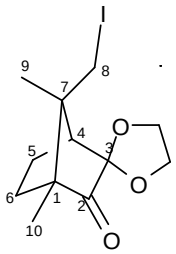

101

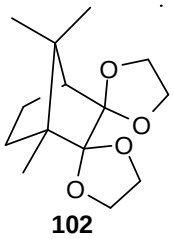

102

***(1*R*,4*S*,7*S*)-(+)-8-Iodocamphorquinone bis(ethylene ketal)* 90*, (1*R*,4*S*,7*R*)-(+)-9-iodocamphorquinone bis(ethylene ketal)* 92*, (1*R*,4*S*,7*S*)-(-)-2,2-(ethylenedioxy)-8-iodocamphorquinone* 100*, (1*R*,4*S*,7*S*)-(+)-3,3-(ethylenedioxy)-8-iodocamphorquinone* 101 and *camphorquinone bis(ethylene ketal)* 102.**

A mixture of 8-iodocamphorquinone **89** (1.30 g, 4.44 mmol), ethylene glycol (13.4 mL) *p*-toluenesulfonic acid (1.40 g, 6.83 mmol) and benzene (42 mL) was boiled under reflux under nitrogen in a flask fitted with a Dean-Stark trap, containing

5Å molecular sieves. After 5 days, the mixture was cooled to room temperature, diluted with diethyl ether (100 mL), washed sequentially with brine (100 mL) and water (3 x 100 mL) and dried (anhydrous Na_2SO_4). The solvent was removed *in vacuo*, and the crude product was chromatographed on silica [flash chromatography; elution with hexane-ethyl acetate (3:1)] to afford *(1*R,*4*S,*7*S)*-(+)-8-iodocamphorquinone bis(ethylene ketal)* **90** (400 mg, 24%) as white crystals. An analytical sample was prepared by further chromatography [HPLC on Partsil 10; elution with hexane-ethyl acetate 4:1] to afford *(1*R,*4*S,*7*S)*-(+)-8-iodocamphorquinone bis(ethylene ketal)* **90,** m.p. 98-104^{o}C (Found $\mathbf{M}^+$: 253.14204. $C_{14}H_{21}O_4$ – I requires *M*, 253.14398); ν_{max}(thin film)/cm^{-1} 1032 and 1018 (C-O-C); $[\alpha]_D^{22}$ = +15.8^o (*c* 1.00, $CHCl_3$); δ_H (400MHz; $CDCl_3$) 0.82 (3H, s, 10-CH_3), 1.10 (3H, d, *J* = 1.1Hz, 9-CH_3), 1.56 (2H, m, 5H_a and 6-H_a), 1.78 (1H, m, 6-H_b), 1.98 (1H, d, *J* = 4.2Hz, 4-H), 2.20 (1H, m, 5-H_b), 3.13 (1H, d, *J* = 9.7 Hz, 8-H_a), 3.92 (8H, m, 2xOCH_2CH_2O) and 4.33 (1H, dd, *J* = 1.2 and 9.7Hz, 8-H_b); δ_C (100MHz; $CDCl_3$) 9.89 (C-10), 19.5 (C-9), 19.8 (C-6), 20.7 (C-8), 31.9 (C-5), 48.5 (C-7), 51.9 (C-4), 53.2 (C-1), 64.2, 64.6, 65.2 and 66.1 (2xOCH_2CH_2O), 113.0 (C-3) and 113.5 (C-2); *m/z* 380 (M^+, 9.2%) and 253 (100);

The residual material from flash chromatography was chromatographed further [HPLC on Partisil 10; elution hexane-EtOAc (4:1)] to afford three fractions.
i) *(1*R,*4*S,*7*R*)-(+)-9-Iodocamphorquinone bis(ethylene ketal)* **92** as white crystals (102mg, 6%), m.p. 57-60^{o}C; ν_{max} (thin film)/cm^{-1} 1096 and 1124 (C-O-C); $[\alpha]_D^{22}$ = +6.4^o (*c* 1.00, $CHCl_3$); δ_H (400MHz; $CDCl_3$) 0.83 (3H, s, 10-CH_3), 1.34 (3H, s, 8-CH_3), 1.46 (2H, m, 5H_a and 6-H_a), 1.83 (1H, m, 6-H_b), 1.87 (1H, d, *J* = 4.0Hz, 4-H), 2.06 (1H, m, 5-H_b), 2.96 (1H, d, *J* = 9.7Hz, 9-H_a), 3.42 (1H, dd, *J* = 1.3 and 9.7Hz, 9-H_b) and 3.92 (8H, m, 2xOCH_2CH_2O); δ_C (100MHz; $CDCl_3$) 10.1 (C-10), 18.5 (C-8), 18.8 (C-9), 20.6 (C-6), 29.1 (C-5), 48.5 (C-7), 52.6 (C-4), 53.7 (C-1), 64.4, 64.6, 65.0 and 66.0 (2xOCH_2CH_2O), 113.0 (C-3) and 115.6 (C-2); *m/z* 380 (M^+, 17.6%) and 253 (100)

ii) *(1*R,*4*S,*7*S*)-(+)-2,2-(Ethylenedioxy)-8-iodocamphorquinone* **100** as yellow oil (19.4 mg, 1.4%), (Found $\mathbf{M}^+$: 307.02175 $C_{11}H_{16}O_2I$ – CH_2O requires *M*, 307.01951); ν_{max}(thin film)/cm^{-1} 1749 (C=O); $[\alpha]_D^{22}$ = +137^o (*c* 1.9 $CHCl_3$); δ_H (400MHz; $CDCl_3$) 0.92 (3H, s, 10-CH_3), 1.16 (3H, d, *J* = 1.0Hz, 9-CH_3), 1.90 (4H, m, 5-CH_2 and 6-

CH_2), 2.23 (1H, d, *J* = 3.9Hz, 4-H), 3.07 (1H, d, *J* = 9.9Hz, 8-H_a), 3.43 (1H, dd, *J* = 1.1 and 9.9Hz, 8-H_b) and 4.16 (4H, m, OCH_2CH_2O); δ_C (100MHz; $CDCl_3$) 9.2 (C-10), 16.5 (C-8), 18.2 (C-9), 20.3 (C-6), 33.7 (C-5), 47.8 (C-7), 50.9 (C-4), 58.2 (C-1), 64.7 and 66.3 (OCH_2CH_2O), 106.4 (C-2) and 215.9 (C=O).

iii) *(1*R,*4*S,*7*S*)-(-)-3,3-(Ethylenedioxy)-8-iodocamphorquinone* **101** (trace amount) as pale yellow oil; ν_{max} (thin film)/cm^{-1} 1757 (C=O); $[\alpha]_D^{22}$ = -16.0 (*c* 0.12 $CHCl_3$); δ_H (400MHz; $CDCl_3$) 1.07 (3H, s, 10-CH_3), 1.08 (3H, s, 9-CH_3), 1.76-2.06 (5H, series of overlapping multiplets, 4-H, 5-CH_2 and 6-CH_2), 3.05 (1H, d, *J* = 10.5Hz, 8-H_a), 3.25 (1H, d, *J* = 10.5Hz, 8-H_b), 4.17 (4H, m, OCH_2CH_2O); δ_C (100MHz; $CDCl_3$) 11.4 (C-8), 18.7 (C-10), 19.4 (C-9) 20.0 (C-6), 31.5 (C-5), 45.1 (C-7), 52.7 (C-4), 59.7 (C-1), 64.5 and 66.3 (OCH_2CH_2O), 106.4 (C-2) and 213.3 (C=O).

iv) Camphorquinone bis(ethylene ketal) **102,** as colourless crystals (trace amount), m.p. 59-63°C; ν_{max}(thin film)/cm^{-1} 1155 and 1115 (C-O); δ_H (400MHz; $CDCl_3$) 0.80, 0.87 and 1.18 (9H, 3xs, 8-, 9- and 10-CH_3), 1.31-2.00 (4H, series of multiplets, 5- and 6-CH_2), 1.68 (1H, d, *J* = 4.6, 4-H), 3.74-4.00 (8H, m, 2xOCH_2CH_2O); δ_C (100MHz; $CDCl_3$) 9.86 (C-9), 20.7 (C-10), 21.0 (C-8), 21.1 (C-5), 29.3 (C-6), 44.5 (C-7), 52.7 (C-1), 53.3 (C-4), 64.2, 64.5, 65.0 and 65.9 (OCH_2CH_2O), 113.5 (C-3) and 114.7 (C-2).

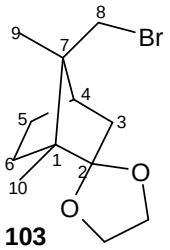

103

***(1*R,*4*R,*7*S*)-(+)-8-Bromocamphor ethylene ketal* 102**

Method A.[120]

Chlorotrimethylsilane (6 mL) was added to a solution of 8-bromocamphor **61** (2.60 g, 11.3 mmol) in ethylene glycol (5.6 mL) under argon, and the resulting mixture was stirred for 7 hours at room temperature. The reaction flask was cooled in an ice-bath and water (10 mL) was added to the reaction mixture. The mixture was then diluted

with Et_2O (100 mL), washed sequentially with brine (100 mL), water (100 mL) and dried (anhydrous $NaSO_4$). The solvent was removed *in vacuo*, and the residue was chromatographed on silica [flash chromatography; elution with hexane-ethyl acetate (4:1)] to afford (1*R*,4*R*,7*S*)-(+)-8-bromocamphor ethylene ketal **103** (1.22 g, 40%) as pale yellow oil.

Method B.[112]

A mixture of 8-bromocamphor **61** (2.00 g, 13.2 mmol), ethylene glycol (15.0 mL), *p*-toluenesulfonic acid monohydrate (2.70 g, 13.1 mmol) and benzene (50 mL) was boiled under reflux in a flask fitted with a Dean-Stark trap, containing 5Å molecular sieves. After 5 days, the mixture was cooled to room temperature, diluted with diethyl ether (100 mL), washed sequentially with saturated brine (100 mL) and water (3 x 100 mL) and dried (anhydrous Na_2SO_4). The solvent was removed *in vacuo*, and the crude product was chromatographed on silica [flash chromatography; elution with hexane-ethyl acetate (4:1)] to afford (1*R*,4*R*,7*S*)-(+)-8-bromocamphor ethylene ketal **101** (1.1g, 46%) as a yellow oil; ν_{max}(thin film)/cm^{-1} 1133 (C-O); $[\alpha]_D^{22} = 9.0^o$ (*c* 1.9, $CHCl_3$), {lit.[120] $[\alpha]_D^{25} = 12.1$ (*c* 1.02, $CHCl_3$)}; δ_H (400MHz; $CDCl_3$) 0.81 (3H, s, 10-CH_3), 1.06 (3H, s, 9-CH_3), 1.26 (1H, m, 6-H_a), 1.48 (2H, m, 3-H_a and 5-H_a), 1.70 (1H, m, 6-H_b), 2.04 (3H, m, 3-H_b, 4-H and 5-H_b), 3.23 (1H, d, *J* = 10.6 Hz, 8-H_a), 3.89 (4H, m, OCH_2CH_2O) and 4.22 (1H, d, *J* = 10.6 Hz, 8-H_b); δ_C (100MHz; $CDCl_3$) 9.83 (C-10), 16.5 (C-9), 26.3 (C-6), 31.1 (C-5), 42.5 (C-8), 43.2 (C-4), 44.1 (C-3), 52.8 (C-7), 53.9 (C-1), 63.9 and 65.0 (OCH_2CH_2O) and 116.3 (C-2); *m/z* 274 (100).

3.2.3.2. Synthesis towards camphor-derived phosphine ligands

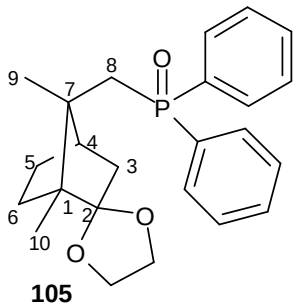

105

(*1*R,*4*R,*7*S)*-(-)-8-(Diphenylphosphinoyl)camphor ethylene ketal*[119] **105

A solution of Ph_2PLi [prepared by stirring a mixture of $ClPPh_2$ (4.50 mL), Li chips (2.50 g) and dry THF (30 mL) at room temperature for 1h and then boiling under reflux for 2h] was added dropwise to a cold (-30^{o}C), stirred solution of 8-bromocamphor ethylene ketal **103** (1.0 g, 3.6 mmol) in dry THF (5 mL) under dry argon. The reaction mixture was stirred overnight at room temperature, and then boiled under reflux for 30 minutes. The mixture was cooled to room temperature and water (20 mL) was carefully added while cooling the flask in an ice-bath. The resulting mixture was treated with 30% H_2O_2 (30 mL) and then diluted with $CHCl_3$ (150 mL). The organic solution was washed sequentially with water (200 mL), 10% aq. KOH (100 mL) and water (150 mL), dried (anhydrous Na_2SO_4) and concentrated *in vauo*. The crude material was chromatographed on silica (gravity chromatography; elution with EtOAc) to afford the (1*R*,4*R*,7*S*)(-)-8-(diphenylphosphinoyl)camphor ethylene ketal **105** (1.10g, 70%) as a viscous pale-yellow oil; ν_{max}(thin film)/cm^{-1} 3053 (ArH); $[\alpha]_D^{22}$ = -7.8^o (*c* 1.30, $CHCl_3$), δ_H (400MHz; $CDCl_3$) 0.78 (3H, s, 10-CH_3), 0.98 (3H, s, 9-CH_3), 1.13 (1H, m, 6-H_a), 1.21 (1H, m, 5-H_a), 1.25 (2H, m, 3-H_a and 4-H), 1.60 (1H, m, 6-H_b), 1.70 (1H, m, 3-H_b), 1.73 (1H, m, 5-H_b), 2.16 (1H, m, 8-H_a), 3.24 (1H, m, 8-H_b), 3.65 (4H, m, OCH_2CH_2O), 7.39 (6H, m, ArH) and 7.63 (4H, m, ArH); δ_C (100MHz; $CDCl_3$) 9.46 (C-10), 18.5 (d, *J* = 1.91 Hz, C-9), 26.9 (C-6), 27.9 (C-5), 32.9 (d, *J* = 71.1Hz, C-8), 41.9 (d, *J* = 2.1Hz, C-4), 44.3 (C-3), 50.7 (d, *J* = 4.9Hz, C-1), 55.2 (d, *J* = 11.5Hz, C-7), 63.4 and 64.9 (OCH_2CH_2O), 116.6 (C-2) and 128-130 (series of overlapping multiplets, ArC); δ_P (162MHz; $CDCl_3$) 31.8 (P=O).

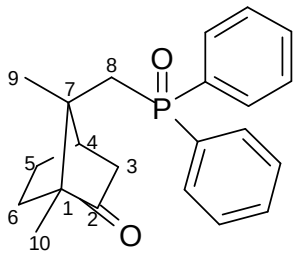

106

(*1*R,*4*R,*7*S)*(+)-8-(Diphenylphosphinoyl)camphor*[119] 106

The monoketal **105** (500 mg, 1.30 mmol) was dissolved in acetone (15 mL). Hydrochloric acid (32%; 1 mL) was added and the solution was left stirring overnight. The reaction mixture was neutralised with 10% aqueous NaOH and the acetone removed *in vacuo*. The product was extracted with chloroform (3 x 20 mL), washed with water and dried (anhydrous $NaSO_4$). The product was recrystalised from heptane to afford (1*R*,4*R*,7*S*)-(+)-8-(diphenylphosphinoyl)camphor **106** as a white amorphous solid in quantitative yield, m.p. 45-49^{o}C (lit.,[119] 55^{o}C); ν_{max} (thin film)/cm^{-1} 1189 (P=O), 1739 (C=O); $[\alpha]_D^{22}$ = 9.5^{o} (*c* 1.0, $CHCl_3$) {lit.[119] $[\alpha]_D^{20}$ = 15.9 (*c* 9.27, MeOH)}; δ_H (400MHz; $CDCl_3$) 0.94 (3H, s, 10-CH_3), 1.03 (3H, s, 9-CH_3), 1.33 (2H, m, 5-H_a and 6-H_a), 1.60 (1H, m, 5-H_b), 1.75 (1H, d, *J* = 18.8Hz, 3-H_a), 1.90 (2H, m, 8-H_a and 6-H_b) 2.19 (2H, m, 3-H_b and 8-H_b) 2.73 (1H, t, *J* = 4.3Hz, 4-H), 7.47 (6H, m, ArH) and 7.76 (4H, m, ArH); δ_C (100MHz; $CDCl_3$) 9.17 (C-10), 17.7 (C-9), 27.0 (C-6), 28.5 (C-5), 33.6 (d, *J* = 70.4, C-8), 40.2 (C-4), 43.2 (C-3), 49.7 (d, *J* = 3.9Hz, C-1), 60.8 (d, *J* = 12.6Hz), 128.7-131.7 (series of overlapping multiplets, ArC) and 219.2 (C-2). δ_P (162MHz; $CDCl_3$) 29.7 (P=O).

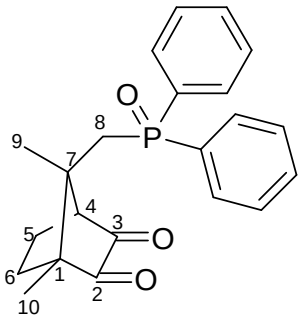

108

(***1*R,*4*S,*7*S*)-(-)-8-(Diphenylphosphinoyl)camphorquinone* **108**

8-(Diphenylphosphinoyl)camphor **106** (600 mg, 1.70 mmol) was dissolved acetic acid (10 mL). Selenium dioxide (600 mg, 5.10 mmol) was added and the resulting suspension was boiled under reflux for 12 hours with stirring. After cooling to room temperature, the black residue was filtered off and washed with methanol. The yellow filtrate and the washings were combined. The volatile organics were evaporated *in vacuo* at *ca.* 50^{o}C. The residue was dissolved in ethyl acetate and sequentially washed with water, a saturated aqueous $NaHCO_3$ and water. The aqueous phase was rendered slightly alkaline and extracted repeatedly with ethyl acetate. The organic extracts were combined, dried (anhydrous Na_2SO_4) and the solvent was evaporated *in vacuo*. The residue was chromatographed [flash chromatography on silica; elution with hexane-ethyl acetate (1: 8)] to afford (*1*R,*4*R,*7*S*)-(-)-8-(diphenylphosphinoyl)-camphorquinone* **108** (257 mg, 41%) as a yellow paste, ν_{max} (thin film)/cm^{-1} 1753 (C=O) and 1187 (P=O); $[\alpha]_D^{22}$ = -82.2^{o} (*c* 1.25, $CHCl_3$); δ_H (400MHz; $CDCl_3$) 1.11 (3H, s, 10-CH_3), 1.22 (3H, s, 9-CH_3), 1.51 (2H, m, 5- and 6-H_a), 1.71 (1H, dd, *J* = 4.97, 10.41Hz, 8-H_a), 1.80 (1H, m, 6-H_b), 2.04 (1H, m, 5-H_b), 2.45 (1H, dd, *J* = 1.96, 13.32Hz, 8-H_b), 2.94 (1H, d, *J* = 5.25Hz) and 7.41-7.72 (10H, series of overlapping multiplets, ArH); δ_C (100MHz; $CDCl_3$) 8.76 (C-10), 15.3 (d, 2.3 Hz, C-9), 22.5 (C-5), 28.4 (C-6), 35.2 (d, *J* = 69.4Hz, C-8), 45.5 (d, *J* = 4.08 Hz, C-1), 55.3 (C-4), 60.6 (d, 11.7Hz, C-7), 129-132 (series of overlapping multiplets, ArC), 202 (C-3) and (C-2); δ_P (162MHz; $CDCl_3$) 30.4 (P=O); *m/z* 368 (M^+, 19%) and 217 (100).

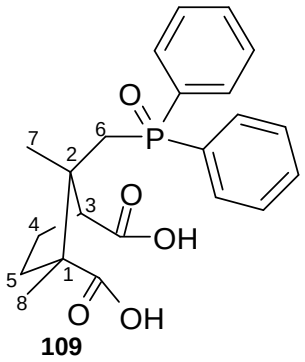

109

***(1*R*,2*S*,3*S*)-2-(Diphenylphosphinoylmethyl)-1,2-dimethyl-1,3-cyclopentane-dicarboxylic acid* 109**

Method A.

A mixture of the phosphine oxide **106** (200 mg, 0.568 mmol), $FeSO_4.7H_2O$ (5 mg, 0.02 mmol) and nitric acid (55%; 6 mL) in water (2 mL) was heated at 100°C for 2 days. The homogeneous solution, which formed after heating the reaction, was cooled to room temperature and the resulting white precipitate was collected by filtration and washed with water (2x10 mL). The solid was dried under reduced pressure to afford (*1*R,*2*S,*3*S)- *2-(diphenylphosphinoylmethyl)-1,2-dimethyl-1,3-cyclopentane-dicarboxylic acid* **109** (170 mg, 75%) as a white powder.

Method B.

8-(Diphenylphosphinoyl)camphorquinone **108** was dissolved in H_2O-THF (2:1; 15 mL). Aqueous NaOCl (15%; 30.0mL) was then added to the resulting solution, which was stirred at room temperature for 3 days. Excess NaOCl was destroyed with sodium thiosulfate. Drop-wise addition of HCl precipitated the product which was then filtered off to afford crude *2-(diphenylphosphinoylmethyl)-1,2-dimethyl-1,3-cyclopentanedicarboxylic acid* **109** (200 mg, 73%) as a white powder, m.p. 260-300°C (not pure) (Found $\mathbf{M}^+$**:** 400.14687. $C_{22}H_{25}O_5P$ requires *M*, 400.14396); ν_{max}(KBr disc)/cm^{-1} 3650-2792 (O-H), 1691 (C=O) and 1119 (P=O); δ_H (400MHz, DMSO-d_6) 1.08 and 1.01 (6H, 2xs, 7- and 8-CH_3), 1.27-3.15 (6H, series of overlapping multiplets, 4-, 5- and 6-CH_2) and 7.47-7.81 (10H, m, ArH); δ_C (100MHz, DMSO-d_6) 20.4 and 22.0 (C-7 and C-8), 30.6 (C-3) 128.4-130.0, (series of overlapping multipletes ArC), 175.2 and 177.0 (C=O); *m/z* 400 (M^+, 1.4%) and 202 (100).

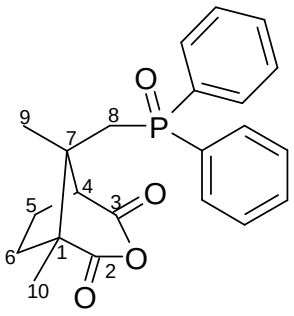

110

***(1*R*,4*S*,7*S*)-(+)-8-(Diphenylphosphinoyl)camphoric anhydride* 110**

Aqueous hydrogen peroxide (30%; 8.00 mL) was added to a solution of 8-(diphenylphosphinoyl)camphorquinone **108** (350 mg, 0.956 mmol) in glacial acetic acid (20.0mL). The resulting solution was stirred for 24 hours at room temperature then added to water (50 mL). The aqueous mixture was extracted with diethyl ether (3 x 50 mL). The combined organic extracts were washed with water (10 x 50 mL) and concentrated *in vacuo*; water (20 mL) was then added again to the residue to precipitate the product. The precipitate was filtered and water was removed under reduced pressure to afford (*1*R,*4*S,*7*S*)-8-(diphenylphosphinoyl)camphoric anhydride* **110** (165 mg, 45%) as white solid, m.p. 126-133^{o}C (Found **M^{+}:** 382.13322. $C_{22}H_{23}O_4P$ requires *M*, 382.13340); ν_{max} (KBr disc)/cm^{-1} 1720 (C=O) and 1163 (C-O), $[\alpha]_D^{33}$ = 2.1^{o} (*c* 1.2 EtOH); δ_H (400MHz, $CDCl_3$) 1.23 and 1.30 (6H, 2xs, 9- and 10-CH_3), 1.59-3.00 (6H, series of overlapping multiplets, 5-, 6- and 8-CH_2), 2.94 (1H, d, *J* = 12.4Hz, 4-H) and 7.49 (10H, m, ArH); δ_C (100MHz, $CDCl_3$) 20.2 (d, *J* = 6.5, C-9), 21.2 (C-10), 31.7 (C-5), 32.3 (C-8), 32.4 (C-6), 50.3 (d, *J* = 4.5Hz, C-7), 53.7 (d, *J* = 3.7Hz, C-4), 57.8 (d, *J* = 7.4, C-1) 128-132 (series of multiplets, ArC), 177 and 179 (C=O); δ_P (162MHz; $CDCl_3$) 29.6 (P=O); *m/z* 382 (M^{+}, 100%).

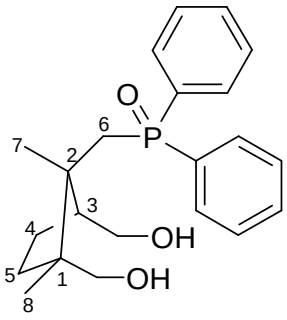

111

***(1*R*,2*S*,3*S*)-(+)-2-(diphenylphosphinoylmethyl)-1,3-bis(hydroxymethyl)-1,2-dimethy-cyclopentane* 111**

Lithium aluminium hydride (LAH) (38.0 mg, 1.00 mmol) was added in small portions to a stirred suspension of the camphoric anhydride **110** (105 mg, 0.275 mmol) in dry diethyl ether (15 mL) under dry argon. The mixture was boiled under reflux for 1 h, and then cooled to room temperature before adding THF (15.0 mL). Excess LAH was quenched cautiously with H_2O, while cooling the flask in an ice-bath. The white precipitate was filtered off and washed with THF. The combined organic solution and washings were separated, dried (anhydrous Na_2SO_4) and concentrated *in vacuo*. The residue was chromatographed (flash chromatography on silica; elution with ethyl acetate) to afford (*1*R,*2*S,*3*S*)-(+)-2-(diphenylphosphinoylmethyl)-1,3-bis(hydroxymethyl)-1,2-dimethylcyclopentane* **111** (64 mg, 63 %) as white crystals, m.p. 141-144^{o}C (Found $\mathbf{M}^+$: 372.18286. $C_{22}H_{29}O_3P$ requires *M*, 372.18543); ν_{max} (thin film)/cm^{-1} 3609-3017 (OH); $[\alpha]_D^{22}$ = 21.6^o (*c* 1.00, $CHCl_3$); δ_H (400MHz; $CDCl_3$) 1.03 (3H, s, 8-CH_3), 1.06 (3H, s, 7-CH_3), 1.42 (3H, m, 4-CH_2, 5-H_a), 1.81 (1H, m, 5-H_b), 2.11 (1H, m, 3-H), 2.55 (2H, m, 6-H), 3.38 (2H, m, C*H*$_2$OH), 3.70 (2H, m, C*H*$_2$OH), 5.01 (1H, s, OH), 7.45 (6H, m, ArH) and 7.77 (4H, m, ArH); δ_C (100MHz; $CDCl_3$) 21.6 (C-8), 22.1 (C-7), 23.6 (C-4), 30.4 (d, *J* = 70.2 Hz, C-6), 32.4 (C-4), 47.8 (d, *J* = 5.2 Hz, C-2), 50.8 (d, *J* = 3.3 Hz, C-1) 52.5 (d, *J* = 7.5 Hz, C-3), 63.1 and 68.3 (2xCH_2OH) and 130.2 (ArC); δ_P (162MHz; $CDCl_3$) 29.3 (P=O); *m/z* 373 (M^+, 100).

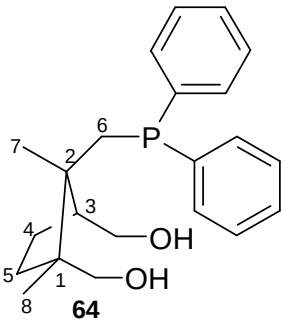

64

Attempted synthesis of *(+)-2-(diphenylphosphinylmethyl)-1,3-bis(hydroxymethyl)-1,2-dimethylcyclopentane* 64

Method A.

The phosphine oxide **111** (100 mg, 0.25 mmol) was dissolved in dry benzene (10mL) under argon. The solution was treated successively with triethyl amine (0.50 mL, 3.0 mmol) and trichlorosilane (0.30 mL, 2.8 mmol) and then boiled under reflux for 4 hours. A white precipitate formed during the reaction. The reaction mixture was diluted with benzene (10mL) and the precipitate filtered off. The filtrate was concentrated *in vacuo* to afford a dark brown residue (10 mg). The NMR analysis of the residue showed the loss of both phenyl groups.

Method B.

The phosphine oxide **111** (110 mg, 0.3 mmol) was dissolved in de-gassed THF-toluene (1:1; 6mL) under argon. Triphenylphosphine was added to the solution and trichlorosilane (0.40 g, 4.0 mmol) was added to resulting mixture. The reaction mixture was stirred for 2 days at 100^{o}C. The cooled mixture was diluted with dichloromethane (5ml), ice (*ca.* 10g) and aqueous NaOH (20%; 10mL). The organic layer was separated, filtered and washed sequentially with saturated aqueous $NaHCO_3$, brine and water, dried (anhydrous Na_2SO_4) and concentrated *in vacuo*. NMR analysis of the residue showed the presence of unconverted phosphinoxide **111**.

Method C.

Hexachlorosilane (1.00 g, 0.25 mmol) was added to the solution of the phosphine oxide **111** (94 mg, 0.25 mmol) in dry benzene (5 mL) under argon. The resulting solution was refluxed under argon for 1.5 hours. The reaction was cooled to 0^{o}C and

then aqueous NaOH (30%; 3mL) was added. The aqueous solution was extracted with benzene (10mL) and separated. The combined organic extracts were filtered, dried (anhydrous Na_2SO_4) and concentrated *in vacuo*. NMR analysis and mass spectrometry showed the presence of unconverted phosphine oxide **111**.

Method D.

The phosphine oxide **111** (140 mg, 0.38 mmol) was dissolved in dry Et_2O (2 mL) under argon. Methyl iodide (0.1 mL) was added to the solution which was stirred for 2 hours at room temperature. The reaction flask was cooled in an ice-bath before lithium aluminium hydride (LAH) (32.3 mg, 0.95 mmol) was added to the reaction solution. The resulting suspension was stirred overnight at room temperature. Excess LAH was quenched cautiously with aqueous HCl (1M; 5 mL). The aqueous layer was extracted with EtOAc (10mL) and the combined organic extracts were dried (anhydrous $MgSO_4$) and concentrated *in vacuo* to afford a dark red residue, NMR analysis showed the presence of the unconverted phosphine oxide **111**.

3.2.3.3. Camphor-derived pyridinyl ligands

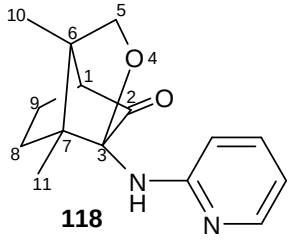

118

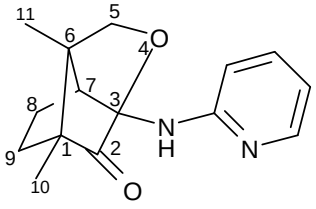

119

***(1*R,*3*R,*6*S,*7*R*-(+)-6,7-dimethyl-3-(2-pyridylamino)-4-oxatricyclo[4.3.0.0^{3,7}]-2-nonanone* 118 and *(1*S,*3*S,*6*S,*7*R*-(-)-1,6-dimethyl-3-(2-pyridylamino)-4-oxa-tricyclo[4.3.0.0^{3,7}]-2-nonanone* 119**

A solution of 2-aminopyridine **117** (47 mg, 0.50 mmol) in THF (1 mL) was cooled in an ice-bath. NaH (19 mg, 0.80 mmol) was cautiously added to the solution and the resulting suspension was stirred for 15 minutes at room temperature under argon. A solution of 8-bromocamphorquinone **88** (100 mg, 0.410 mmol) in THF (1 mL) was added drop-wise to the reaction mixture and stirring was continued overnight at room

temperature. The reaction was quenched with water (10 mL) followed by extraction with ethyl acetate (2x 20 mL). The combined organic extracts were sequentially washed with water (20 mL), saturated aqueous $NaHCO_3$ (20 mL), brine (20 mL) and water (20 mL) and dried (anhydrous $MgSO_4$). The solvent was removed *in vacuo* and the residue was chromatographed [flash chromatography on silica; elution with hexane-ethyl acetate (2:1)] to afford two fractions.

i) *(1*R,*3*R,*6*S,7R*-(-)-6,7-Dimethyl-3-(2-pyridylamino)-4-oxatricyclo[4.3.0.0^{3,7}]-2-nonanone* **118** as soft yellow solid (25.0 mg, 24%), m.p. 92-100^{o}C; (Found **M^{+}:** 258.13536. $C_{15}H_{18}O_2N_2$ requires *M*, 258.13683); ν_{max} (thin film)/cm^{-1} 1764 (C=O) and 1602 (NH); $[\alpha]_D^{22}$ = +121.1^{o} (*c* 1.5, $CHCl_3$); δ_H (400MHz; $CDCl_3$) 1.03 (3H, s, 10-CH_3), 1.09 (3H, s, 11-CH_3), 1.55 (1H, m, 8-H_a) 1.67 (1H, m, 9-H_a), 1.84 (1H, m, 8-H_b), 2.08 (1H, m, 9-H_b) 2.51 (1H, d, *J* = 4.4 Hz, 1-H) 3.87 (1H, d, *J* = 8.2 Hz, 5-H_a), 3.99 (1H, d, *J* = 8.2 Hz, 5-H_b), 5.28 (1H, s, NH), 6.70 (1H, m, 4'-H), 7.10 (1H, d, *J* = 8.5 Hz, 3'-H), 7.44 (1H, m, 5'-H) and 8.06 (1H, d, *J* = 4.8 Hz, 6'-H); δ_C (100MHz; $CDCl_3$) 9.79 (C-10), 10.9 (C-11), 24.8 (C-8), 25.4 (C-9) 52.3 (C-1), 56.6 (C-6), 57.8 (C-1), 71.4 (C-5), 97.5 (C-3), 110.8 (C-3'), 115.3 (C-4') 137.3 (C-5'), 147.2 (C-6') 156.3 (C-2') and 208.0 (C-2); *m/z* 258 (M^+, 100%).

ii) *(1*S,*3*S,*6*S,7R*-(-)-1,6-Dimethyl-3-(2-pyridylamino)-4-oxatricyclo[4.3.0.0^{3,7}]-2-nonanone* **119** as a colourless oil (10.0 mg, 9.5%); (Found **M^{+}:** 258.12365. $C_{15}H_{18}O_2N_2$ requires *M*, 258.13683); ν_{max}(thin film)/cm^{-1} 1757 (C=O) and 1598 (NH); $[\alpha]_D^{22}$ = -78.0^{o} (*c* = 0.5, $CHCl_3$); δ_H (400MHz; $CDCl_3$) 1.11 and 1.12 (6H, 2xs, 10- and 11-CH_3), 1.49 (1H, m, 8-H) 1.59 (1H, m, 9-H), 1.72 (1H, m, 8-H), 1.95 (1H, m, 9-H), 3.30 (1H, d, *J* = 5.1 Hz, 7-H), 3.75 (1H, d, *J* = 8.1 Hz, 5-H_a) 3.87 (1H, d, *J* = 8.1 Hz, 5-H_b), 5.55 (1H, s, NH), 6.72 (2H, m, 4'- and 5'-H), 7.46 (1H, m, 3'-H) and 8.24 (1H, m, 6'-H); δ_C (100MHz; $CDCl_3$) 8.21 (C-10), 11.03 (C-11), 16.9 (C-8), 34.2 (C-9), 50.5 (C-7), 53.1 (C-1), 57.0 (C-6), 69.1 (C-5), 95.3 (C-3), 110.0 (C-4'), 115.2 (C-5'), 137.4 (C-3'), 148.2 (C-6'), 156.1 (C-2') and 209.0 (C-2); *m/z* 258 (M^+, 100%).

***Attempted synthesis of 8-(2-pyridylamino)camphor ethylene ketal* 121**

The general procedure used for the formation of tricyclic compounds **118** and **119** was followed using 8-bromocamphor ethylene ketal **103** (300 mg, 1.09 mmol),

2-aminopyridine (141 mg, 1.50 mmol) and sodium hydride (48.0 mg, 2 mmol). Unconverted 8-bromo ketal **103** was recovered after the reaction.

3.2.3.4. Camphor-derived *N*-heterocyclic carbene (NHC) ligands

Attempted displacement of bromine atom in anhydride* 113 *or diketone* 87 *by 1-phenylarylimidazole.

Method A.

1-Phenylimidazole **122** (0.10 mL, 0.77 mmol) was added to a solution of anhydride **114** (200 mg, 0.77 mmol) or diketone **88** (0.77 mmol) in dry acetonitrile (10 mL). The solutions were stirred for 2 days at room temperature and progress was monitored by thin layer chromatography (TLC). After 2 days, TLC analysis showed no change in the starting materials. Furthermore, the NMR analysis confirmed the presence of unchanged starting materials.

Method B.

The general procedure described for Method A was followed using 1-phenylimidazole **122** (0.10 mL, 0.77 mmol), diketone (188 mg, 0.77 mmol) and silver acetate, but only unconverted starting materials were detected by TLC and NMR analysis.

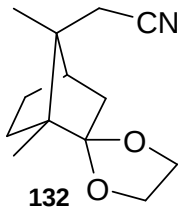

132

***(1*R*,4*R*,7*S*)-8-Cyanocamphor ethylene ketal*[119] 132**

Sodium cyanide (1.80 g, 38.8 mmol) was added to a stirred solution of 8-bromocamphor ethylene ketal **103** (2.00 g, 7.17 mmole) in dry dimethyl sulfoxide (30 mL) and stirring was continued at 60^{o}C under argon for 8 days. After cooling, the reaction mixture was added to water (200 mL) and the product extracted with diethyl ether (2 x 100 mL). The combined organic solutions were washed with water (3 x

200 mL), dried (anhydrous $NaSO_4$) and concentrated *in vacuo* to afford (*1*R,*4*R,*7*S)-8-cyanocamphor ethylene ketal **132** as a yellow oil (1.12 g, 69.0 %); ν_{max} (thin film)/cm^{-1} 2243 (CN); $[\alpha]_D^{22}$ = -0.125° (*c* 1.1, $CHCl_3$), {lit.,[119] $[\alpha]_D^{25}$ = +5.06 (*c* 2.35, C_2H_5OH); δ_H (400MHz; $CDCl_3$) 0.82 (3H, s, 10-CH_3), 1.07 (3H, s, 9-CH_3), 1.24 (1H, m, 5-H_a), 1.32 (1H, m, 6-H_a), 1.52 (1H, d, *J* = 13.7 Hz, 3-H_a), 1.52 (1H, m, 5-H_b), 1.97 (3H, m, 3-H_b, 4-H and 5-H_b), 2.28 (1H, d, *J* = 17.2, 8-H_a), 2.94 (1H, d, *J* = 17.2, 8-H_b) and 3.86 (4H, m, OCH_2CH_2O); δ_C (100MHz; $CDCl_3$) 9.54 (C-10), 17.4 (C-9), 22.9 (C-8), 26.5 (C-5), 29.4 (C-6), 43.2 (C-4), 44.3 (C-3), 49.6 (C-7), 52.9 (C-1), 64.0 and 65.1 (OCH_2CH_2O), 115.9 (C-2) and 119.6 (CN).

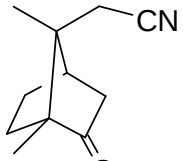

133

***8-Cyanocamphor* 133**

8-Cyanocamphor ethylene ketal **132** (300 mg, 1.3 mmol) was dissolved in acetone (10 mL). Hydrochloric acid (32%; 1 mL) was added and the solution was left stirring overnight. The reaction mixture was neutralised with 10% aqueous NaOH and the acetone removed *in vacuo*. The aqueous residue was extracted with chloroform (3 x 20 mL), and the combined organic extracts were washed with water and dried (anhydrous $NaSO_4$). Evaporation of the solvent *in vacuo* afforded crude 8-cyanocamphor **133** (165 mg, 71%); ν_{max}(thin film)/cm^{-1} 2243 (CN) and 1742 (C=O); δ_C (100MHz; $CDCl_3$) 9.53, 17.0, 23.3, 27.0, 30.4, 41.6, 43.1, 49.4, 58.3, 118.1 and 217.0; which was used without further purification.

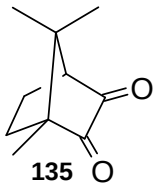

135

***Attempted oxidation of 8-cyanocamphor* 133**

8-Cyanocamphor **133** (160 mg, 0.91mmol) was dissolved acetic acid (10.0 mL). Selenium dioxide (295 mg, 2.66 mmol) was added and the resulting suspension was boiled under reflux for 12 hours with stirring. After cooling to room temperature, the black residue was filtered off and washed with methanol. The dark green filtrate and the washings were combined. The volatile organics were evaporated *in vacuo* at *ca.* 50^{o}C. The residue was dissolved in ethyl acetate and the organic solution was washed sequentially with water, saturated aqueous $NaHCO_3$ and water. The aqueous phase was rendered slightly alkaline and extracted repeatedly with ethyl acetate. The organic extracts were combined, dried (anhydrous Na_2SO_4) and the solvent was evaporated *in vacuo*. The residue was chromatographed [flash chromatography on silica; elution with hexane-ethyl acetate (1: 4)] to afford a yellow fraction which was chromatographed further [HPLC on Partisil 10; elution with hexane-EtOAc (6:1)] to afford (1*R*,4*S*)-camphorquinone **135** as yellow crystals (23 mg, 40.5%; based on the sample used in HPLC), m.p.173-179^{o}C (lit.[138] 198-201^{o}C); ν_{max} (thin film)/cm^{-1} 1763 and 1749 (C=O); δ_H (400MHz; $CDCl_3$) 0.92, 1.05, 1.09 (9H, 3 x s, 8-, 9- and 10-CH_3), 1.58-2.18 (4H, series of multiplets, 5- and 6-CH_2) 2.62 (1H, d, J = 5.3Hz, 4-H); (100MHz; $CDCl_3$) 8.77, 17.4 and 21.1 (C-8, C-9 and C-10), 22.2 and 29.9 (C-5 and C-6), 42.6 (C-7), 58.0 (C-4), 58.6 (C-1) 202.8 and 204.8 (2xC=O); *m/z* 166 (M^+, 22.6%) and 94 (100).

3.2.4. Ruthenium Complexation Studies

Note: The Grubbs' first generation catalyst was transferred to round bottom flask in a glove box filled with argon. Rigorous anhydrous conditions were followed in the following experiment.

***Attempted complexation of ligand* 110 *with the Grubbs' first-generation catalyst* $Ru(=CHPh)Cl_2(PCy_3)_2$ [103]**

A solution of the dihydroxy compound **111** (88.2 mg, 0.237 mmol) in dry benzene (5 mL) was added dropwise to a cooled suspension of potassium hydride (38 mg, 0.95 mmol) in benzene (5 mL). The mixture was stirred for 2 hours at room temperature and then the solids were allowed to settle. The supernatant liquid was then transferred by canula into a flask containing the Grubbs' first generation catalyst $Ru(=CHPh)Cl_2(PCy_3)_2$ **4** (65 mg, 0.079 mmol) and the resulting mixture stirred for 24 hours at room temperature. The solvent was removed by freeze-drying and the resulting solids were suspended in benzene (0.5 mL) and pentane (50 mL). CuCl (78 mg, 0.79 mmol) was added to the suspension and the mixture stirred for 20 minutes, and then cooled to -30^{o}C for 24 hours. The organic supernatant liquid was decanted and solvent removed *in vacuo* to afford a black solid. No identifiable product could be detected by NMR spectroscopy.

4. REFERENCES

1. A. Frennet and C. Hubert, *J. Mol. Catal. A, Chemical,* 2000, **163**, 163.

2. F.G. Donnan, *J. Chem. Soc.*, 1933, 316.

3. I. Langmuir, *J. Chem. Soc.*, 1912, **34**, 860.

4. F. Cavani and F. Trifiro, *Catalysis Today*, 1997, **34**, 269.

5. C. Masters, "*Homogeneous Transition-metal Catalysis: A gentle art*", Chapman and Hall, London, 1981, pp.1-218.

6. C.A. Tolman, *Chem. Soc. Rev.*, 1972, **1**, 337.

7. F.A. Cotton, G. Wilkinson and P.L. Gans, *"Basic Inorganic Chemistry, 2nd Edition"*, John Wiley and Sons, New York, 1987, pp. 190-193.

8. L.S. Meriwether and M.L. Fiene, *J. Am. Chem. Soc.*, 1959, **81**, 4200.

9. C.A. Tolman, *J. Am. Chem. Soc.*, 1970, **92**, 2953.

10. D.C. Smith, E.D. Stevens and S.P. Nolan, *Inorg. Chem.*, 1999, **38**, 5277.

11. (a) J. A. Widegren and R.G. Finke, *J. Mol. Catal. A: Chemical,* 2003, **198**, 117; (b) D.T. Thompson, *Coord. Chem. Rev.*, 1996, **154**, 179.

12. (a) B. Cornils and W.A. Herrmann, *J. Catal*, 2003, **216,** 23; (b) P.W.N.M. van Leeuwen, P.C.J. Kamer, J.N.H. Reek and P. Dierkes, *Chem. Rev.*, 2000**, 100**, 2741.

13. (a) J. Barrault, Y. Pouilloux, J. M. Clacens, C. Vanhove and S. Bancquart, *Catalysis Today*, 2002, **75**, 177; (b) G.W. Parshall and R. E. Putcher, *J. Chem. Educ.*, 1986, **63**, 189.

14. M. Asadullah, S. Ito, K. Kunimori, M. Yanada and K. Tomishige, *Environ. Sci. Technol.*, 2002, **36**, 4476.

15. R. Eisenberg and D.N. Nocera, *Inorg. Chem.*, 2005, **44**, 6799.

16. M.A. Grele and A.J. Colussi, *J. Phys. Chem.*, 1982, **86**, 4844; S.W. Benson *J. Phys. Chem.*, 1985, **89**, 4366.

17. R.L. Banks and G.C. Bailey, *Industrial and Chemical Engineering Product Research and Development*, 1964, **3**, 170.

18. N. Calderon, *Acc. Chem. Res.*, 1972, **5**, 127.

19. T. Opstal and F. Verpoort, *J. Mol. Catal., A, Chem.*, 2003, **200**, 49.

20. R.H. Grubbs and W. Tumas, *Science*, 1989, **243**, 907.

21. G. Natta, G.D. Asta, G. Mazzati, I. Pasquone, A. Valvassoni and A. Zambelli, *J. Am. Chem. Soc*., 1961, **83,** 3343.

22. P. J. Flory, *J. Am. Chem. Soc.*, 1940, **62**, 1561.

23. L.R. Gilliom and R.H. Grubbs, *J. Am. Chem. Soc*., 1986, **103**, 733.

24. L. Louie and R.H. Grubbs, *Organometallics,* 2002, **21**, 2153

25. S.E. Lehman, Jr. and K.B. Wagener, *Organometallics*, 2005, **24**, 1477

26. K.B. Wagener, J.M. Boncella and J.G. Nel, *Macromolecules*, 1991, **24**, 2649.

27. (a) M. R. Buchmeiser, *Chem. Rev.*, 2000, **100**, 1565; (b) J**.** Tsuji and S. Hashiguchi, *Tetrahedron Lett*., 1980, **21**, 2955.

28. R.H. Grubbs, S.J. Miller and G. C. Fu, *Acc. Chem. Res.*, 1995**, 28,** 446.

29. A. Grigg, W. Martin, J. Morris and V. Sridharan, *Tetrahedron Lett.*, 2003, **44**, 4899.

30. S. H. Hong and R. H. Grubbs, *J. Am. Chem. Soc.*, 2006, **128**, 3508

31. (a) V. Dragutan, I. Dragutan, L. Delaude and A. Demonceau, *Coord. Chem. Rev.* 2006, in press; (b) T.M. Trnka and R.H. Grubbs, *Acc. Chem. Res.*, 2001, **34**, 18. (c) M.L. Randall and M.L. Snapper, *J. Mol. Catal. A, Chem*., 1998, **133**, 29; (d) K.J. Ivin, *J. Mol. Catal. A, Chem.*, 1998, **133**, 1; S.K. Armstrong, *J. Chem. Soc., Perkin Trans*. 1, 1998, 371; (e) R. H. Grubbs and S. Chang, *Tetrahedron*, 1998, **54,** 4413; (f) C. Pariya, K.N. Jayaprakash and A. Sarkar, *Coord. Chem. Reviews*, 1998, **168**, 1; (g) G.D. Cuny, J. Cao and J.R. Hauske, *Tetrahedron Lett.*, 1997, **38**, 5237.

32. A.K. Chatterjee, T. Choi, D.P. Sanders and R.H. Grubbs, *J. Am. Chem. Soc.*, 2003, **125**, 1136.

33. A.K. Chatterjee, J.P. Morgan, M.Scholl and R.H. Grubbs, *J. Am. Chem. Soc.*, 2000, **122**, 3783.

34. J.A. Tallarico, M.L. Randall and M.L. Snapper, *Tetrahedron,* 1997, **53**, 16511.

35. C. Adlhart and P. Chen, *J. Am. Chem. Soc.*, 2004, **126**, 3496.

36. J.C. Mol, *J. Mol. Catal. A, Chem.*, 2004, **213**, 39.

37. J.S. Plotkin, *Catalysis Today*, 2005, **106**, 10;

38. P.P. O'Neill and J.J. Rooney, *J. Am. Chem. Soc.*, 1972, **94**, 4383.

39. E.F. Lutz, *J. Chem. Educ.*, 1986, **63**, 202.

40. M. Yamazaki, *J. Mol. Catal. A, Chem.*, 2004, **213,** 81.

41. A.S. Williams, *Synthesis*, 1999, 1707.

42. E. Marcus and W. Peter, U.S. Patent 6573391, 2003.

43. J. Prunet, *Curr. Topics Med. Chem.*, 2005, **5**, 1559.

44. H. Hagiwara, T. Katsumi, V.P. Kamata, T. Hoshi, T. Suzuki and M. Ando, *J. Org. Chem.*, 2000, **65**, 7231.

45. T. Misaki, R. Nagase, K. Mutsumoto and Y. Tanabe, *J. Am. Chem. Soc.*, 2005, **127**, 2854.

46. D.F. Taber and K.J. Frankowski, *J. Chem. Educ.*, 2006, **83**, 283.

47. K. Eshima, M. Yuasa, H. Nishide and E. Tsuchida, *J. Chem. Soc., Chem. Commun.*, 1985, 130.

48. K. Tanaka, *J. Mol. Catal.*, 1988, **46**, 87.

49. J.C. Mol, *Green Chemistry*, 2002, **4**, 5.

50. E. Verkuijlen, F. Kepteijn, J.C. Mol and C. Boelhouwer, *J. Chem. Soc., Chem. Commun.*, 1977, 198.

51. T.J. Kartz, S.J. Lee and M.A. Shippel, *J. Mol. Catal.*, 1980, **8**, 219.

52. G.C. Bazan, J.H., Oskam, H.N. Cho, L.Y. Park and R.R. Schrock, *J. Am. Chem. Soc.*, 1991, **113**, 6899.

53. R.H. Grubbs, *J. Macromolecular Science Pure and Appl., Chem.*, 1994, **A31**, 1821.

54. B.M. Novak and R.H. Grubbs, *J. Am. Chem. Soc.*, 1988, **110**, 960

55. B.M. Novak and R.H. Grubbs, *J. Am. Chem. Soc.*, 1988, **110**, 7542

56. S.T. Nguyen, L.K. Johnson, R.H., Grubbs and J.W. Ziller, *J. Am. Chem. Soc.*, 1992, **114**, 3974.

57. S.T. Nguyen, R.H., Grubbs and J.W. Ziller, *J. Am. Chem. Soc.*, 1993, **115**, 9858.

58. P. Schwab, R.H. Grubbs and J.W. Ziller, *J. Am. Chem. Soc.*, 1996, **118,** 100.

59. E.L. Dias, S.T. Nguyen and R.H. Grubbs, *J. Am. Chem. Soc.*, 1997, **119**, 3887.

60. (a) M. Scholl, T.M. Trnka, J.P. Morgan and R.H. Grubbs, *Tetrahedron. Lett.*, 1999, **40**, 2247. (b) M. Scholl, S. Ding, C.W. Lee and R.H. Grubbs, *Org. Lett.*, 1999, **1**, 953. (c) T. Weskamp, W.C. Schattenmann, M. Spiegler and W.A. Herrmann, *Angew., Chem., Int. Ed.*, 1998, **37**, 2490.

61. S.M. Hansen, F. Rominger, M. Metz and P. Hofmann, *Chem. Eur. J.*, 1999, **5**, 557.

62. J.S. Kingsbury, J.P.A. Harrity, P.J. Bonitatebus, Jr. and A.H. Hoveyda, *J. Am. Chem. Soc.*, 1999, **121**, 791.

63. J.P.A. Harrity, M.S. Visser, J.D. Gleason and A.H. Hoveyda, *J. Am. Chem. Soc.* 1997, **119**, 1488.

64. M.S. Sanford, J.A. Love and R.H. Grubbs, *J. Am. Chem. Soc.*, 2001, **123**, 6543.

65. D.R. Anderson, D.D. Hickstein, D.J. O'Leary and R.H. Grubbs, *J. Am. Chem. Soc.*, 2006, **128**, 8386.

66. J.A. Tallarico, P.J. Bonitatebus, Jr. and M.L. Snapper, *J. Am. Chem. Soc.* 1997, **119**, 7157.

67. P. Romero and E. Piers, *J. Am. Chem. Soc.*, 2005, **127**, 5032.

68. C. Adhart, C. Hiderling, H. Baumann and P. Chen, *J. Am. Chem. Soc.*, 2000, **122**, 8204.

69. O.M. Aagaard, R.J. Meier and F. Buda, *J. Am. Chem. Soc.* 1998, **120**, 7174.

70. S.F. Vyboishchikov, M. Bühl and W. Thiel, *Chem. Eur. J.*, 2002, **8,** 3962.

71. F. Bernardi, A. Bottoni and G.P. Miscione, *Organometallics*, 2003, **22**, 940.

72. L. Cavallo, *J. Am. Chem. Soc.*, 2002, **124**, 8965.

73. C.H. Suresh and N. Koga, *Organometallics*, 2004, **23**, 76.

74. I. Sabbagh and P.T. Kaye, *Journal of Molecular Structure: THEOCHEM*, 2006, **763**, 37.

75. S. Formine, S.M. Vargas and M.A. Tlenkopatchev, *Organometallics*, 2003, **22**, 93.

76. M.S. Sanford, J.A. Love and R.H. Grubbs, *Organometallics*, 2001, **20**, 5314.

77. T. Weskamp, F.J. Kohl and W.A. Herrmann, *Tetrahedron Lett.*, 1999, **40**, 4787.

78. M. Ulman and R.H. Grubbs, *J. Org. Chem.*, 1999, **64**, 7202.

79. S. Chang, L. Jones II, C. Wang, L.M. Henling and R.H. Grubbs, *Organometallics*, 1998, **17**, 3460.

80. (a) R. Drozdazak, B. Allaert, N. Ledoux, I. Dragutan, V. Dragutan and F. Verpoort, *Adv. Synth. Catal.*, 2005, **347**, 1721; (b) B.D. Clercq and F. Verpoort, *Adv. Synth. Catal.*, 2002, **344**, 639.

81. B.D. Clercq and F. Verpoort, *Tetrahedron Lett.*, 2002, **43**, 9101.

82. S.B. Garber, J.S. Kingsbury, B.L. Gray and A.H. Hoveyda, *J. Am. Chem. Soc.* 2000, **122**, 8168.

83. Q. Yao and A.R. Motta, *Tetrahedron Lett.*, 2004, **45**, 2447.

84. (a) T.S. Halbach, S. Mix, D. Fischer, S. Maechling, J.O. Krause, C. Sievers, S. Blechert, O. Nuyken and M. R. Buchmeiser, *J. Org. Chem.*, 2005, **70**, 4687; (b) J.O. Krause, O. Nuyken, K. Wurst and M. R. Buchmeiser, *Chem. Eur. J.*, 2004, **10**, 777.

85. T.J. Seiders, D.W. Ward and R.H. Grubbs, *Org. Lett.*, 2001, **3**, 3225.

86. J.J. van Veldhuizen, S.B. Garber, J.S. Kingsbury and A.H. Hoveyda, *J. Am. Chem. Soc.*, 2002, **124**, 4954.

87. J.J. van Veldhuizen, J.E. Campbell, R.E. Giudici and A.H. Hoveyda, *J. Am. Chem. Soc.*, 2005, **127**, 6877.

88. W. Day and R.H. Grubbs, *J. Am. Chem. Soc.*, 2004, **126**, 7414.

89. D. Amoroso, G.P.A. Yap and D.E. Fogg, *Organometallics*, 2002, **21**, 3335.

90. W. Janse van Rensburg, P.J. Steynberg, W.H. Meyer, M.M. Kirk, D.W. Serfontein and G.S. Forman, *J. Am. Chem. Soc.*, 2004, **126**, 14332.

91. T. Ung, A. Hejl, R.H. Grubbs and Y. Schrodi, *Organometallics*, 2004, **23,** 5399.

92. T.A. Kirkland, D.M. Lynn and R.H. Grubbs, *J. Org. Chem*., 1998, **63,** 9904.

93. D.M. Lynn, B. Mohr and R.H. Grubbs, *J. Am. Chem. Soc.*, 1998, **120**, 1627.

94. D.M. Lynn, B. Mohr, R.H. Grubbs, L.M. Henling and M.W. Day, *J. Am. Chem. Soc.*, 2000, **122**, 6601.

95. J. P. Gallivan, J. P. Jordan and R. H. Grubbs, *Tetrahedron Lett.*, 2005, **46**, 2577.

96. S.H. Hong and R.H. Grubbs, *J. Am. Chem. Soc*., 2006, **128**, 3508.

97. K.W. Wellington, Ph.D. Thesis, Rhodes University, 1999**.**

98. J.P. Hagemann, Ph.D. Thesis, Rhodes University, 1997**.**

99. A. Daubinet, Ph.D. Thesis, Rhodes University, 2001.

100. (a) B.S.B. Gxoyiya, MSc. Thesis, Rhodes University, 2003; (b) T.R. Tshikudo, MSc. Thesis, Rhodes University, 2002.

101. I.T. Sabbagh, Ph.D. Thesis, Rhodes University, 2005.

102. T.P. Curran, C.W.Borysenko, S.M. Abelleira and R.J. Messier, *J. Org. Chem.*, 1994, **59**, 3522.

103. M.S. Sanford, L.M. Henling, M.W. Day and R.H. Grubbs, *Angew. Chem. Int. Ed.*, 2000, **39**, 3451.

104. J.O. Krause, O. Nuyken, K. Wurst and M.R. Buchmeiser, *Chem.Eur. J.*, 2004, **10**, 777.

105. B. Askew, P. Ballester, C. Buhr, K.S. Jeong, S. Jones, K. Parris, K. Williams and J. Rebek, *J. Am. Chem. Soc.*, 1989, **111**, 1082.

106. B.W. Baldwin, T. Hirose, Z. Wang, T. Uchimaru and A. Yliniemelä, *Bull. Chem. Soc. Jpn.*, 1997, **70**, 1895.

107. M.L. Dougan, J.L. Chin, K. Solt and D.E. Hansen, *Bioorg. Med. Chem. Lett.*, 2004, **14**, 4153.

108. Q. Ye, I.V. Komarov, A.J. Kirby and M. Jones, *J. Org. Chem.*, 2002, **67**, 9288.

109. R.E. Banks, N.J. Lawrence and A.L. Popplewell, *J. Chem. Soc., Chem. Commun.*, 1994, 343

110. K. Tanemura, T. Suzuki, Y. Nishida, K. Satsumabayashi and T. Horaguchi, *Chem. Comm.*, 2004, 470.

111. J.W. Apsimon, *J. Chem. Phys.*, 1957, **27**, 226.

112. I.V. Komarov, A. Monsees, A. Spannenberg, W. Baumann, U. Schmidt, C. Fischer and A. Börner, *Eur. J. Org. Chem.*, 2003, 138.

113. R. Antkowiak and W.Z. Antkowiak, *Polish J. Chem.*, 1994, **68**, 2297.

114. P. Cachia, N. Darby, C. R. Eck and T. Money, *J. Chem. Soc., Perkin I*, 1976, 359.

115. I.V. Komarov, A. Monsees, R. Kadyrov, C. Fischer, U. Schmidt and A. Börner, *Tetrahedron Asymm.*, 2002, **13**, 1615.

116. K.A. Lobb, unpublished work.

117. (a) C.J. Collins and C.K. Johnson, *J. Am. Chem. Soc.*, 1973, **95**, 4766; (b) C.J. Collins and C.K. Johnson, *J. Am. Chem. Soc.*, 1974, **96**, 2514.

118. R. Klein, MSc. Thesis, Rhodes University, 1999.

119. I.V. Komarov, M.V. Gorichko and M.Y. Kornilov, *Tetrahedron Asymm.*, 1997, **8**, 435.

120. D.L. Kuo and T. Money, *Can. J. Chem.*, 1988, **66**, 1794.

121. Z. Yang, L. Wang, Z. Zhou, Q. Zhou and C. Tang, *Tetrahedron Asymm.*, 2001, **12**, 1579.

122. E.J. Corey and H.L. Pearce, *J. Am. Chem. Soc.*, 1979, **101**, 5845.

123. T. Imamoto, S. Kikuchi, T. Miura and Y. Wada, *Org. Lett.*, 2001, **3**, 87.

124. H. Wu, J. Yu and J.B. Spencer, *Org. Lett.*, 2004, **6**, 4675.

125. K. Naumann, G. Zon and K. Mislow, *J. Am. Chem. Soc.*, 1969, **91**, 7012.

126. S. Wagaw and S.L. Buchwald, *J. Org. Chem.*, 1996**, 61**, 7240.

127. S.J. Dominianni and T.T. Yen, *J. Med. Chem.*, 1989, **32**, 2301.

128. E. Alessio, G. Mestroni, A. Bergamo and G. Sava, *Curr. Topics Med. Chem.*, 2004, **4**, 1525.

129. E. Pretch and A. Fűrst, Carbon-13 NMR Chemical Shift Prediction Module, SoftShell International Ltd., 1990.

130. (a) Modgraph Consultants. *NMR Predict*., http://www.modgraph.co.uk/, 2006; (b) R.J. Abraham, B. Bardsley M. Mobli and R.J. Smith, *Magn. Reson. Chem*., 2005, **43**, 3.; and (c) J. Meiler, W. Maier, M. Will and R. Meusinger, *J. Magn. Res.*, 2002, **157**, 242.

131. (a) B. Delley, *J. Chem. Phys.*, 1990, **92**, 508; (b) B. Delley, *J. Chem. Phys.*, 1996, **100**, 6107; (c) B. Delley, *J. Chem. Phys.*, 2000, **113**, 7756.

132. J.P. Perdew and Y. Wang, *Phys. Rev.*, 1992, **B 45**, 13244.

133. W. Kohl, L.J. Sham, *Phys. Rev.*, 1965, **140**, A1133

134. P. Pulay, *J. Comput. Chem.*, 1982, **3**, 556.

135. D.D. Perrin and W.L.F. Armarego, *"Purification of Laboratory Chemicals"*, Pergamon Press, Oxford, 1988.

136. D.S. Kemp and K.S. Patrakis, *J. Org. Chem.*, 1981, **46**, 5140.

137. (a) C.R. Eck, R.W. Mills and T. Money, *J. Chem. Soc., Chem. Commun.*, 1973, 911; (b) C.R. Eck, R.W. Mills and T. Money, *J. Chem. Soc., Perkin Trans. 1*, 1975, 251.

138. B. Pfrunder and C. Tamm, *Helv. Chim. Acta,* 1969, **52**, 1630.

5. APPENDIX

5.1 CRYSTALLOGRAPHIC DATA FOR 8-IODOCAMPHOQUINONE BIS(ETHYLENE KETAL) 90

Table 9: Crystal data and structure refinement for compound **90**

Empirical formula	$C_{14}\ H_{21}\ I\ O_4$
Formula Weight	380.21
Temperature	113 K
Wavelength	0.71073 Å
Crystal System	Monoclinic
Space group	C2(No. 5)
Unit cell dimensions	a = 16.3127(4) Å $\alpha = 90^o$
	b = 7.1753(2) Å $\beta = 90^o$
	c = 12.5202(4) Å $\gamma = 90^o$
Volume	1452.54(7) $Å^3$
Z	4
Density calculated	1.739 g/cm^3
Absorption coefficient	2.212 mm^{-1}
F(000)	760
Crystal Size [mm]	0.14 x 0.15 x 0.15 mm^3
Theta range for data collection	3.3 to 25.3^o
Index Ranges	-19<=h<=19, -8<=k<=8, -15<=l<=15
Reflections collected	16587
Independent reflections	2643 [R(int) = 0.047]
Completeness of data to theta = 25.3^o	99%
Absorption correction	Empirical
Max. and min. transmission	0.7470 and 0.7326
Refinement method	Full-matrix least-squares on F^2
Data / restraints / parameters	2643 / 0 / 174
Goodness-of-fit on F^2	1.11
Final R indices [I>2sigma(I)]	R_1 = 0.0204, wR_2 = 0.0498
R indices (all data)	R_1 = 0.0240, wR_2 = 0.0503
Absolute structure parameter	0.02(2)
Largest diff. peak and hole	1.27 and -1.17 $e.Å^{-3}$

Table 10: Atomic coordinates and equivalent isotropic displacement parameters for compound **90**. U(eq) is defined as one third of the trace of the orthogonalized U^{ij} tensor.

Atom	**x**	**y**	**z**	**U(eq) [Å^2]**
C(1)	0.23150(19)	0.8545(4)	0.7316(2)	0.0174(8)
C(2)	0.20872(18)	0.7282(4)	0.8240(2)	0.0167(8)
C(3)	0.20813(19)	0.5264(6)	0.7807(2)	0.0216(9)
C(4)	0.1295(2)	0.5201(4)	0.6948(2)	0.0227(10)
C(5)	0.09320(19)	0.7186(4)	0.7007(2)	0.0181(9)
C(6)	0.14952(19)	0.8513(4)	0.6471(2)	0.0181(8)
C(7)	0.26462(19)	0.7576(5)	0.9305(2)	0.0209(9)
C(8)	0.11405(18)	0.7656(4)	0.8226(2)	0.0171(8)
C(9)	0.0723(2)	0.6339(5)	0.8958(3)	0.0239(9)
C(10)	0.09795(18)	0.9661(4)	0.8566(3)	0.0194(8)
C(13)	0.3354(2)	1.0722(8)	0.7536(3)	0.0335(10)
C(14)	0.3507(2)	0.9426(5)	0.6658(3)	0.0247(10)
C(17)	0.1376(3)	1.1055(5)	0.5370(3)	0.0437(15)
C(18)	0.1494(3)	0.9377(5)	0.4697(3)	0.0376(13)
O(12)	0.25121(12)	1.0405(5)	0.76565(16)	0.0207(6)
O(15)	0.30203(13)	0.7841(3)	0.68993(18)	0.0209(7)
O(16)	0.11113(13)	1.0275(4)	0.63104(16)	0.0223(7)
O(19)	0.16535(15)	0.7897(3)	0.54448(18)	0.0253(7)
I(11)	-0.03012(1)	1.05359(5)	0.82465(1)	0.0231(1)

Table 11: Hydrogen coordinates and isotropic displacement parameters for compound **90**.

	x	**y**	**z**	**U(iso) [Å^2]**
H(3A)	0.20400	0.43510	0.83900	0.0260
H(3B)	0.25870	0.50020	0.74740	0.0260
H(4A)	0.14430	0.49370	0.62210	0.0270
H(4B)	0.08990	0.42450	0.71320	0.0270
H(5)	0.03320	0.72860	0.67210	0.0220
H(7A)	0.24310	0.68650	0.98750	0.0310
H(7B)	0.26600	0.89040	0.94900	0.0310
H(7C)	0.32070	0.71490	0.92330	0.0310
H(9A)	0.09410	0.65810	0.97130	0.0360
H(9B)	0.08380	0.50440	0.87790	0.0360
H(9C)	0.01250	0.65520	0.88490	0.0360
H(10A)	0.13190	1.05140	0.81840	0.0230
H(10B)	0.11670	0.97880	0.93470	0.0230
H(13A)	0.37210	1.04330	0.82110	0.0400
H(13B)	0.34440	1.20320	0.73320	0.0400
H(14A)	0.33090	0.99510	0.59380	0.0300
H(14B)	0.41010	0.91050	0.66970	0.0300
H(17A)	0.18990	1.17530	0.55470	0.0530
H(17B)	0.09500	1.18980	0.49970	0.0530
H(18A)	0.09910	0.91230	0.41840	0.0450
H(18B)	0.19660	0.95580	0.42860	0.0450

Table 12: Anisotropic displacement parameters ($Å^2$ x 10^3) for compound **90**. The anisotropic displacement factor exponent takes the form: $-2p^2[h^2a^{*2}U^{11} + \ldots + 2h\ k\ a^*\ b^*U^{12}]$

	U^{11}	U^{22}	U^{33}	U^{23}	U^{13}	U^{12}
C(1)	21(15)	12(13)	21(15)	-2(12)	7(12)	1(11)
C(2)	21(15)	14(14)	16(15)	-1(11)	3(11)	2(11)
C(3)	29(15)	15(2)	22(13)	-2(14)	8(11)	2(13)
C(4)	30(16)	16(2)	22(14)	-4(12)	4(11)	0.4(12)
C(5)	20(15)	16(16)	19(15)	-3(11)	3(12)	-1(12)
C(6)	23(15)	13(14)	19(15)	1(12)	6(12)	4(11)
C(7)	20(15)	23(15)	20(15)	-1(13)	0.3(12)	3(12)
C(8)	18(14)	16(14)	17(14)	-0.4(12)	3(11)	1(11)
C(9)	26(17)	24(14)	23(17)	1(13)	10(13)	-2(13)
C(10)	15(15)	21(14)	21(15)	-6(12)	1(12)	3(12)
C(13)	29(15)	30(2)	43(18)	-1(2)	11(13)	-10(2)
C(14)	26(17)	22(17)	28(18)	4(13)	10(13)	-4(13)
C(17)	77(3)	31(3)	25(18)	8(15)	15(18)	12(17)
C(18)	65(3)	31(2)	16(18)	7(15)	4(17)	4(18)
O(12)	21(9)	12(10)	30(10)	-3(14)	7(7)	5(13)
O(15)	20(11)	16(11)	29(12)	0(9)	12(9)	0.4(8)
O(16)	31(10))	17(15)	19(9)	5(10)	5(7)	9(10
O(19)	40(14)	22(12)	15(11)	0.5(9)	7(9)	4(10)
I(11)	17(1)	25(1)	26(1)	4.4(1)	2(1)	4(1)

Table 13: Bond lengths [Å] for compound **90**

C(1)-C(2)	1.553(4)	C(3)-H(3A)	0.9900
C(1)-C(6)	1.592(4)	C(3)-H(3B)	0.9900
C(2)-C(3)	1.546(5)	C(4)-H(4A)	0.9900
C(2)-C(7)	1.527(4)	C(4)-H(4B)	0.9900
C(2)-C(8)	1.565(4)	C(5)-H(5)	1.0000
C(3)-C(4)	1.562(4)	C(7)-H(7A)	0.9800
C(4)-C(5)	1.548(4)	C(7)-H(7B)	0.9800
C(5)-C(6)	1.538(4)	C(7)-H(7C)	0.9800
C(5)-C(8)	1.556(4)	C(9)-H(9A)	0.9800
C(8)-C(9)	1.537(5)	C(9)-H(9B)	0.9800
C(8)-C(10)	1.533(4)	C(9)-H(9C)	0.9800
C(13)-C(14)	1.486(6)	C(10)-H(10A)	0.9900
C(17)-C(18)	1.497(5)	C(10)-H(10B)	0.9900
O(12)-(C1)	1.425(4)	C(13)-H(13A)	0.9900
O(12)-C(13)	1.420(4)	C(13)-H(13B)	0.9900
O(15)-C(1)	1.418(4)	C(14)-H(14A)	0.9900
O(15)-C(14)	1.442(4)	C(14)-H(14B)	0.9900
O(16)-C(6)	1.413(4)	C(17)-H(17A)	0.9900
O(16)-C(17)	1.422(4)	C(17)-H(17B)	0.9900
O(19)-C(6)	1.415(3)	C(18)-H(18A)	0.9900
O(19)-C(18)	1.417(4)	C(18)-H(18B)	0.9900
I(11)-C(10)	2.167(3)		

Table 14: Bond Angles [°] for compound **90**

C(1)-O(12)-C(13)	107.5(3)	C(2)-C(8)-C(9)	113.7(2)
C(1)-O(15)-C(14)	107.0(2)	C(2)-C(8)-C(10)	111.3(2)
C(6)-O(16)-C(17)	107.0(2)	C(5)-C(8)-C(9)	113.3(2)
C(6)-O(19)-C(18)	109.1(2)	C(5)-C(8)-C(10)	116.9(2)
O(12)-C(1)-O(15)	106.4(2)	C(9)-C(8)-C(10)	107.8(2)
O(12)-C(1)-C(2)	113.0(2)	I(11)-C(10)-C(8)	114.7(2)
O(12)-C(1)-C(6)	110.4(2)	O(12)-C(13)-C(14)	103.8(3)
O(15)-C(1)-C(2)	110.6(2)	O(15)-C(14)-C(13)	100.8(3)
O(15)-C(1)-C(6)	113.7(2)	O(16)-C(17)-C(18)	103.0(3)
C(2)-C(1)-C(6)	102.9(2)	O(19)-C(18)-C(17)	104.9(3)
C(1)-C(2)-C(3)	106.0(2)	C(2)-C(3)-H(3A)	111.00
C(1)-C(2)-C(7)	113.3(2)	C(2)-C(3)-H(3B)	111.00
C(1)-C(2)-C(8)	103.0(2)	C(4)-C(3)-H(3A)	111.00
C(3)-C(2)-C(7)	114.3(2)	C(4)-C(3)-H(3B)	111.00
C(3)-C(2)-C(8)	101.3(2)	H(3A)-C(3)-H(3B)	109.00
C(7)-C(2)-C(8)	117.4(2)	C(3)-C(4)-H(4A)	111.00
C(2)-C(3)-C(4)	103.6(3)	C(3)-C(4)-H(4B)	111.00
C(3)-C(4)-C(5)	103.0(2)	C(5)-C(4)-H(4A)	111.00
C(4)-C(5)-C(6)	107.1(2)	C(5)-C(4)-H(4B)	111.00
C(4)-C(5)-C(8)	102.2(2)	H(4A)-C(4)-H4B	109.00
C(6)-C(5)-C(8)	103.2(2)	C(4)-C(5)-H(5)	114.00
O(16)-C(6)-O(19)	106.3(2)	C(6)-C(5)-H(5)	114.00
O(16)-C(6)-C(1)	113.5(2)	C(8)-C(5)-H(5)	114.00
O(16)-C(6)-C(5)	109.7(2)	C(2)-C(7)-H(7A)	110.00
O(19)-C(6)-C(1)	111.7(2)	C(2)-C(7)-H(7B)	109.00
O(19)-C(6)-C(5)	113.2(2)	C(2)-C(7)-H(7C)	109.00
C(1)-C(6)-C(5)	102.5(2)	H(7A)-C(7)-H(7B)	109.00
C(2)-C(8)-C(5)	93.5(2)	H(7A)-C(7)-H(7C)	109.00
H(7B)-C(7)-H(7C)	109.00	H(13A)-C(13)-H(13B)	109.00
C(8)-C(9)-H(9A)	109.00	O(15)-C(14)-H(14A)	112.00
C(8)-C(9)-H(9B)	109.00	O(15)-C(14)-H(14B)	112.00

C(8)-C(9)-H(9C)	109.00	C(13)-C(14)-H(14A)	112.00
H(9A)-C(9)-H(9B)	109.00	C(13)-C(14)-H(14B)	112.00
H(9A)-C(9)-H(9C)	110.00	H(14A)-C(14)-H(14B)	109.00
H(9B)-C(9)-H(9C)	109.00	O(16)-C(17)-H(17A)	111.00
I(11)-C(10)-H(10A)	109.00	O(16)-C(17)-H(17B)	111.00
I(11)-C(10)-H(10B)	109.00	C(18)-C(17)-H(17A)	111.00
C(8)-C(10)-H(10A)	109.00	C(18)-C(17)-H(17B)	111.00
C(8)-C(10)-H(10B)	109.00	H(17A)-C(17)-H(17B)	109.00
H(10A)-C(10)-H(10B)	108.00	O(19)-C(18)-H(18A)	111.00
O(12)-C(13)-H(13A)	111.00	O(19)-C(18)-H(18B)	111.00
O(12)-C(13)-H(13B)	111.00	C(17)-C(18)-H(18A)	111.00
C(14)-C(13)-H(13A)	111.00	C(17)-C(18)-H(18B)	111.00
C(14)-C(13)-H(13B)	111.00	H(18A)-C(18)-H(18B)	109.00

Table 15: Torsion angles [^{o}] for compound **90**

C(13)-O(12)-C(1)-O(15)	-5.5(3)
C(13)-O(12)-C(1)-C(2)	116.0(3)
C(13)-O(12)-C(1)-C(6)	-129.3(3)
C(1)-O(12)-C(13)-C(14)	26.9(4)
C(14)-O(15)-C(1)-O(12)	-19.0(3)
C(14)-O(15)-C(1)-C(6)	102.7(3)
C(1)-O(15)-C(14)-C(13)	34.5(3)
C(14)-O(15)-C(1)-C(2)	-142.1(2)
C(17)-O(16)-C(6)-C(5)	-149.0(3)
C(17)-O(16)-C(6)-C(1)	97.0(3)
C(6)-O(16)-C(17)-C(18)	31.6(4)
C(17)-O(16)-C(6)-O(19)	-26.2(3)
C(18)-O(19)-C(6)-O(16)	9.3(3)
C(6)-O(19)-C(18)-C(17)	10.1(4)
C(18)-O(19)-C(6)-C(5)	129.8(3)
C(18)-O(19)-C(6)-C(1)	-115.1(3)
O(12)-C(1)-C(6)-O(16)	-4.8(3)
O(15)-C(1)-C(2)-C(8)	-154.8(2)
O(15)-C(1)-C(6)-O(16)	-124.2(2)
C(6)-C(1)-C(2)-C(3)	73.0(3)
C(6)-C(1)-C(2)-C(7)	-160.9(2)
O(12)-C(1)-C(2)-C(3)	-167.9(2)
O(12)-C(1)-C(2)-C(7)	-41.8(3)
O(12)-C(1)-C(2)-C(8)	86.1(3)
O(15)-C(1)-C(2)-C(3)	-48.8(3)
O(15)-C(1)-C(2)-C(7)	77.3(3)
C(6)-C(1)-C(2)-C(8)	-33.0(3)
O(15)-C(1)-C(6)-O(19)	-4.0(3)
O(12)-C(1)-C(6)-O(19)	115.5(2)
O(12)-C(1)-C(6)-C(5)	-123.0(2)
C(2)-C(1)-C(6)-O(16)	116.1(2)

C(2)-C(1)-C(6)-O(19)	-123.7(2)
O(15)-C(1)-C(6)-C(5)	117.6(2)
C(2)-C(1)-C(6)-C(5)	-2.1(3)
C(1)-C(2)-C(8)-C(9)	171.1(2)
C(1)-C(2)-C(8)-C(5)	53.8(2)
C(8)-C(2)-C(3)-C(4)	36.3(2)
C(3)-C(2)-C(8)-C(5)	-55.9(2)
C(7)-C(2)-C(8)-C(10)	58.3(3)
C(7)-C(2)-C(8)-C(5)	179.0(3)
C(1)-C(2)-C(3)-C(4)	-70.9(3)
C(7)-C(2)-C(3)-C(4)	163.5(2)
C(1)-C(2)-C(8)-C(10)	-66.9(3)
C(4)-C(5)-C(6)-O(16)	168.6(2)
C(7)-C(2)-C(8)-C(9)	-63.7(3)
C(3)-C(2)-C(8)-C(9)	61.5(3)
C(3)-C(2)-C(8)-C(10)	-176.5(2)
C(2)-C(3)-C(4)-C(5)	-1.1(3)
C(3)-C(4)-C(5)-C(8)	-34.8(3)
C(3)-C(4)-C(5)-C(6)	73.3(2)
C(8)-C(5)-C(6)-O(16)	-84.0(3)
C(8)-C(5)-C(6)-O(19)	157.4(2)
C(8)-C(5)-C(6)-C(1)	36.9(3)
C(6)-C(5)-C(8)-C(9)	-173.4(2)
C(4)-C(5)-C(8)-C(9)	-62.3(3)
C(4)-C(5)-C(6)-O(19)	50.0(3)
C(4)-C(5)-C(6)-C(1)	-70.5(2)
C(4)-C(5)-C(8)-C(2)	55.5(2)
C(6)-C(5)-C(8)-C(10)	60.4(3)
C(4)-C(5)-C(8)-C(10)	171.5(2)
C(6)-C(5)-C(8)-C(2)	-55.6(2)
C(9)-C(8)-C(10)-I(11)	-67.5(3)
C(2)-C(8)-C(10)-I(11)	167.19(18)

C(5)-C(8)-C(10)-I(11)	61.5(3)
O(12)-C(13)-C(14)-O(15)	-37.1(4)
O(16)-C(17)-C(18)-O(19)	-25.3(4)

5.2. CRYSTALLOGRAPHIC DATA FOR 9-IODOCAMPHOQUINONE BIS(ETHYLENE KETAL) 92

Table 16: Crystal data and structure refinement for compound **92**

Empirical formula	$C_{14}\ H_{21}\ I\ O_4$
Formula Weight	380.21
Temperature	113 K
Wavelength	0.71073 Å
Crystal System	Monoclinic
Space group	P21 (No. 4)
Unit cell dimensions	a = 7.2272(14) Å $\alpha = 90^o$
	b = 22.840(5) Å $\beta = 90^o$
	c = 13.149(3) Å $\gamma = 90^o$
Volume	2168.9(8) $Å^3$
Z	6
Density calculated	1.747 g/cm^3
Absorption coefficient	2.223 mm^{-1}
F(000)	1140
Crystal Size	0.06 x 0.07 x 0.09 mm^3
Theta range for data collection	3.6 to 25.3^o
Index Ranges	-8<=h<=8, -27<=k<=27,-15<=l<=15
Reflections collected	58200
Independent reflections	7847 [R(int) = 0.111]
Completeness of data to theta = 25.3^o	99%
Absorption correction	Empirical
Max. and min. transmission	0.8782 and 0.8250
Refinement method	Full-matrix least-squares on F^2
Data / restraints / parameters	7847 / 0 / 520
Goodness-of-fit on F^2	0.97
Final R indices [I>2sigma(I)]	R_1 = 0.0343, wR_2 = 0.0519
R indices (all data)	R_1 = 0.0542, wR_2 = 0.0566
Absolute structure parameter	0.039(14)
Largest diff. peak and hole	0.59 and -1.10 $e.Å^{-3}$

Table 17: Atomic coordinates and equivalent isotropic displacement parameters for compound **92**. U(eq) is defined as one third of the trace of the orthogonalized U^{ij} tensor.

Atom	**x**	**y**	**z**	**U(eq) [Å^2]**
C(1)	0.9762(7)	0.0936(2)	0.1665(5)	0.0187(17)
C(2)	0.9644(6)	0.1239(2)	0.2705(4)	0.0150(17)
C(3)	0.8363(7)	0.0849(2)	0.3336(4)	0.0200(17)
C(4)	0.6379(7)	0.0985(2)	0.2904(4)	0.0216(17)
C(5)	0.6758(6)	0.1382(2)	0.1995(4)	0.0168(17)
C(6)	0.7685(7)	0.1005(2)	0.1193(4)	0.0164(17)
C(7)	1.1514(7)	0.1356(3)	0.3217(5)	0.028(2)
C(8)	0.8351(7)	0.1775(2)	0.2422(4)	0.0150(17)
C(9)	0.9101(7)	0.2216(2)	0.1678(4)	0.0214(17)
C(10)	0.7914(8)	0.2112(2)	0.3405(5)	0.0273(19)
C(13)	1.1983(8)	0.0770(3)	0.0489(5)	0.0258(19)
C(14)	1.1931(8)	0.0253(2)	0.1178(5)	0.0261(19)
C(17)	0.7152(7)	0.0825(2)	-0.0538(4)	0.0239(17)
C(18)	0.7130(8)	0.0263(2)	0.0084(4)	0.0250(19)
O(12)	1.1104(4)	0.12159(15)	0.1070(3)	0.0197(11)
O(15)	1.0272(5)	0.03345(15)	0.1726(3)	0.0224(11)
O(16)	0.7651(5)	0.12654(15)	0.0204(3)	0.0205(12)
O(19)	0.6746(5)	0.04651(15)	0.1076(3)	0.0206(12)
I(11)	0.55671(5)	0.26927(2)	0.32297(3)	0.0284(1)

Table 18: Hydrogen coordinates and isotropic displacement parameters for compound **92**.

Atom	**x**	**y**	**z**	**U(iso)**
H(3A)	0.8484	0.0949	0.4068	0.024
H(3B)	0.8665	0.0429	0.3249	0.024
H(4A)	0.5726	0.0623	0.2683	0.026
H(4B)	0.5638	0.119	0.3412	0.026
H(5A)	0.5649	0.1604	0.1729	0.02
H(7A)	1.218	0.0986	0.3317	0.042
H(7B)	1.1346	0.1543	0.3878	0.042
H(7C)	1.2229	0.1616	0.2787	0.042
H(9A)	0.8199	0.2532	0.1566	0.032
H(9B)	0.9322	0.2021	0.1029	0.032
H(9C)	1.0267	0.2379	0.1958	0.032
H(10A)	0.9016	0.2344	0.3626	0.033
H(10B)	0.7672	0.1826	0.395	0.033
H(13A)	1.3272	0.0879	0.0343	0.031
H(13B)	1.1286	0.0694	-0.0161	0.031
H(14A)	1.1878	-0.0117	0.0783	0.031
H(14B)	1.3034	0.0244	0.1648	0.031
H(17A)	0.8078	0.0803	-0.1073	0.029
H(17B)	0.5919	0.0906	-0.0862	0.029
H(18A)	0.6153	-0.0007	-0.0179	0.03
H(18B)	0.8342	0.0062	0.0078	0.03

Table 19: Anisotropic displacement parameters ($Å^2$ x 10^3) for compound **92**.

Atom	**U^{11}**	**U^{22}**	**U^{33}**	**U^{23}**	**U^{13}**	**U^{12}**
C(1)	18(3)	20(3)	18(3)	8(2)	-1(2)	1(2)
C(2)	12(3)	20(3)	13(3)	5(2)	1(2)	1(2)
C(3)	24(3)	26(3)	10(3)	5(3)	0(2)	-4(2)
C(4)	23(3)	023(3)	19(3)	0(3)	3(3)	-5(2)
C(5)	12(3)	025(3)	13(3)	-3(3)	-3(2)	-1(2)
C(6)	18(3)	13(3)	18(3)	8(2)	-3(2)	0(2)
C(7)	22(3)	34(4)	27(4)	-2(3)	-4(3)	1(3)
C(8)	15(3)	15(3)	15(3)	-1(2)	-1(2)	-1(2)
C(9)	24(3)	19(3)	21(3)	-3(3)	-1(3)	-4(2)
O(12)	19(18)	19(2)	22(2)	2(17)	11(17)	1(16)
O(15)	20(19)	19(2)	029(2)	5(17)	6(17)	6(16)
O(16)	31(2)	20(2)	10(2)	1(17)	-4(17)	2(17)
O(19)	21(2)	18(2)	23(2)	-1(18)	3(17)	-4(17)
I(11)	30(2)	26(2)	30(2)	-9(2)	5(2)	4(2)

Table 20: Bond distances (Å) for compound **92.**

C(1)-C(2)	1.538(8)	C(3)-H(3A)	0.99
C(1)-C6	1.610(7)	C(3)- H(3B)	0.99
C(2)-C(3)	1.548(7)	C(4)-H(4A)	0.99
C(2)-C(7)	1.511(7)	C(4)-H(4B)	0.99
C(2)-C(8)	1.576(7)	C(5)-H(5A)	1
C(3)-C(4)	1.553(7)	C(7)-H(7A)	0.98
C(4)-C(5)	1.533(7)	C(7)-H(7B)	0.98
C(5)-C(8)	1.548(7)	C(7)-H(7C)	0.98
C(5)-C(6)	1.535(7)	C(9)-H(9B)	0.98
C(8)-C(10)	1.547(8)	C(9)-H(9A)	0.98
C(8)-C(9)	1.519(7)	C(9)-H(9C)	0.98
C(13)-C(14)	1.490(9)	C(10)-H(10A)	0.99
C(17)-C(18)	1.522(7)	C(10)-H(10B)	0.99
O(12)-C(13)	1.436(7)	C(13)-H(13A)	0.99
O(12)-C(1)	1.421(6)	C(13)-H(13B)	0.99
O(15)-C(1)	1.424(6)	C(14)-H(14B)	0.99
O(15)-C(14)	1.434(7)	C(14)-H(14A)	0.99
O(16)-C(17)	1.438(6)	C(17)-H(17A)	0.99
O(16)-C(6)	1.429(6)	C(17)-H(17B)	0.99
O(19)-C(6)	1.413(6)	C(18)-H(18B)	0.99
O(19)-C(18)	1.421(7)	C(18)-H(18A)	0.99
I(11)-C(10)	2.159(5)		

Table 21: Bond Angles[^{o}] for compound **92**

C(1)-O(12)-C(13)	107.4(4)	C(4)-C(5)-C(6)	107.4(4)
C(1)-O(15)-C(14)	108.5(4)	O(19)-C(6)-C(1)	113.2(4)
C(6)-O(16)-C(17)	108.8(4)	O(16)-C(6)-C(5)	113.5(4)
C(6)-O(19)-C(18)	105.9(4)	O(16)-C(6)-O(19)	105.8(4)
O(15)-C(1)-C(6)	110.6(4)	O(16)-C(6)-C(1)	112.0(4)
O(15)-C(1)-C(2)	114.0(5)	C(1)-C(6)-C(5)	102.4(4)
O(12)-C(1)-C(6)	112.9(4)	O(19)-C(6)-C(5)	110.1(4)
C(2)-C(1)-C(6)	102.5(4)	C(5)-C(8)-C(10)	114.8(4)
O(12)-C(1)-O(15)	106.5(4)	C(9)-C(8)-C(10)	107.3(4)
O(12)-C(1)-C(2)	110.4(4)	C(5)-C(8)-C(9)	115.5(4)
C(7)-C(2)-C(8)	118.7(4)	C(2)-C(8)-C(9)	116.4(4)
C(1)-C(2)-C(3)	105.8(4)	C(2)-C(8)-C(10)	109.1(4)
C(1)-C(2)-C(7)	113.4(4)	C(2)-C(8)-C(5)	93.5(3)
C(3)-C(2)-C(8)	102.3(4)	I(11)-C(10)-C(8)	113.6(4)
C(3)-C(2)-C(7)	114.0(5)	O(12)-C(13)-C(14)	102.5(5)
C(1)-C(2)-C(8)	101.1(4)	O(15)-C(14)-C(13)	104.1(4)
C(2)-C(3)-C(4)	104.6(4)	O(16)-C(17)-C(18)	103.5(4)
C(3)-C(4)-C(5)	102.3(4)	O(19)-C(18)-C(17)	103.0(4)
C(4)-C(5)-C(8)	102.3(4)	C(4)-C(3)-H(3A)	111
C(6)-C(5)-C(8)	103.7(4)	C(4)-C(3)-H(3B)	111
C(4)-C(5)-H(5A)	114	C(2)-C(3)-H(3B)	111
C(8)-C(5)-H(5A)	114	C(2)-C(3)-H(3A)	111
C(6)-C(5)-H(5A)	114	H(3A)-C(3)-H(3B)	109
H(7B)-C(7)-H(7C)	109	H(4A)-C(4)-H(4B)	109
H(7A)-C(7)-H(7B)	110	C(5)-C(4)-H(4B)	111
H(7A)-C(7)-H(7C)	109	C(5)-C(4)-H(4A)	111
C(2)-C(7)-H(7A)	110	C(3)-C(4)-H(4A)	111
C(2)-C(7)-H(7B)	109	C(3)-C(4)-H(4B)	111
C(2)-C(7)-H(7C)	109	H(14A)-C(14)-H(14B)	109
H(9A)-C(9)-H(9C)	110	C(13)-C(14)-H(14A)	111
C(8)-C(9)-H(9A)	109	O(16)-C(17)-H(17B)	111

H(9A)-C(9)-H(9B)	109	C(18)-C(17)-H(17A)	111
C(8)-C(9)-H(9B)	109	O(16)-C(17)-H(17A)	111
H(9B)-C(9)-H(9C)	109	H(17A)-C(17)-H(17B)	109
C(8)-C(9)-H(9C)	109	C(18)-C(17)-H(17B)	111
I(11)-C(10)-H(10B)	109	H(18A)-C(18)-H(18B)	109
C(8)-C(10)-H(10A)	109	C(17)-C(18)-H(18B)	111
I(11)-C(10)-H(10A)	109	O(19)-C(18)-H(18B)	111
C(8)-C(10)-H(10B)	109	C(17)-C(18)-H(18A)	111
H(10)-C(10)-H(10B)	108	O(19)-C(18)-H(18A)	111
C(14)-C(13)-H(13B)	111	O(12)-C(13)-H(13A)	111
H(13A)-C(13)-H(13B)	109	O(15)-C(14)-H(14A)	111
O(12)-C(13)-H(13B)	111	C(13)-C(14)-H(14B)	111
C(14)-C(13)-H(13A)	111	O(15)-C(14)-H(14B)	111

Table 22: Torsion Angles [^{o}] for compound **92**

C(13)-O(12)-C(1)-O(15)	20.3(6)
C(13)-O(12)-C(1)-C(2)	144.6(4)
C(13)-O(12)-C(1)-C(6)	-101.3(5)
C(1)-O(12)-C(13)-C(14)	-32.0(5)
C(14)-O(15)-C(1)-O(12)	0.6(6)
C(14)-O(15)-C(1)-C(6)	123.7(5)
C(1)-O(15)-C(14)-C(13)	-20.2(6)
C(14)-O(15)-C(1)-C(2)	-121.4(5)
C(17)-O(16)-C(6)-C(5)	-136.1(4)
C(17)-O(16)-C(6)-C(1)	108.5(4)
C(6)-O(16)-C(17)-C(18)	-6.9(5)
C(17)-O(16)-C(6)-O(19)	-15.2(5)
C(18)-O(19)-C(6)-O(16)	32.9(5)
C(6)-O(19)-C(18)-C(17)	-36.4(5)
C(18)-O(19)-C(6)-C(5)	155.9(4)
C(18)-O(19)-C(6)-C(1)	-90.2(5)
O(15)-C(1)-C(6)-O(16)	-111.4(5)
O(15)-C(1)-C(6)-O(19)	8.2(6)
C(6)-C(1)-C(2)-C(7)	-167.2(4)
C(6)-C(1)-C2-C(8)	-39.0(4)
O(12)-C(1)-C(6)-O(19)	127.4(4)
O(12)-C(1)-C(6)-O(16)	7.9(6)
O(12)-C(1)-C(6)-C(5)	-114.1(4)
C(2)-C(1)-C(6)-C(5)	4.7(5)
C(6)-C(1)-C(2)-C(3)	67.2(4)
O(15)-C(1)-C(2)-C(3)	-52.3(5)
O(15)-C(1)-C(2)-C(7)	73.3(6)
O(15)-C(1)-C(6)-C(5)	126.7(5)
C(2)-C(1)-C(6)-O(16)	126.7(4)
C(2)-C(1)-C(6)-O(19)	-113.8(4)
O(12)-C(1)-C(2)-C(8)	81.5(4)

O(12)-C(1)-C(2)-C(7)	-46.6(6)
O(12)-C(1)-C(2)-C(3)	-172.2(4)
O(15)-C(1)-C(2)-C(8)	-158.6(4)
C(3)-C(2)-C(8)-C(10)	66.0(5)
C(7)-C(2)-C(8)-C(9)	61.2(6)
C(1)-C(2)-C(8)-C(10)	175.0(4)
C(7)-C(2)-C(8)-C(5)	-178.1(5)
C(3)-C(2)-C(8)-C(5)	-51.8(4)
C(8)-C(2)-C(3)-C(4)	29.2(5)
C(1)-C(2)-C(8)-C(9)	-63.5(5)
C(3)-C(2)-C(8)-C(9)	-172.5(4)
C(1)-C(2)-C(8)-C(5)	57.3(4)
C(7)-C(2)-C(8)-C(10)	-60.4(6)
C(7)-C(2)-C(3)-C(4)	158.5(4)
C(1)-C(2)-C(3)-C(4)	-76.2(4)
C(2)-C(3)-C(4)-C(5)	6.3(5)
C(3)-C(4)-C(5)-C(8)	-40.6(4)
C(3)-C(4)-C(5)-C(6)	68.2(4)
C(6)-C(5)-C(8)-C(10)	-167.8(4)
C(4)-C(5)-C(8)-C(2)	56.8(4)
C(4)-C(5)-C(8)-C(10)	-56.2(5)
C(6)-C(5)-C(8)-C(9)	66.6(5)
C(6)-C(5)-C(8)-C(2)	-54.9(4)
C(8)-C(5)-C(6)-O(19)	152.8(4)
C(4)-C(5)-C(8)-C(9)	178.3(4)
C(8)-C(5)-C(6)-C(1)	32.2(5)
C(8)-C(5)-C(6)-O(16)	-88.8(5)
C(4)-C(5)-C(6)-O(19)	45.0(5)
C(4)-C(5)-C(6)-C(1)	-75.6(4)
C(4)-C(5)-C(6)-O(16)	163.4(4)
C(5)-C(8)-C(10)-I(11)	-59.6(5)
C(2)-C(8)-C(10)-I(11)	-163.0(3)

C(9)-C(8)-C(10)-I(11)	70.1(4)
O(12)-C(13)-C(14)-O(15)	31.5(5)
O(16)-C(17)-C(18)-O(19)	26.2(5)

5.3. CRYSTALLOGRAPHIC DATA FOR 2-(DIPHENYLPHOSPHINOYLMETHYL)-1,3-BIS(HYDROXYMETHYL)-1,2-DIMETHYCYCLOPENTANE 111

Table 23: Crystal data and structure refinement for compound **111**

Crystal Data	
Formula	$C_{22}H_{29}O_3P$
Formula Weight	372.42
Crystal System	Orthorhombic
Space group	P212121 (No. 19)
a, b, c [Angstrom]	8.6703(2) 13.1990(3) 16.8725(4)
V	1930.88(8) $Å^3$
Z	4
Density calculated	1.281 g/cm^3
Absorption coefficient	0.161 mm^{-1}
F(000)	800
Crystal Size [mm]	0.06 x 0.08 x 0.11 mm^3
Data Collection	
Temperature	113 K
Wavelength	0.71073 Å
Theta Min-Max	4.8 to 25.7^o
Dataset	-10: 10 ; -16: 16 ; -20: 20
Tot., Uniq. Data, R(int)	32436, 3650, 0.084
Observed data [I > 2.0 sigma(I)]	3015
Refinement	
Nref, Npar	3650, 240
R, wR2, S	0.0330, 0.0751, 1.02
w = 1/[\s^2^(Fo^2^)+(0.0397P)^2^]	where P=(Fo^2^+2Fc^2^)/3
Max. and Av. Shift/Error	0.00, 0.00
Flack x	0.00(8)
Min. and Max. Resd. Dens. [e/Ang^3]	-0.20, 0.20

Table 24: Atomic coordinates and equivalent isotropic displacement parameters for compound **111**. U(eq) is defined as one third of the trace orthogonalized U^{ij} tensor.

Atom	**x**	**y**	**z**	**U(eq) [Å^2]**
C(1)	0.5862(2)	0.51409(13)	0.75916(10)	0.0208(5)
C(2)	0.4169(2)	0.50574(14)	0.79349(10)	0.0244(6)
C(3)	0.3872(2)	0.61283(15)	0.82929(12)	0.0293(7)
C(4)	0.5435(2)	0.66523(14)	0.83875(12)	0.0281(7)
C(5)	0.6635(2)	0.58210(14)	0.82353(11)	0.0241(6)
C(6)	0.6702(2)	0.41260(14)	0.75261(11)	0.0250(6)
C(7)	0.8270(2)	0.62035(15)	0.80969(11)	0.0270(6)
C(9)	0.2893(2)	0.48293(15)	0.73400(12)	0.0280(6)
C(11)	0.4086(3)	0.42455(15)	0.85861(11)	0.0305(6)
C(12)	0.5910(2)	0.57301(13)	0.67849(10)	0.0217(5)
C(15)	0.5887(2)	0.60831(14)	0.51110(10)	0.0218(5)
C(16)	0.6690(2)	0.69894(15)	0.52035(11)	0.0261(6)
C(17)	0.6719(2)	0.77022(15)	0.45987(12)	0.0289(7)
C(18)	0.5934(2)	0.75207(15)	0.38977(11)	0.0272(6)
C(19)	0.5121(2)	0.66285(15)	0.38012(12)	0.0281(6)
C(20)	0.5102(2)	0.59113(14)	0.44029(11)	0.0248(6)
C(21)	0.7691(2)	0.44423(14)	0.57132(11)	0.0210(6)
C(22)	0.7707(2)	0.33936(14)	0.56251(11)	0.0248(6)
C(23)	0.9094(2)	0.28790(15)	0.55528(11)	0.0284(6)
C(24)	1.0476(2)	0.34086(15)	0.55708(11)	0.0274(7)
C(25)	1.0463(2)	0.44550(15)	0.56454(11)	0.0282(7)
C(26)	0.9088(2)	0.49690(14)	0.57142(10)	0.0253(5)
O(8)	0.84420(16)	0.70043(10)	0.75393(8)	0.0298(4)
O(10)	0.29763(16)	0.38396(10)	0.70024(8)	0.0285(4)
O(14)	0.45472(14)	0.43642(9)	0.57036(8)	0.0260(4)
P(13)	0.58659(6)	0.50775(4)	0.58407(3)	0.0213(1)

Table 25: Hydrogen coordinates and isotropic displacement parameters for compound **111**.

Atom	**x**	**y**	**z**	**U(iso)**
H(3A)	0.3356	0.6067	0.8814	0.035
H(3B)	0.3199	0.6528	0.7936	0.035
H(4A)	0.5549	0.6933	0.8929	0.034
H(4B)	0.5547	0.721	0.7999	0.034
H(5)	0.6675	0.5403	0.8729	0.029
H(6A)	0.7745	0.4238	0.7319	0.038
H(6B)	0.6134	0.3679	0.7166	0.038
H(6C)	0.6767	0.3811	0.8051	0.038
H(7A)	0.8692	0.6435	0.8611	0.032
H(7B)	0.8909	0.5625	0.7918	0.032
H(8)	0.8108	0.7546	0.7737	0.036
H(9A)	0.1884	0.4907	0.7607	0.034
H(9B)	0.2942	0.5335	0.6908	0.034
H(10)	0.3472	0.3864	0.6575	0.034
H(11A)	0.3084	0.4284	0.8853	0.046
H(11B)	0.4911	0.4361	0.8973	0.046
H(11C)	0.4211	0.3573	0.8348	0.046
H(12A)	0.6859	0.6148	0.679	0.026
H(12B)	0.5029	0.6207	0.6788	0.026
H(16)	0.7223	0.7121	0.5685	0.031
H(17)	0.7277	0.8315	0.4666	0.035
H(18)	0.5955	0.8009	0.3484	0.033
H(19)	0.4575	0.6506	0.3323	0.034
H(20)	0.4549	0.5297	0.4331	0.03
H(22)	0.6763	0.3029	0.5614	0.03
H(23)	0.9098	0.2164	0.5491	0.034
H(24)	1.1428	0.3056	0.5532	0.033
H(25)	1.1408	0.4819	0.5649	0.034
H(26)	0.9089	0.5686	0.5763	0.03

Table 26: Anisotropic displacement parameters ($Å^2$ x 10^3) for compound **111**. The anisotropic displacement factor exponent takes the form: $-2p^2[h^2a^{*2}U^{11} + \ldots + 2h\ k\ a^*\ b^*U^{12}]$.

Atom	**U^{11}**	**U^{22}**	**U^{33}**	**U^{23}**	**U^{13}**	**U^{12}**
C(1)	25(9)	20(9)	20(9)	1(8)	0(8)	1(9)
C(2)	26(10)	21(10)	27(9)	-1(8)	2(9)	-1(10)
C(3)	30(12)	25(11)	33(11)	-3(9)	5(10)	0(9)
C(4)	32(12)	25(11)	27(11)	-6(9)	7(9)	-4(9)
C(5)	31(11)	22(11)	19(9)	0(8)	0(9)	-2(9)
C(6)	28(11)	21(10)	26(10)	1(8)	-1(9)	3(9)
C(7)	29(11)	23(11)	29(11)	-1(9)	-4(9)	-3(9)
C(9)	29(11)	20(11)	35(11)	-1(9)	2(9)	-1(9)
C(11)	30(11)	32(11)	30(11)	3(9)	3(10)	-4(11)
C(12)	24(10)	18(9)	23(9)	-2(7)	-0(9)	2(9)
C(15)	21(9)	21(10)	23(9)	-1(8)	0.0007(9)	5(10)
C(16)	31(12)	23(11)	25(10)	-3(9)	-5(9)	3(10)
C(17)	32(12)	21(11)	34(12)	3(9)	-1(10)	-3(10)
C(18)	31(11)	24(11)	27(10)	5(8)	2(10)	5(11)
C(19)	27(11)	33(12)	24(10)	-2(9)	-2(9)	7(10)
C(20)	21(10)	22(10)	31(11)	-1(8)	-2(8)	2(9)
C(21)	27(11)	19(10)	17(9)	-1(8)	-0(8)	1(8)
C(22)	27(11)	23(11)	25(10)	-2(8)	-2(9)	-3(9)
C(23)	34(11)	21(10)	30(10)	-5(8)	-2(10)	6(10)
C(24)	27(12)	31(12)	25(11)	-5(9)	-2(9)	7(9)
C(25)	25(11)	31(12)	29(11)	0(9)	-2(9)	1(9)
C(26)	26(9)	19(9)	31(10)	1(9)	-1(9)-	1(10)
O(8)	34(8)	23(7)	33(8)	-2(6)	6(6)	-4(7)
O(10)	31(8)	23(7)	32(8)	-1(6)	1(6)	-3(6)
O(14)	25(7)	23(7)	30(7)	-3(6)	-2(6)	-3(6)
P(13)	22(2)	18(2)	23(2)	-2(2)	-1(2)	1(2)

Table 27: Bond lengths [Å] for compound **111**

C(1)–C(6)	1.529(3)	C(6)-H(6C)	0.98
C(1)-C(12)	1.568(2)	C(7)-H(7A)	0.99
C(1)-C(2)	1.582(2)	C(7)-H(7B)	0.99
C(1)-C(5)	1.560(3)	C(9)-H(9A)	0.99
C(2)-C(11)	1.537(3)	C(9)-H(9B)	0.99
C(2)-C(3)	1.559(3)	C(11)-H(11A)	0.98
C(2)-C(9)	1.524(3)	C(11)-H(11B)	0.98
C(3)-C(4)	1.530(3)	C(11)-H(11C)	0.98
C(4)-C(5)	1.534(3)	C(12)-H(12A)	0.99
C(5)-C(7)	1.523(2)	C(12)-H(12B)	0.99
C(15)-C(20)	1.394(2)	C(16)-H(16)	0.95
C(15)-C(16)	1.393(3)	C(17)-H(17)	0.95
C(16)-C(17)	1.388(3)	C(18)-H(18)	0.95
C(17)-C(18)	1.386(3)	C(19)-H(19)	0.95
C(18)-C(19)	1.382(3)	C(20)-H(20)	0.95
C(19)-C(20)	1.388(3)	C(22)-H(22)	0.95
C(21)-C(26)	1.397(2)	C(23)-H(23)	0.95
C(21)-C(22)	1.392(3)	C(24)-H(24)	0.95
C(22)-C(23)	1.387(3)	C(25)-H(25)	0.95
C(23)-C(24)	1.388(3)	C(26)-H(26)	0.95
C(24)-C(25)	1.387(3)	P(13)-O(14)	1.4991(13)
C(25)-C(26)	1.377(3)	P(13)-C(12)	1.8115(18)
C(3)-H(3A)	0.99	P(13)-C(15)	1.8105(19)
C(3)-H(3B)	0.99	P(13)-C(21)	1.8037(18)
C(4)-H(4A)	0.99	O(8)-C(7)	1.423(2)
C(4)-H(4B)	0.99	O(10)-C(9)	1.427(2)
C(5)-H(5)	1	O(8)-H(8)	0.84
C(6)-H(6A)	0.98	O(10)-H(10)	0.84
C(6)-H(6B)	0.98		

Table 28: Bond Angles[^{o}] for compound **111**

C1-C2 -C11	110.73(16)	C24-C25-C26	123.95(13)
C1-C2-C3	103.42(14)	C4-C3-H3A	118.68(16)
C1-C2 -C9	116.50(14)	C4-C3-H3B	117.31(14)
C1-C5-C4	103.69(14)	C5-C4-H4A	120.58(17)
C1-C5-C7	118.94(15)	C5-C4-H4B	120.10(18)
C1-C6-H6A	109	C1-C12-H12A	119.90(18)
C1-C6-H6B	109	C1-C12-H12B	120.06(18)
C1-C6-H6C	110	H12A-C12-H12B	120.68(17)
C12-P13-C15	104.43(8)	C15-C16-C17	118.92(13)
C12-P13-C21	107.90(8)	C16-C17-C18	119.10(16)
C15-P13-C21	104.53(8)	C17-C18-C19	121.96(14)
C2-C1-C12	112.15(14)	C21-C22-C23	120.34(17)
C2-C1-C5	100.59(13)	C22-C21-C26	120.02(18)
C2-C1-C6	114.05(14)	P13-C21-C22	119.78(17)
C2-C11-H11A	110	C24-C23-H23	120.36(17)
C2-C11-H11B	109	C23-C24-H24	120.38(17)
C2-C11-H11C	109	C25-C24-H24	110
C2-C3-C4	107.70(14)	H3A-C3-H3B	110
C2-C9-H9A	109	C21-C22-H22	110
C2-C9 -H9B	109	C23-C22-H22	110
C3-C2-C11	110.34(15)	C2-C3-H3A	108
C3-C2-C9	108.33(15)	C21-C26-C25	111
C3-C4-C5	105.07(15)	C3-C4-H4A	111
C4-C5-C7	114.83(15)	C3-C4-H4B	111
C5-C1-C12	107.91(14)	P13-C21-C26	111
C5-C1-C6	110.48(14)	C22-C23-C24	109
C5-C7-H7A	108	C19-C18-H18	106
C5-C7-H7B	108	C18-C19-H19	106
C6-C1-C12	111.05(14)	C23-C24-C25	107
C7-C5-H5	106	P13-C12-H12B	107
C7-O8-H8	109	C18-C19-C20	107

C9-C2-C11	107.41(16)	C2-C3-H3B	107
C9-O10-H10	109	C15-C20-C19	120
H11A-C11-H11B	109	C24-C25-H25	120
H11A-C11-H11C	109	C26-C25-H25	120
H11B-C11-H11C	109	C21-C26-H26	120
H6A-C6-H6B	109	C15-C16-H16	120
H6A-C6-H6C	109	C17-C16-H16	120
H6B-C6-H6C	110	C16-C17-H17	120
H7A-C7-H7B	107	C20-C19-H19	120
H9A-C9-H9B	108	C22-C23-H23	120
O10-C9-C2	114.02(15)	C1-C5-H5	120
O10-C9-H9A	109	C15-C20-H20	120
O10-C9-H9B	109	C19-C20 -H20	120
O14-P13-C12	116.77(8)	P13 -C15-C16	120
O14-P13-C15	111.30(8)	C16 -C15 -C20	120
O14-P13-C21	111.03(8)	P13-C15-C20	120
O8-C7-C5	116.44(15)	H4A-C4-H4B	120
O8-C7-H7A	108	C18-C17-H17	120
O8-C7-H7B	108	C17-C18-H18	120
P13-C12-C1	121.80(12)	C4-C5-H5	120
P13-C12-H12A	107	C25-C26 -H26	120

Table 29: Torsion Angles [^{o}] for compound **111**

C21-P13-C12-C1	-70.82(15)
O14-P13-C15-C16	162.01(15)
C12-P13-C15-C16	35.17(17)
C21-P13-C15 -C16	-78.07(17)
O14-P13-C15-C20	-20.86(17)
C12-P13-C15-C20	-147.69(14)
C21-P13-C15-C20	99.07(15)
O14-P13-C12-C1	55.01(16)
O14-P13-C21-C22	-9.04(18)
C12-P13-C21-C22	120.11(15)
C15-P13-C21-C22	-129.15(15)
O14-P13-C21-C26	172.10(14)
C12-P13-C21-C26	-58.75(17)
C15-P13-C21-C26	52.00(17)
C15-P13-C12-C1	178.37(13)
C12-C1-C2-C9	41.3(2)
C12-C1-C2-C11	164.41(14)
C2-C1-C5-C7	-173.17(15)
C6-C1-C5-C4	-165.04(14)
C6-C1-C5-C7	66.0(2)
C12-C1-C5-C4	73.39(17)
C6-C1-C2-C11	37.1(2)
C12-C1-C2-C3	-77.40(16)
C2-C1-C5-C4	-44.22(16)
C5-C1-C2-C3	37.04(16)
C5-C1-C2-C9	155.74(15)
C5-C1-C2-C11	-81.15(17)
C6-C1-C2-C3	155.28(15)
C6-C1-C2-C9	-86.02(19)
C12-C1-C5-C7	-55.6(2)
C5-C1-C12-P13	154.97(12)

C6-C1-C12-P13	33.76(19)
C2-C1-C12-P13	-95.15(16)
C11-C2-C9-O10	-57.2(2)
C3-C2-C9-O10	-176.36(15)
C1-C2-C3-C4	-17.06(18)
C1-C2-C9-O10	67.6(2)
C9-C2-C3-C4	-141.28(16)
C11-C2-C3-C4	101.40(19)
C2-C3-C4-C5	-10.4(2)
C3-C4-C5-C1	34.32(18)
C3-C4-C5-C7	165.74(16)
C1-C5-C7-O8	75.0(2)
C4-C5-C7-O8	-48.7(2)
P13-C15-C16-C17	176.47(14)
C16-C15-C20-C19	0.1(3)
C20-C15-C16-C17	-0.6(3)
P13-C15-C20-C19	-177.22(14)
C15-C16-C17-C18	0.6(3)
C16-C17-C18-C19	0.0(3)
C17-C18-C19-C20	-0.6(3)
C18 -C19-C20-C15	0.5(3)
P13-C21-C22-C23	-177.82(14)
C26-C21-C22-C23	1.1(3)
P13-C21-C26-C25	177.53(14)
C22-C21-C26-C25	-1.3(3)
C21-C22-C23-C24	0.2(3)
C22-C23-C24-C25	-1.3(3)
C23-C24-C25-C26	1.0(3)
C24-C25-C26-C21	0.3(3)

Table 30: Hydrogen bonds for compound **111** [bond lengths (d) in Å, bond angles (<) in degrees).

D--H…A	**d(D-H)**	**d(H…A)**	**d(D…A)**	**<(DHA)**
O(8) -- H(8) .. O(10)	0.84	2	2.8246(19)	168
O(10) -- H(10) .. O(14)	0.84	1.86	2.6715(19)	161
C(4) -- H(4B) .. O(10)	0.99	2.5	3.266(2)	134
C(11)-- H(11C) .. O10	0.98	2.53	2.890(2)	101
C(12)-- H(12A) .. O(8)	0.99	2.18	3.044(2)	145